

ALMA MATER STUDIORUM – UNIVERSITA' DI BOLOGNA

II FACOLTA' DI INGEGNERIA

Dipartimento di Ingegneria delle Costruzioni Meccaniche,
Nucleari, Aeronautiche e di Metallurgia

DOTTORATO DI RICERCA IN
DISEGNO E METODI DELL'INGEGNERIA INDUSTRIALE

Ciclo XXII

Settore scientifico-disciplinare di afferenza: ING-IND05

**DESIGN, ASSEMBLY AND TEST OF AN AIRBORNE
AUTOMATED IMAGING SYSTEM FOR
ENVIRONMENTAL MONITORING**

Presentata da:

Ing. Nicola Melega

Coordinatore Dottorato

Prof. Franco Persiani

Relatore

Prof. Paolo Tortora

Esame finale anno 2010

Abstract

Remote sensing and photogrammetry are key technologies for several activities such mapping, agriculture, land use or soil and air pollution monitoring. In this study an airborne autonomous and fully automated system for photogrammetry and remote sensing purposes is presented. State of the art technologies in this field have been reviewed, in order to define a set of requirements needed to lead the develop of this new system. The proposed solution demonstrates the feasibility of very high resolution image acquisition (working in the visible portion of the electromagnetic spectrum, in the Red-Green-Blue and nIR bands) from a standard equipped ultra light aircraft, without the need of any specific navigation system or modifications to the aircraft structure. The camera system geometry has been studied both in terms of number of elements and relative positioning. A compatible hardware layout has been developed using industrial PC-boards, a GPS receiver and an IMU, and a 3D CAD model of the whole system has been assembled. A planning tool, partially based on the use of a geographical browser, was necessary to generate typical multi-stripes flight trajectories used during photogrammetric campaigns, and has been developed as part of this thesis.

An engineering model of the system, with reduced performances, has been designed and assembled as a test bed for the final architecture and has been used during both laboratory and flight tests. This prototype already implements the “tunnel in the sky” visual interface which helps the pilot to follow the planned trajectory. Three flight campaigns have been carried out aimed at understanding the system’s functionalities and at verifying the actual capability of reproducing the planned flight trajectories during normal operations.

During the flight campaigns, high resolution images were acquired and post-processing operations have been carried out creating mosaics from the acquired images and presenting them using the above-mentioned graphical geobrowser.

Table of Contents

Table of Contents	i
List of Figures	iii
List of Tables	vii
Chapter 1. Introduction.....	1
Chapter 2. Background.....	4
2.1 AMSC.....	5
2.2 STARS	10
2.3 LCCES	13
Chapter 3. Remote Sensing and Photogrammetry, State of the Art Technologies.....	17
3.1 Airborne Sensors	18
3.1.1 Airborne Digital Cameras.....	19
3.1.2 Airborne Pushbroom Line Scanners.....	23
Chapter 4. FASTER.....	25
4.1 Underlying Idea.....	25
4.2 Proposed Solution	27
4.3 FASTER Cameras Geometry	30
4.4 FASTER components.....	32
Chapter 5. FASTER Planning Software	37
5.1 Photogrammetric Aerial Mission	37
5.2 FASTER planning software layout	40
5.3 Google Earth Geobrowsing Solution	41
5.3.1 KML/KMZ Exchange Format	43
5.3.2 Reading KML/KMZ in Matlab.....	43
5.4 FASTER Flight Planner	45
5.4.1 Universal Transverse Mercator Coordinate System.....	46
5.4.2 Trajectory Determination	49
Chapter 6. FASTER Engineering Model.....	57

Table of Contents

6.1	FASTER EM Hardware layout	60
6.1.1	Sensors And Data Logger	61
6.1.2	Visualization and data storage	64
6.1.3	Sensing Device	66
6.2	Power Subsystem	68
6.3	Airborne External POD Assembly	69
6.4	Airborne Internal Management and Computing Unit Assembly	73
6.5	FASTER EM Software Description	75
6.5.1	Garmin GPS 18 5Hz Acquisition Block.....	78
6.5.2	Crossbow NAV420 Acquisition Block	81
6.5.3	Magnetometer acquisition block	85
6.5.4	Canon EOS 450D Management Block.....	85
6.5.5	Tunnel in The Sky Management Block.....	89
6.5.6	Virtual Tunnel Block	90
6.5.7	Datalog Block	93
6.5.8	Pilot Interface Block.....	94
6.6	Tunnel In The Sky Visual Interface	95
6.7	Canon Camera Control Software	98
Chapter 7.	Results of the test campaigns.....	101
7.1	Laboratory Tests.....	101
7.2	Flight tests	108
7.2.1	First Test Campaign.....	110
7.2.2	Second Test Campaign	114
7.2.3	Third test campaign	119
Chapter 8.	Conclusions.....	125
Appendix-A	Converting Geographical Coordinates to UTM.....	127
Bibliography	129

List of Figures

Figure 1: Dalsa FTF2020M sensor	6
Figure 2: Dalsa demoboard with FTF2020M sensor support	6
Figure 3: Acquisition method, e.g 6 bands image	7
Figure 4: E.F.L = 200 mm, Telephoto Ratio = 0.9, Overall Length = 180 mm, F/# = 4, B.F.L = 60 mm.....	7
Figure 5: AMSC standard ray tracing analysis	8
Figure 6: AMSC plotting of the MTF (b)	8
Figure 7: Spot shape of the ALMASat-1 Sun Sensor wide angle lens used as test bed for the development of the calibration procedures for the AMSC	9
Figure 8: Electronics Layout Block Diagram	10
Figure 9: STARS simulation environment diagram	11
Figure 10: STARS laboratory test-bed	11
Figure 11: Experimental results on printed target (from 0 to 5° rotation along z-axis).....	12
Figure 12: LEO Conditions.....	14
Figure 13: GEO conditions	14
Figure 14: LCCES LEO optical layout.....	14
Figure 15: LCCES GEO optical layout	14
Figure 16: LCCES LEO optical configuration standard raytrace analysis	15
Figure 17: LCCES GEO optical configuration standard raytrace report.....	15
Figure 18: LEO configuration assembly.....	16
Figure 19: GEO configuration assembly	16
Figure 20: Carl Zeiss VOS 40 [Ref. (1)] and a DSLR Canon EOS 1D [Ref (2)].....	19
Figure 21: ADS Agri-View multispectral camera [Ref. (1)] and Track' Air oblique MIDAS system [Ref. (2)]	20
Figure 22: Applanix DSS439 [Ref. (1)] and DiMAC Wide+ [Ref. (2)].....	21
Figure 23: Vexcel UltraCAm Xp [Ref. (1)] and the Intergraph DMC [Ref. (2)]	22
Figure 24: Multiple cameras system geometries [Ref. (1), (2)].....	23

List of Figures

Figure 25: Leica ADS40 sensor head and assembly [.....	24
Figure 26: Direct Georeferencing System, reference frames [Ref. (1)]	26
Figure 27: FASTER selected cameras system geometry	31
Figure 28: FASTER camera ground projections	32
Figure 29: Prosilica GE4000 [Ref. (1)] and the Zeiss Distagon 28 mm F/2.8 [Ref. (2)] ..	33
Figure 30: FASTER 3D model assembly	34
Figure 31: FASTER 3D model assembly, pc-box and SSDs mount	35
Figure 32: FASTER 3D model canopy.....	35
Figure 33: Flight plan scheme [Ref. (1)]	38
Figure 34: Crab angle representation [Ref. (1)].....	39
Figure 35: FASTER planning software block diagram	40
Figure 36: Google Earth geobrowser GUI.....	42
Figure 37: Google Earth SRTM DEM implementation.....	42
Figure 38: Example of polygon surrounding the Forlì Ridolfi Airport	44
Figure 39: Imported KMZ in the Matlab environment	45
Figure 40: UTM System [Ref. (27)]	47
Figure 41: Ridolfi-area.kmz converted in UTM coordinates.....	48
Figure 42: Example of plotting: target area, surrounding square area, DEM area	50
Figure 43: DEM extraction from the ASTER database, tile ASTGTM44N011E	50
Figure 44: FASTER flight planner - computed flight height [m]	51
Figure 45: Standard 45/180 procedure turn [Ref. (3)]	52
Figure 46: Planned trajectory	53
Figure 47: <i>FASTER_planner.m</i> script output.....	54
Figure 48: Particular of the target area	54
Figure 49: Planned trajectory exported in a KML file and visualized inside Google Earth	55
Figure 50: Airborne internal management and computing system functional layout.....	59
Figure 51: FASTER EM Hardware Layout	61
Figure 52: Advantech 3353 PC104+ board and mechanical drawing [Ref. (4)]	62
Figure 53: Garmin GPS 18x 5Hz and its mechanical drawing [Ref. (5)]	63
Figure 54: Crossbow NAV420 and its mechanical drawing [Ref. (6)]	64
Figure 55: VIA EPIA EN15000 board and mechanical drawing [Ref. (7)]	65
Figure 56: Litemax 8.4" high brightness LCD display and its mechanical drawing [Ref. (11)].....	66

List of Figures

Figure 57: Canon EOS 450 and Canon EF28 f/2.8 [Re. (12)].....	66
Figure 58: Canon EOS 450D fixed in the rapid prototyping base; lens focus ring has been blocked to avoid ring movements during flight.....	67
Figure 59: M2-ATX-140W power supply [Ref. (14)] (a) and the DC-DC converter used to power the camera (b)	69
Figure 60: Tecnam P92 selected mounting area for the external POD.....	71
Figure 61: Canopy section	72
Figure 62: Canopy lower side features	72
Figure 63: FASTER EM fiberglass canopy installed on Tecnam P92 passenger side	73
Figure 64: FASTER airborne internal and computing unit front panel.....	74
Figure 65: FASTER airborne internal and computing unit installed onboard the Tecnam P92	74
Figure 66: FASTER airborne internal and computing unit inside view of the rack box ...	75
Figure 67: FASTER EM Simulink model	77
Figure 68: Garmin GPS 18 5Hz acquisition block sheme	80
Figure 69: Crossbow NAV420 acquisition block scheme.....	84
Figure 70: Magnetometer acquisition block scheme	85
Figure 71: Camera shot signal generation	87
Figure 72: Canon EOS 450 remote connections panel	87
Figure 73: Canon EOS 450D Management Block Scheme.....	88
Figure 74: Tunnel in the sky management block scheme.....	90
Figure 75: Virtual Tunnel block scheme	92
Figure 76:Datalog block scheme	93
Figure 77: FASTER status monitor block scheme	94
Figure 78: FASTER Acquisition Display	95
Figure 79: Pilot visual interface inside the Tecnam P92 cockpit.....	95
Figure 80: Guidance tunnel ver. 1.....	96
Figure 81: Guidance tunnel updated version	97
Figure 82:Guidance tunnel interface provided with interactive buttons.....	98
Figure 83: Camera control center screenshot.....	99
Figure 84: FASTER CIL layout.....	103
Figure 85: FASTER HIL layout	104
Figure 86: Simulation of the third flight campaign (Brisighella area) using the HIL setup	105

List of Figures

Figure 87: Brisighella area, planned vs HIL simulated trajectory	106
Figure 88: Brisighella area, distance between planned and HIL simulated trajectories, whole flight	107
Figure 89: Brisighella area, HIL simulated altitude profile vs planned, whole flight	107
Figure 90: C-shaped bracket used to install the external POD on the passenger side of the P92 fuselage	108
Figure 91: FASTER EM LCD monitor mounted on the metal support.....	109
Figure 92:FASTER external POD installed on the Tecnam P92.....	109
Figure 93: First flight campaign trajectory	110
Figure 94: First flight campaign, planned vs flown trajectory.....	111
Figure 95: First flight campaign, initial part of planned vs flown trajectory.....	112
Figure 96: First flight campaign, distance between planned and flown trajectories	112
Figure 97: First flight campaign, planned vs flown altitude	113
Figure 98: First flight campaign, high resolution Google Earth layer created from an acquired image	114
Figure 99:Second flight campaign, circuit over Verginese airfield.....	115
Figure 100:Second flight campaign, planned vs flown trajectory	115
Figure 101:Second flight campaign, Pilot training system.....	116
Figure 102: Second flight campaign, selected waypoints of the flown trajectory used to compute the distance from the planned trajectory	117
Figure 103: Second flight campaign, distance between planned and flown trajectory ...	117
Figure 104: Second flight campaign, planned vs flown altitude	118
Figure 105: Second flight campaign, Google Earth layer created from an acquired image	118
Figure 106: Brisighella target area.....	119
Figure 107:Third flight campaign, planned vs flown trajectories.....	120
Figure 108: Third flight campaign, distance between planned and flown trajectories....	120
Figure 109: Third flight campaign, planned vs flight altitude	121
Figure 110: Third flight campaign, distance between planned and flown trajectories, 1 st stripe.....	121
Figure 111: Brisighella mosaic, cropped image	122
Figure 112: Third flight campaign, Brisighella mosaic	123
Figure 113: Geographical to UTM coordinates conversion, geometrical problem	127

List of Tables

Table 1: LCCES Microbolometer specifications.....	13
Table 2: FASTER system requirements	29
Table 3:FASTER final model vs Engineering Model characteristics.....	36
Table 4: Datum	48
Table 5: <i>FASTER_planner.m</i> computed flight parameters	55
Table 6: FASTER functional requirements and some notes on their implementation on EM model.....	58
Table 7: Crossbow NAV420 measurement accuracy	64
Table 8: M2-ATX-140W maximum power characteristics	68
Table 9:FASTER EM measured power consumption	69
Table 10: GPGGA sentence structiure.....	79
Table 11: GPVTG sentence structiure	79
Table 12: GPRMC sentence structiure	79
Table 13: GPTMV sentence structiure	79
Table 14: NAV420 Angle Mode Packet list	82
Table 15: NAV420 BIT message definition	83
Table 16:Log file structure.....	93

Chapter 1. Introduction

Since 2003, the Microsatellite Laboratory of II Faculty of Engineering of the University of Bologna has been involved in the design and realization of small satellite missions based on the ALMASat multipurpose platform. After the realization of the first microsatellite, ALMASat-1, it is currently under development a second Earth observation mission, named ALMASat-EO. Goal of this second mission is the acquisition of mid-resolution Earth images (in the visible band) of the Italian territory.

Besides the modification of the original ALMASat-1 bus, an entirely new optical payload has to be assembled to achieve all mission requirements. The AMSC is a novel concept of digital multispectral camera, based on the use of an LCD tunable filter instead of a traditional filter wheel. This payload implies the use of new electronic architectures that must ensure sufficient computational power to enable onboard image processing (image compression and geographical tagging). Effect of all these new features is a longer development phase and the need of specific tests necessary to reach an high reliability level, compatible with typical space operations.

In order to perform both functional and radiometric tests, in an environment similar to that in which the AMSC will operate, an aerial platform will be used. This solution, that has several advantages, because of its complexity resulted in a completely independent project, with more specific requirements compared to being just a test bed for ALMASat-EO sensor.

FASTER stands for *Fully Automated SysTem for Environmental monitoRing* and this acronym resumes the enhanced functionality given to the original test platform. The project is jointly carried out together with the Flight Mechanics Laboratory of the II Faculty of Engineering. Aim of the project is the realization of a compact, direct georeferencing system capable to acquire very high resolution images in different bands of the electromagnetic spectrum suitable to be mounted on very light aircraft platforms. One of the most challenging objective to achieve is make a system which is independent

from the airplane (without fuselage modifications or the need of specific navigation instruments) in which is installed. Thus it will be possible to move the system from an airplane to another without affecting performances.

This work is organized as follows: in *Chapter 2* background experiences are presented introducing how the idea to realize such a system was conceived. Past activities, like the development of the ALMASat-EO Multispectral Camera, permitted to acquire important skills in the field of digital sensor electronics and optical design. Skills that have been consolidated during the STARS and LCCES projects which involved the use of high frame rate and Thermal Infrared sensors, jointly with the development of image processing algorithms.

Chapter 3 describes the state of the art technologies currently used in remote sensing and photogrammetric devices. In this section a survey on existing instruments is presented ranging from aerial to satellite platform, highlighting pros and cons of each solution. Field applications are investigated too, trying to identify in which direction research is moving and what are the most interesting innovation that are coming in the future.

In *Chapter 4* the FASTER system is discussed. FASTER is a remote sensing instrument specifically designed to be installed on board ULAs. Goal of the project is the realization of a compact and inexpensive autonomous system that can be mounted on the aircraft without the need of further modifications. The hardware layout and three dimensional models of the various parts of the system are shown. The proposed final configuration utilizes three cameras working in the visible spectrum two of which are tilted in the cross-track direction of 15° in order to obtain a larger swath width on the ground. This optimizes the elapsed mission time with respect to single camera configuration. The third camera is equipped with a nIR filter which that allow the extraction of the NDVI index, useful to monitor the vegetation status.

Photogrammetric or remote sensing aerial campaigns must be carefully planned before execution so a flight planner software has been developed to support the aerial platform. The planning software and its implementation in the Matlab environment is presented on *Chapter 5* showing already planned missions examples.

An engineering model of the FASTER system has been realized, with reduced capabilities, in order to start a complete test campaign on the instrument. The FASTER EM is discussed in *Chapter 6*, presenting the hardware list and the management software which has been expressly realized. Here is also shown the pilot guidance interface

indispensable when using aircraft without navigation instruments. The interface monitors system status and offers the same information normally provided by a multi function display installed onboard commercial aviation aircrafts.

The FASTER EM has been tested during three flight campaigns and their results are reported in *Chapter 7*. These early test campaigns were essentially a series of functional tests that verified the correct data exchange between different subsystem. Attention was paid in the tuning of the guidance tunnel which required major changes in order to be completely usable by the pilot. During the last flight campaign over a thousand images were acquired and they have been used to test preliminary mosaicing algorithms.

In the final Chapter, conclusions and future work are discussed. The FASTER project, despite the work already done, is still in an early development stage. Future plans involve a new set of test campaigns to determine the georeferencing accuracy of the system and the installation of second camera for terrain direct three dimensional reconstruction. In fact an accurate high resolution 3D terrain model assures better results during the orthorectification process.

Chapter 2. Background

In this Chapter a brief description of all the preparatory activities carried out during the three years PhD course is reported, emphasizing those that led to the definition of the subject of this work.

In Section 2.1 the AMSC project is discussed in detail; this study allowed to deepen themes such as the development of optical systems for remote sensing purposes. Digital sensor technologies, their electronic integration and optical layouting using CAO (Computer Aided Optics) software are only part of the background knowledge acquired in the course of this work. The AMSC project aimed to the development of a digital multispectral camera equipped with an innovative tunable LCD filter ended with the need to find a suitable platform to carry out functional tests on the prototype model, because of the inherent difficulties in reproducing the same operational conditions.

Sections 2.2 and 2.3 describe two projects directly related to the previous one because they are possible candidates for an image based attitude determination sensor that will be utilized onboard the ALMASat-EO mission. STARS is a very accurate three axial standalone attitude determination sensor that processes Earth image sequences in the visible spectrum. STARS involves the use of an high frame rate detector which is significantly different from that used on the AMSC and many image process algorithms must be run in real time mode. LCCES is also an Earth sensor but working in the Thermal Infrared spectrum. This project has much in common with both STARS and AMSC because of the use of an image based sensing device and the development of custom optics. This study is built around a new detector type, the uncooled microbolometer, which allows the development of small size and low power systems without substantial performances loss. Optics are also characterized by the use of Germanium lens which have its own transmission window in the TIR spectrum.

All these experiences led to the idea to develop a common test bed capable to replicate all the functions that will be available on the ALMASat-EO microsatellite in an operational environment different from a standard laboratory equipment.

The idea has subsequently evolved in a more generic and expandable aerial platform, not only a test bed, able to manage remote sensing instrumentations and equipped with attitude and positioning sensors for high accuracy data georeferencing. The FASTER system, that will be described in the following Chapters, aggregates all the results obtained with the previous projects in a unique system that has diversified applications.

2.1 AMSC

The AMSC (ALMASat MultiSpectral Camera) is a spaceborne camera that will fly onboard ALMASat-EO, the second microsatellite of the University of Bologna. The idea was to extend the capabilities of the ALMASat-1 standard bus in order to achieve Earth observation capabilities, to do this a completely new device has to be developed. The development of the optical payload for an Earth observation microsatellite mission is always difficult due to the high number of constraints that have to be considered when dealing with the reduced dimensions and low-power available on the spacecraft. As a matter of fact, most of the widely available systems presently used to acquire Earth images, as *pushbroom* or *wiskhbroom* scanners, cannot be used onboard a microsatellite mainly because of the high power and data rate they require.

On the other hand, a common *still camera* with no moving parts and a *discrete* mode of operation instead of a *continuous* one (scanner), seems to be the right choice in order to reduce power consumption and complexity of the system; in particular, the main advantage of this system is that the linear sensor is replaced by a two-dimensional one able to acquire instantaneously an entire scene, thus preserving the correct geometry and reducing the number of frames necessary to acquire the target area. Moreover, a low frame rate allows the use of a *Full Frame CCD* ensuring the highest resolution. The camera has been designed in order to fit the available space dedicated to the payload, onboard the ALMASat-EO spacecraft bus, which consists in an additional cube (300x300x300 mm) placed in the lower part of the original ALMASat-1 bus.

In the first phase, major efforts were devoted to the definition of the system requirements and the selection of suitable enabling technologies which could allow the use of imaging Earth sensors on board an Earth orbiting spacecraft. The type of sensor

that best fits the implementation of a system for the acquisition of satellite images is a CCD (although CMOS based devices are currently the best choice in order to reduce power consumption). This stems mainly from the high sensitivity of silicon at wavelengths of less than $1.1 \mu\text{m}$, ideal if one is interested in capturing images in the visible spectrum ($0.4\text{-}0.7 \mu\text{m}$) or nIR (near infrared).

Among all manufacturers taken into consideration, the selected device is a DALSA FTF 2020M which is a squared full frame CCD with 2048×2048 pixels ($12 \mu\text{m}$ side) with 100% optical fill factor and a considerably high dynamic range (which represents an equivalent measure for the contrast the device is able to achieve). As stated by the final M in the product code the sensor is monochrome with no reported Bayern filter in front of the sensible area.

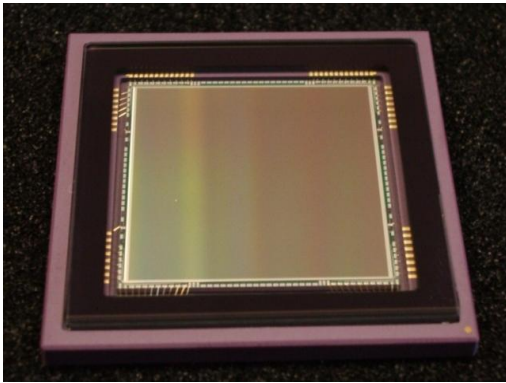


Figure 1: Dalsa FTF2020M sensor



Figure 2: Dalsa demoboard with FTF2020M sensor support

Typically, in digital still cameras, multispectral capabilities are achieved by using mechanical wheels that rotate optical filters in front of the sensor. To avoid moving parts inside the instrument, which could compromise the success of the entire mission, a LCD continuous tuneable filter will be placed in-between the sensor and the optics, to provide better multispectral capabilities than the mechanical wheel. Multispectral images will be generated overlapping single band images and creating arrays with a maximum of 10 spectral bands. The time the filter takes to switch between one wavelength to another is typically 50 to 150 ms depending on the value of λ . AMSC will be one of the first spaceborne instrument based on the use of a tunable filter.

CRI (Cambridge Research Inc, manufacturer of the filter) has already tested the correct operation of the filter in vacuum conditions; it was found that the filter did not experience mechanical damages or deformations during the test and that the optical

tuning error is consistent with the one measured prior to the test. One of the main issues connected to the use of this kind of filter is the need of custom-designed optics instead of a commercial one; this is due to the filter causing a variation of the *B.F.L.* (*Back Focal Length*) which, in turn, results in a shift of the focus of the system. The filter has an aperture of 35 mm, thus matching the dimensions of the CCD (main diagonal of 34.76 mm) and the wavelength can be varied between 400 and 720 nm (in the *visible spectrum*) with steps of 20 nm.

The number of bands and the value of the acquired wavelengths can be selected (both after launch, and during the whole mission lifetime) by storing appropriate palette onboard. This allows a flexible use of the instrument and enables a rapid response on specific targets, especially during disaster monitoring or for environmental and agricultural purposes.

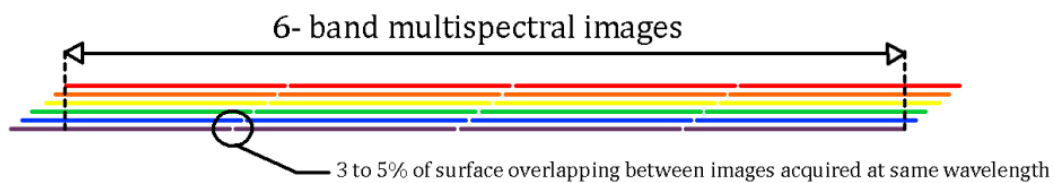


Figure 3: Acquisition method, e.g 6 bands image

Diffraction optics have been designed (starting from a telephoto layout with a ratio of 0.9) in order to correct the 6 cm shift of the focal plane due to the filter housing, with a fixed focal length of 200 mm; five lenses are divided into two main groups and then inserted in a titanium case which will provide the necessary stiffness during the launch phase, and avoid misalignments between each lens.

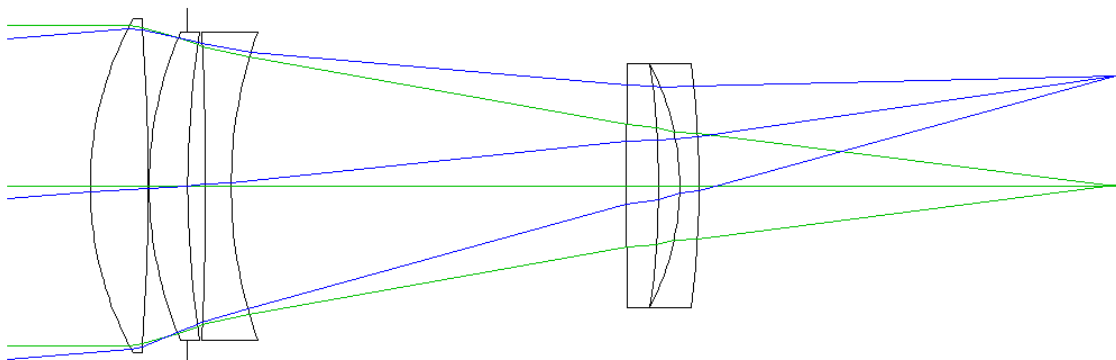


Figure 4: E.F.L = 200 mm, Telephoto Ratio = 0.9, Overall Length = 180 mm, F/# = 4, B.F.L = 60 mm

Background

A complete set of analysis has been done on the selected optical layout in order to determine the expected performances of the lens in terms of both distortion and MTF as shown in the following figures.

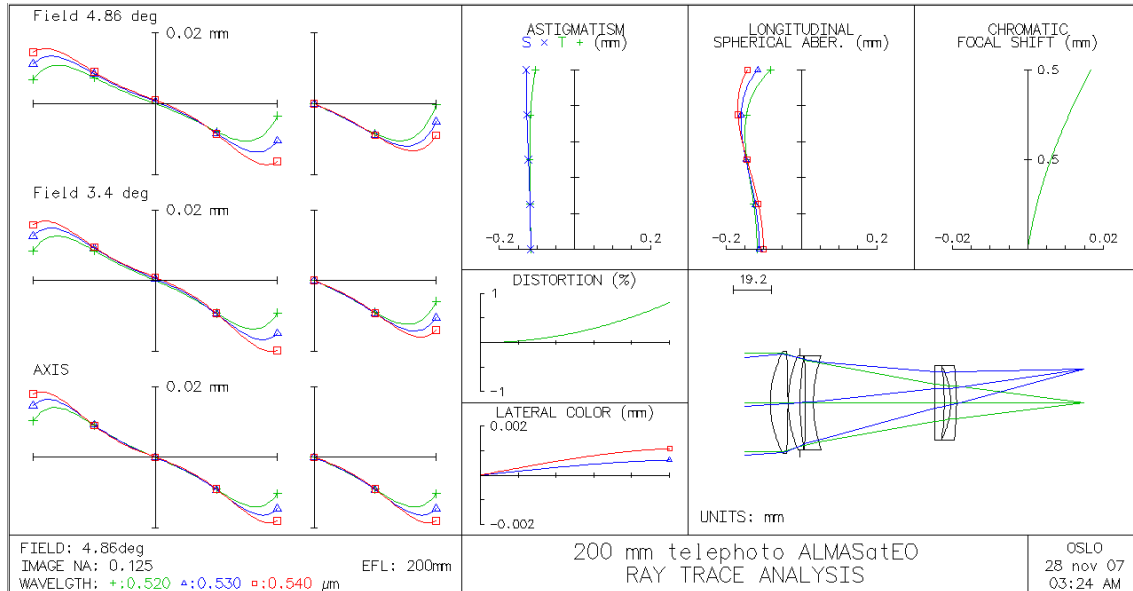


Figure 5: AMSC standard ray tracing analysis

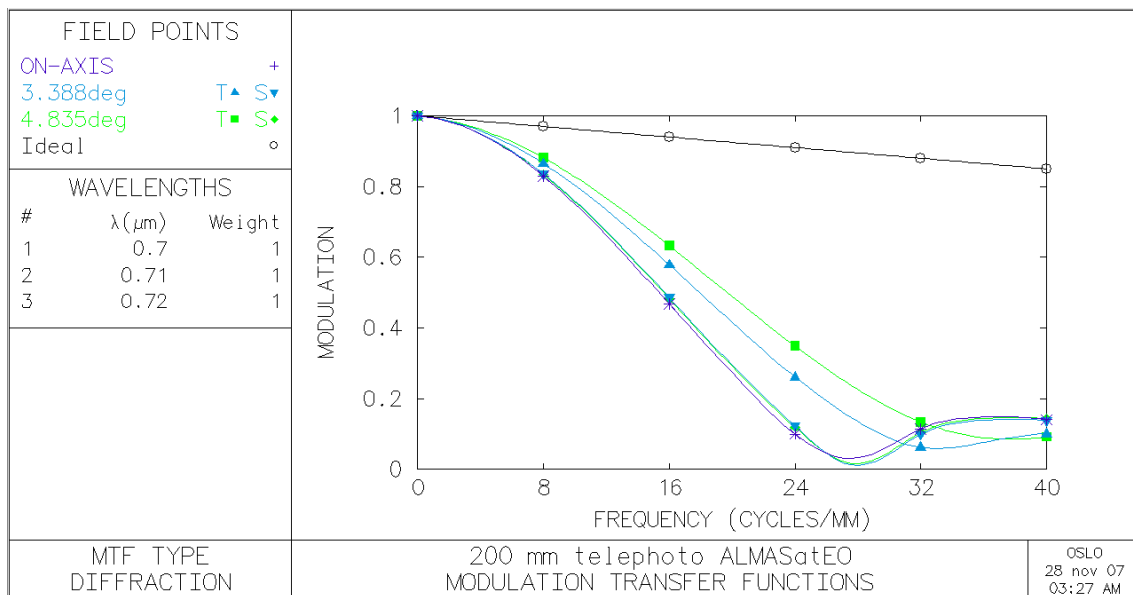


Figure 6: AMSC plotting of the MTF (b)

Lens will be custom built by a specialized manufacturer (currently Gestione SILO is the selected company) and after the production phase a final test campaign on the flight model will be carried out. AMSC optics will be tested using a small optical bench (QC Bench made by Optikos) that will be helpful to determine the real performances of the

system. The optical bench is currently used to test performances of the wide angle CCTV lens of the ALMASat-1 sun sensors. Procedures has been developed to retrieve the exact distortion function of optical system.

In the following pictures some examples of the spot shape on the optical axis (a), at 30° of hFOV (b) and near the full field (c) of the 130° wide angle lens.

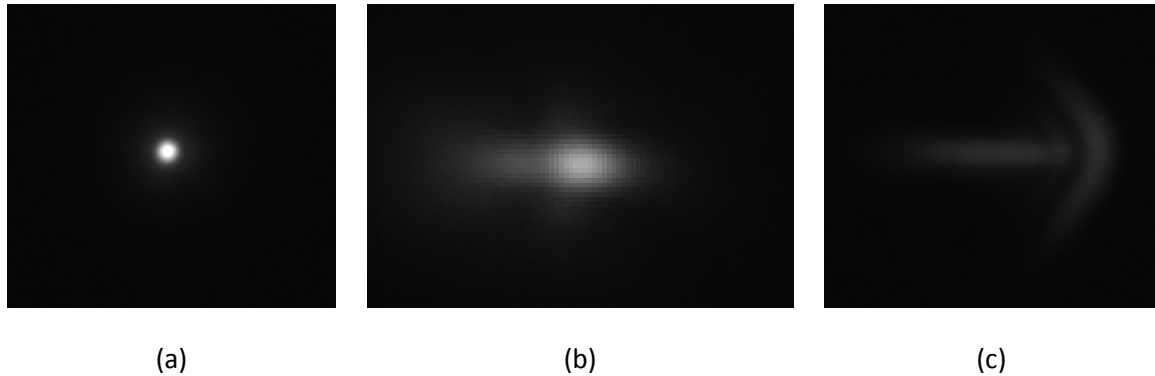


Figure 7: Spot shape of the ALMASat-1 Sun Sensor wide angle lens used as test bed for the development of the calibration procedures for the AMSC

The camera electronics is currently under development and a preliminary layout is shown in Figure 8. The CCD will be controlled by a flexible FPGA (currently under test a Xilinx Virtex 5) that can be customized to use a variety of different sensors. The filter will be connected to a proprietary box linked to the FPGA via RS-232 interface. The entire system will be managed by a platform based on an ARM7 microprocessor able to store images in a commercial flash memory drive and also send data via CAN BUS to the S-band transmitter. Each image acquired by the sensor is currently in the order of 50 Mbit for a single band image, thus the use of an appropriate compression algorithm is necessary. One of the most flexible algorithms that can be used on-board to reduce the image dimensions is the JPEG2000, the new international standard for image data compression which uses latest compression techniques based on wavelet technology.

The JPEG2000 provides for both lossless or lossy compression in the same architecture with different compression ratios. Compression ratios usually vary between 2:1 in lossless mode to 15:1 in lossy mode with unnoticeable artefacts, allowing further use of the images for analysis.

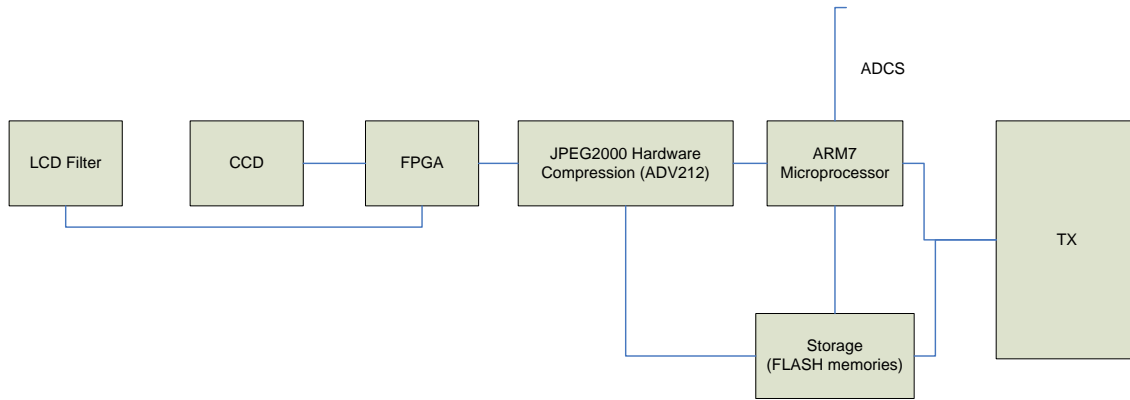


Figure 8: Electronics Layout Block Diagram

The result is a 50 Mbit image reduced down to 3 Mbit. JPEG2000 also provides quality features like region of interest coding (ROI) and different types of progressive transmission. The AMSC will guarantee a ground resolution of about 40 m from an altitude of 720 km.

2.2 STARS

In the framework of the project internally funded by the University of Bologna, named STARS - *Standalone Three-Axis spacecraft oRientation Sensor*, a team composed by two separate departments, DIEM and DEIS, investigated the feasibility of a novel standalone spacecraft attitude sensor, capable of estimating the full three-axis orientation of an Earth-orbiting satellite. The underlying idea is that by capturing from space a sequence of images of the Earth surface (in the visible bands) and elaborating them in pairs through feature extraction, feature matching, homography estimation and finally attitude estimation.

The following project steps have been carried out: selection of enabling technologies, definition of the attitude determination algorithm, numerical simulations followed by an acquisition campaign on a experimental test-bed.

In the early phase the selection of suitable enabling technologies was performed in order to allow the use of imaging Earth sensors as standalone attitude sensing hardware on board an Earth orbiting spacecraft, then the attitude determination algorithm was selected. To do this a dedicated simulation environment was developed and its structure is shown on Figure 9. Inside the Microsatellite Laboratory a Matlab/Simulink model was generated to simulate a spacecraft orbit, giving the instantaneous position (altitude, latitude and longitude) and orientation (in form of quaternions).

Background

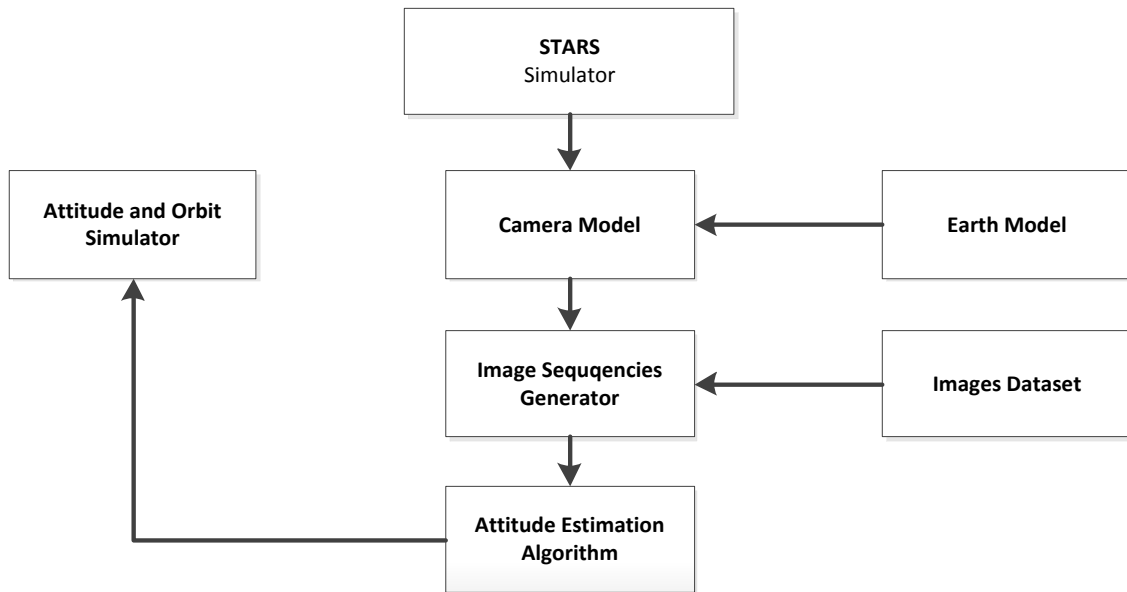


Figure 9: STARS simulation environment diagram

The output of the model was used as a reference to test the image processing algorithms employed to retrieve the spacecraft attitude from Earth image pairs. Synthetic Earth images were extracted from the Landsat 7 database that has a global coverage and it is based on visible panchromatic frames with 15 *m* of ground sampling distance. Most of the effort of the simulation part was spent to determine what type (and their magnitude) of errors were involved in the entire process.



Figure 10: STARS laboratory test-bed

In particular the work that has been carried out at the II Faculty of Engineering is relative to the realization of a test-bed capable of test on really acquired images the algorithm previously selected.

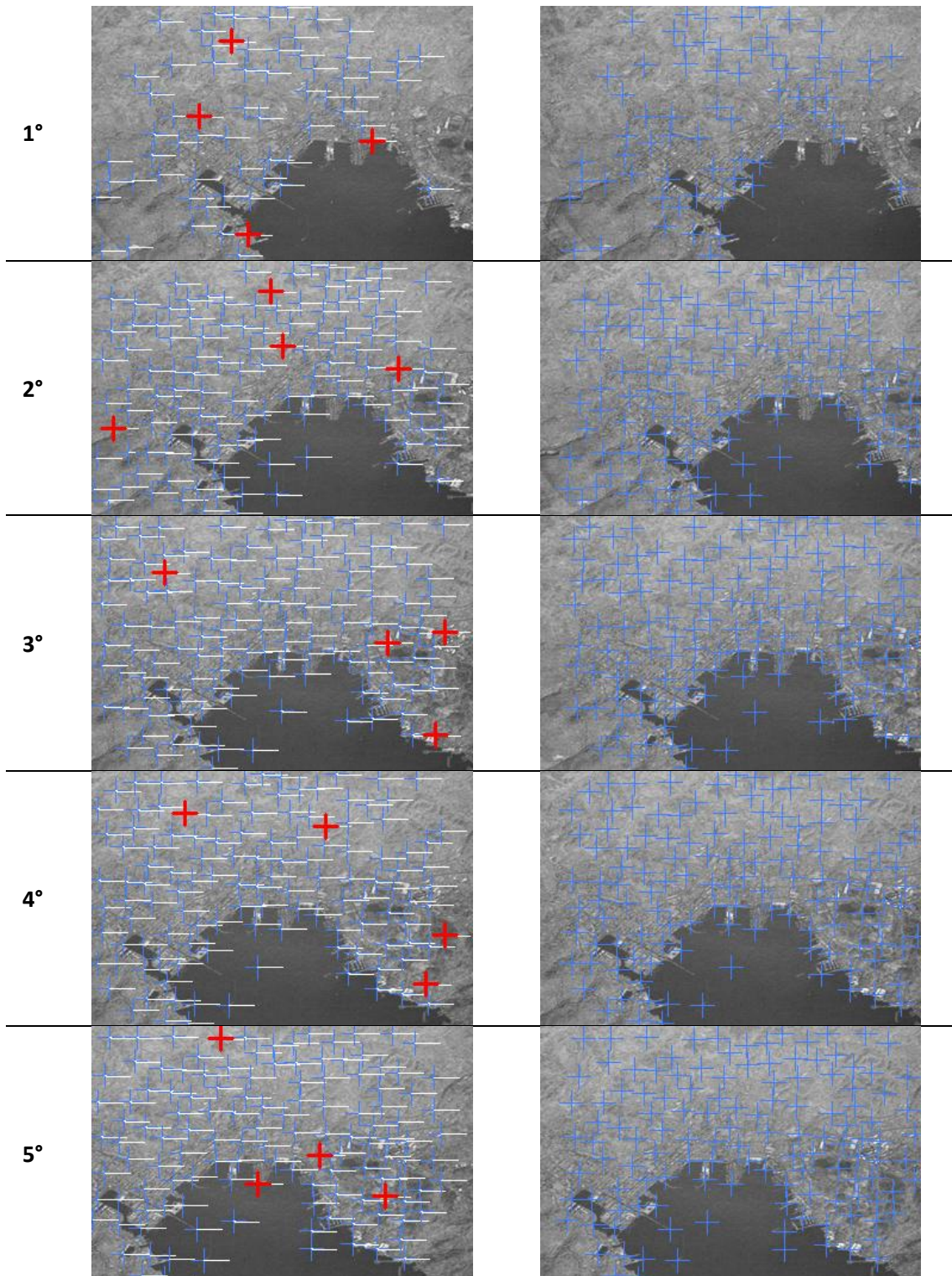


Figure 11: Experimental results on printed target (from 0 to 5° rotation along z-axis)

Test-bed is made up of three main components: a DSLR camera (Digital Single Lens Reflex) which simulate the STARS sensing device, a referenced AI platform equipped with a fine pointing rotating device controlled via an RS232 serial interface and a target image. The same Landsat 7 image used for numerical simulations, was printed and used as a target for a 1 DOF platform. Preliminary results showed that the algorithm was able to work also with real images (affected by high noise level due to printing characteristics) with reduced performances and an accuracy of about 100 arcseconds (0.02°) on the controlled angle was achieved [Ref (1)].

2.3 LCCES

The objective of this study was to investigate the possibility to develop a Low Cost Coarse Earth Sensor suitable for LEO and GEO orbits and to be used either as a stand-alone sensor or as temporary back-up for more accurate attitude sensor like star trackers. A sensor like the LCCES will be a potential candidate for the ALMASat-EO mission because of its capability of functioning also during eclipse; the LCCES will guarantee a coarse attitude determination when sun sensors aren't functioning in order to avoid long re-aligning maneuvers when passing from eclipse to daylight during orbiting. Thanks to the experience acquired with the AMSC the LCCES is based on an uncooled thermal detector, an area scan microbolometer made by ULIS, with 384×288 pixels ($25 \mu\text{m}$ pitch) designed for high end applications (see Table 1).

This device is not space qualified, but is compliant to the standard MIL-STD 810F and MIL-STD 883 and it has been selected as sensing device for the MERTIS spectral imager that will probably fly onboard the BepiColombo mission. Two preliminary optical layouts able to maintain the Earth disc inside the optical FOV were proposed.

Parameters	Values
Pixel dimension	$25 \mu\text{m} \times 25 \mu\text{m}$
Thermal time constant	3.8 to 9 ms
Optical fill factor	>80%
Spectral response	8-14 μm
Absorption	> 85%
Thermal coefficient resistance	> 2.2%/K
Resistance non uniformity	< 2%

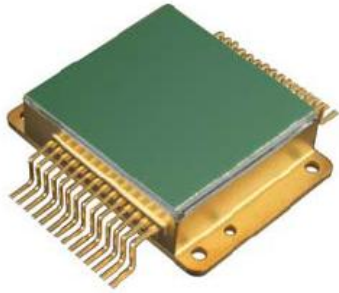


Table 1: LCCES Microbolometer specifications

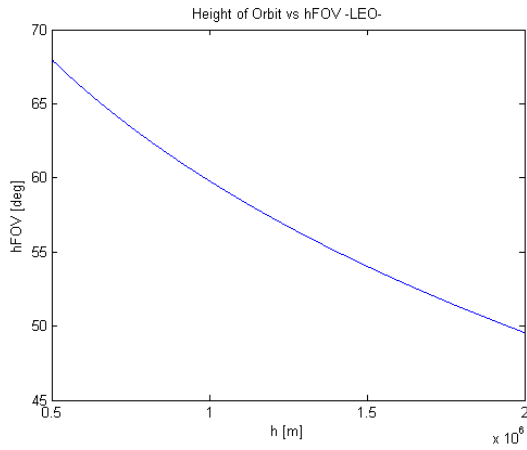


Figure 12: LEO Conditions

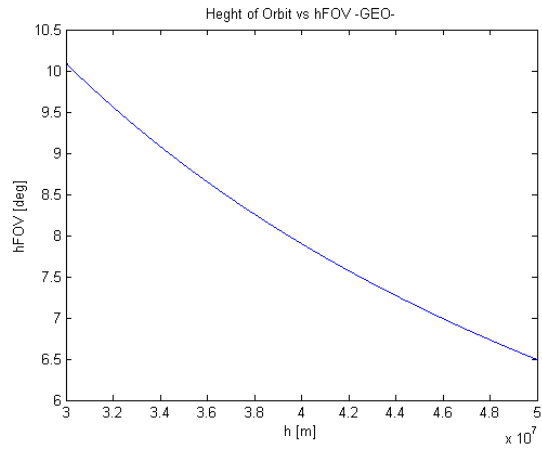


Figure 13: GEO conditions

Figures above refers to the *hFOV* (Half Field of View) and lead to a maximum full aperture of 136.04° for LEO conditions and 20.2° for GEO. In order to achieve these performances with a sufficient image quality, an all reflective systems (which not suffer chromatic aberrations) may not be an appropriate choice due to the optical obscuration of some configurations (Cassegrain) which becomes relevant at these wavelengths and mainly because of the their small FOV which can't satisfy LEO requirements. Another critical aspect is represented by the alignment of the system especially in case of off axis mirrors. A refractive system instead, can reach large FOVs maintaining an adequate image quality in term of optical aberrations and distortion due to the use of Germanium (with a refractive index $n=4$) for the thermal IR wavelengths (8-14 μm). This permit to achieve LEO requested values of FOV with a relative small amount of optical elements, as shown in the following figures.

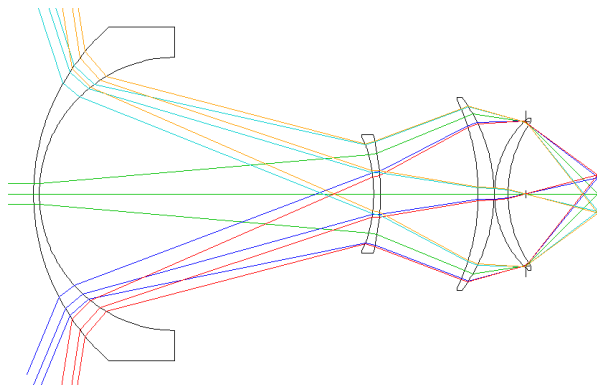


Figure 14: LCCES LEO optical layout

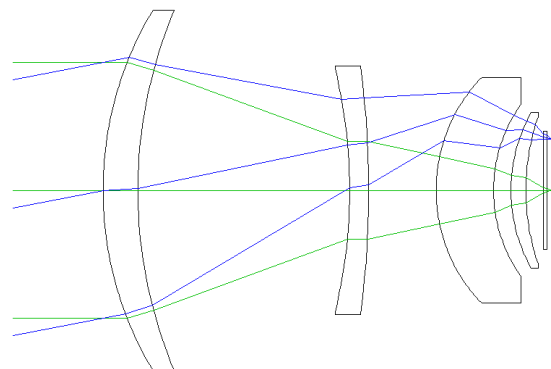


Figure 15: LCCES GEO optical layout

Each optical configuration has been preliminarily evaluated using a CAO (*Computer Aided Optics*) software, OSLO, finding the expected values of aberrations (1st, 3rd and 5th

Background

order), astigmatism, distortion, MTF and PSF as reported in the following diagrams. In this approach lens coating hasn't been taken into account although in a more refined layout optimization it's important to properly simulate its effects.

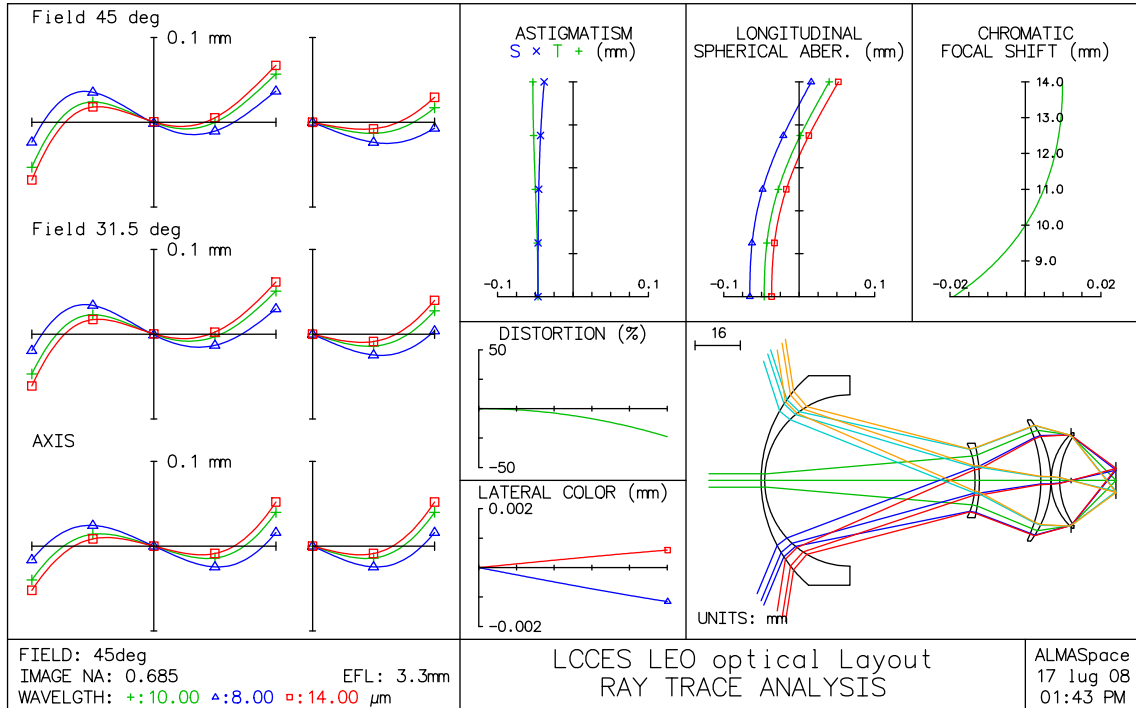


Figure 16: LCCES LEO optical configuration standard raytrace analysis

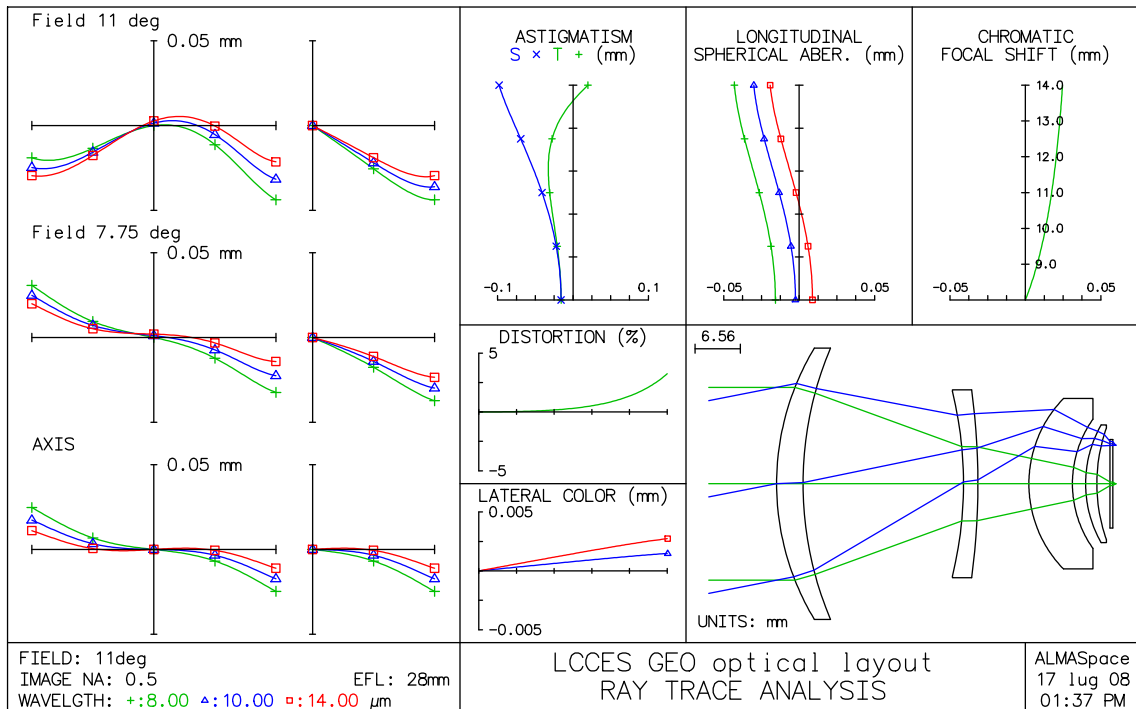


Figure 17: LCCES GEO optical configuration standard raytrace report

The preliminary layout of the ES housing consist of a common electronics box both for LEO and GEO sensor, in front of an interchangeable LEO and GEO optical head. Since LEO optical assembly dimensions are quite larger than GEO ones, the preliminary housing layout has been dimensioned upon LEO optical assembly. Traditional materials and production technologies shall be privileged thought the use of composites, in particular carbon-fiber, for the optical housing may grant better structural performances. Carbon-fiber optical housing could be a valid alternative to standard aluminum and shall be considered in case of high overall weight due to aluminum use.

The selected preliminary configuration provides a common electronics enclosure both for LEO and GEO sensor, in front of an interchangeable optical head. Thanks to this solution the electronic board is the same both for LEO (Figure 18) and GEO (Figure19) optics ensuring modularity and reliability. The bottom of the sensor act as interface with the spacecraft providing power and data connector(s) and an additional electronics bay for additional plug-in boards integration. Thus it is possible to increase sensor capabilities simply by adding compatible interface, data elaboration and data storage units inside the electronics bay.

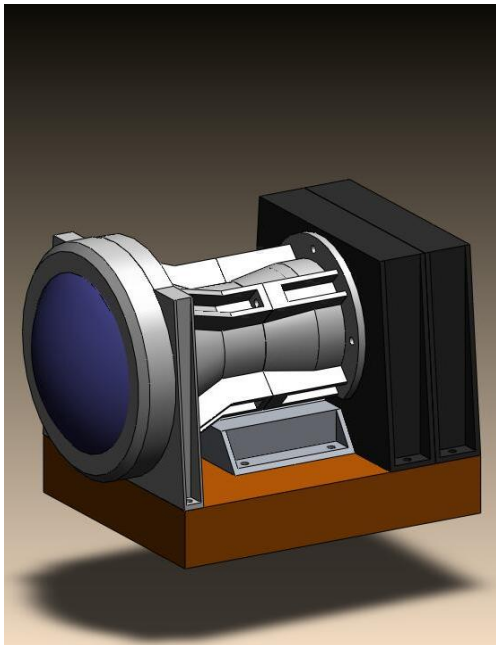


Figure 18: LEO configuration assembly

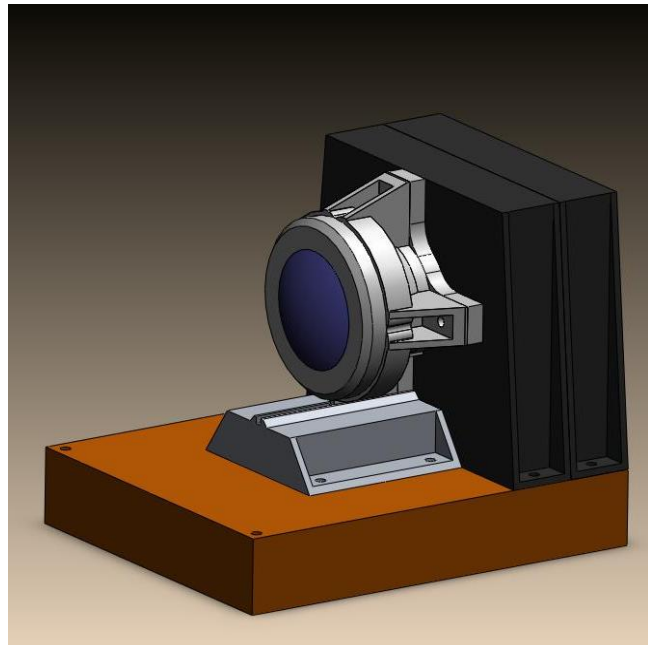


Figure19: GEO configuration assembly

Chapter 3. Remote Sensing and Photogrammetry, State of the Art Technologies

In this chapter a survey on the state of the technologies used in the field of remote sensing and photogrammetry is presented. Before introducing instruments and their performances, it is right and proper to clearly define what, today, remote sensing and photogrammetry are:

- “**Photogrammetry** is the art, science and technology of obtaining information about physical objects and the environment through process of recording, measuring and interpreting photographic images and patterns of recorded radiant electromagnetic energy and other phenomena.” (*Wolf and Dewitt, 2000*);
- “**Remote Sensing** is the science of measuring or inferring the physical properties of an object or medium, using a sensor that is at some distance from the object or medium. Typically, the term is used to describe measurements of electromagnetic radiation scattered or emitted from Earth’s atmosphere or surface using instruments on aircraft or satellites. A more general definition would also include measurements of other planets or moons in the solar system using interplanetary probes. The term Earth Observation is now also in widespread use, but its use is normally restricted to describing regional-to-global scale measurements from satellites. More recently, however, the Group on Earth Observation has broadened this term to include the collection, processing, modelling, and dissemination of data about the Earth system collected through in situ, airborne and space-based observations, using satellites, buoys, seismometers, and other devices.” (*Woodhouse, 2006*)

These two concepts are often merged together and can be seen as a part of a new, modern discipline, which integrates acquisition, modelling analysis, and management of

spatially referenced data (data could be remote sensed or retrieved through a photogrammetric process) named **Geomatics** [Ref. (2)]. It uses terrestrial, marine, airborne, and satellite-based sensors to acquire spatial and other data. It also includes the process of transforming spatially referenced data from different sources into common information systems with well defined accuracy characteristics. Geomatics applications areas include: the environment, land management and reform, urban and subdivision planning, infrastructure management, natural resource monitoring and development, coastal zone management and mapping, archaeological excavation and survey and disaster informatics for disaster risk reduction and response.

In the last twenty years, thanks to the development of digital sensors, one of the fields that had the strongest growth is that of high or very high resolution imagers both airborne and spaceborne. This type of instruments played a major role in the development of modern geographic information systems (*GIS*), constituting one of the main data source for land management and mapping; but also other applications, like precision farming or air pollution monitoring, can take serious advantages from increasing resolution. The new generation of Earth observation satellites are able to acquire image data at 0.4 m of ground resolution almost reaching the values obtained by aerial surveys.

In the following sections a review of the state of the art technologies used for airborne sensors is presented in order to better identify the subject of this work.

3.1 Airborne Sensors

In the last decade, digital photogrammetry has progressively replaced traditional aerial photography based on large format films, leading to a great reduction in size and cost of the instruments. One of the major benefits of digital photogrammetry is the elimination of degrading effects of film which improves the dynamic range of the images (thus the overall image quality). This means that image acquisition can be done under poorer illumination conditions than required for film increasing the number of acquisition per day and throughout the year, [Ref (3)]. Digitalized data is also easier to be managed allowing a faster post processing phase reducing the delivery time of the final product.

Available airborne sensors differs for technical realization, geometric, radiometric and spectral properties but also image formats vary greatly. These instruments typically have an high geometric performance level but recently there have been significant improvements regarding spectral and radiometric performances becoming usufeul also for

remote sensing applications. A possible classification of airborne sensors can be done based on the two principal architecture currently adopted [Ref. (4)]:

- Airborne digital cameras, that produce frame images;
- Airborne pushbroom line scanners, that produce continuous strip imagery of the terrain

3.1.1 Airborne Digital Cameras

Airborne digital cameras can be further subdivided into three specific categories:

- *Small format*, cameras equipped with sensors up to 16 Megapixels;
- *Medium format*, cameras equipped with sensors between 16 and 50 Megapixels;
- *Large format*, cameras with large sensors with more than 50 Megapixels.

Small format cameras are usually frame cameras equipped with CCD or CMOS two-dimensional arrays, monochrome or coupled with mosaic RGB filters to produce colour images or IR filters for false-colour images. An example of monochrome camera is the Carl Zeiss VOS 40 which uses an high speed, 4 Megapixels CCD area array and can be equipped with lens up to 500 mm of focal length. Colour camera are the most diffuse because they are based on consumer DSLR cameras aimed at the professional photography market. For airborne use they are fitted to anti-vibration mount together with an electronic unit that controls the timing and exposure of the image. In some cases a GPS and IMU units can be adopted to generate tilt data to help carry out the rectification of the images (Figure 20).



Figure 20: Carl Zeiss VOS 40 [Ref. (5)] and a DSLR Canon EOS 1D [Ref(6)]

Instead of using an RGB filter to achieve colour registration, cameras can also be equipped with three separate CCDs in conjunction with an optical beam splitter. This solution avoid the interpolation necessary using a Bayern filter enabling higher spectral performances. Systems made by Airborne Data System and Integrated Spectronics utilize this simultaneous method to acquire the Red, Green and Blue spectral bands.

The New Metric Camera made by the VTT research institute in Finland utilizes nine squared CCDs in its focal plane (pixel pitch 4 μm). The individual image produced by the CCDs array is approximately 10000 pixels (in the across-track direction) x 1600 pixels (in the along-track direction). This solution, called multiple arrays camera, is also used by the G2010 camera developed by Global Imaging Technologies but in this case each CCD is coupled with its lens while in NMC a single lens for entire set of detectors is used.

Another adopted technical solution is the use of multiple cameras put together in a unique assembly. The multiple camera approach can be used to acquire colour or false colour images; three to four monochrome cameras are coupled, with their optical axis parallel to one another and their shutter synchronized to operate simultaneously to cover the same target area. To produce the final image different spectral bands are fused together to generate a colour image. An example is the ADS Agri-View with four small format cameras acquiring the Red, Green, Blue and nIR bands.

Using multiple cameras it is possible to acquire oblique images like the the Track'Air MIDAS system which makes use of five Canon EOS 1D used to acquire one vertical and four oblique colour photos simultaneously. Oblique images produced by these systems are very useful in 3D building reconstruction because the camera is able to see vertical side of constructions.



Figure 21: ADS Agri-View multispectral camera [Ref. (7)] and Track'Air oblique MIDAS system [Ref. (8)]

Medium format cameras that are in current use have been modified from existing film cameras built by Hasselblad, Rollei, Mamiya and Contax with the film magazine replaced by a modern digital back. Digital backs have been developed by several companies like Phase One, Imacon and Jenoptik and most of these devices uses the biggest CCDs available on the market with up to 65 Megapixels.

The largest supplier of medium format airborne digital frame cameras are Applanix (a Trimble company) and Rollei. The Applanix product is the Digital Sensor System (*DSS*) which is available in three different models, from 16 to 39 Mpixels. The system is supplied with the Applanix POS/AV, which integrates an high grade IMU and a differential GPS receiver, and a crab angle remover to be fixed inside the aircraft. The DSS is also available in several multiple cameras configuration ranging from 2 to 4. Rollei Aerial Industrial Camera (*AIC*) and IGI DigiCAM are very similar to the DSS but they are not supplied with crab angle removers. Three-axis stabilized mounts are available for medium format cameras and are able to compensate for roll and pitch movements of $\pm 23^\circ$ and heading changes of $\pm 13^\circ$.

The Digital Modular Aerial Camera (*DiMAC*) is a multicamera solution composed by up to four cameras installed inside a cylindrical housing. Each camera is equipped with a 22 Megapixels CCD with a pixel pitch of 9 μm . One of the most important feature of this camera is its forward motion compensation (*FMC*) technology which shift the image plane of the sensor opposite to the motion direction with a proportional speed. The FMC permits a longer exposure time avoiding image blurring. The output image is given by the geometrical composition of the four single frames resulting in a 6500x8500 pixels photo. The swath width from an altitude of 2000 m is about 1500 m and the corresponding GSD (with 80 mm lenses) is 0.23 m.



Figure 22:Applanix DSS439 [Ref.(9)] and DiMAC Wide+ [Ref. (10)]

Large format cameras are typically sets of multiple medium-format cameras coupled together to form an integrated unit, notwithstanding some military devices, used for reconnaissance, employs very large CCD array (up to 100 Megapixels) which are available in very limited quantities. The resulting images or sub images are then rectified and stitched together to form a single, large format, digital monochromatic image.

The Vexcel UltraCam-Xp (*UC-Xp*) is composed by four in-line lens arrangement used in conjunction with multiple monochrome CCDs. Images are coloured using pan-sharpening technique using data from the four additional small format multispectral images that are collected simultaneously. UC-Xp generates panchromatic images of 17130 x 11310 pixels while multispectral (RGB + nIR) images are 5770 x 3770 pixels. GSD from an altitude of 500 m is about 2.9 cm.



Figure 23: Vexcel UltraCAM Xp [Ref. (11)] and the Intergraph DMC [Ref.(12)]

The Intergraph DMC is another example of large format camera. Inside an external rigid body are installed two separate lens groups. The first one is composed by four 120 mm lenses placed in the housing center, each camera uses a 7168x4096 pixels CCD with a pixel pitch of 12 μm . Cameras are slightly tilted in order to create a small overlapping zone between every frame. Acquired images are 13824x7680 pixels. Other four, small format cameras, equipped with wide angle lenses, are used to for the RGB + nIR bands, as in the UC-Xp. From an altitude of 2000 m the resulting swath width is about 2880 m

for panchromatic images and 2800 for multispectral data, while the achievable GSD is 0.19 m. In the following image, geometries of multicamera systems are reported.

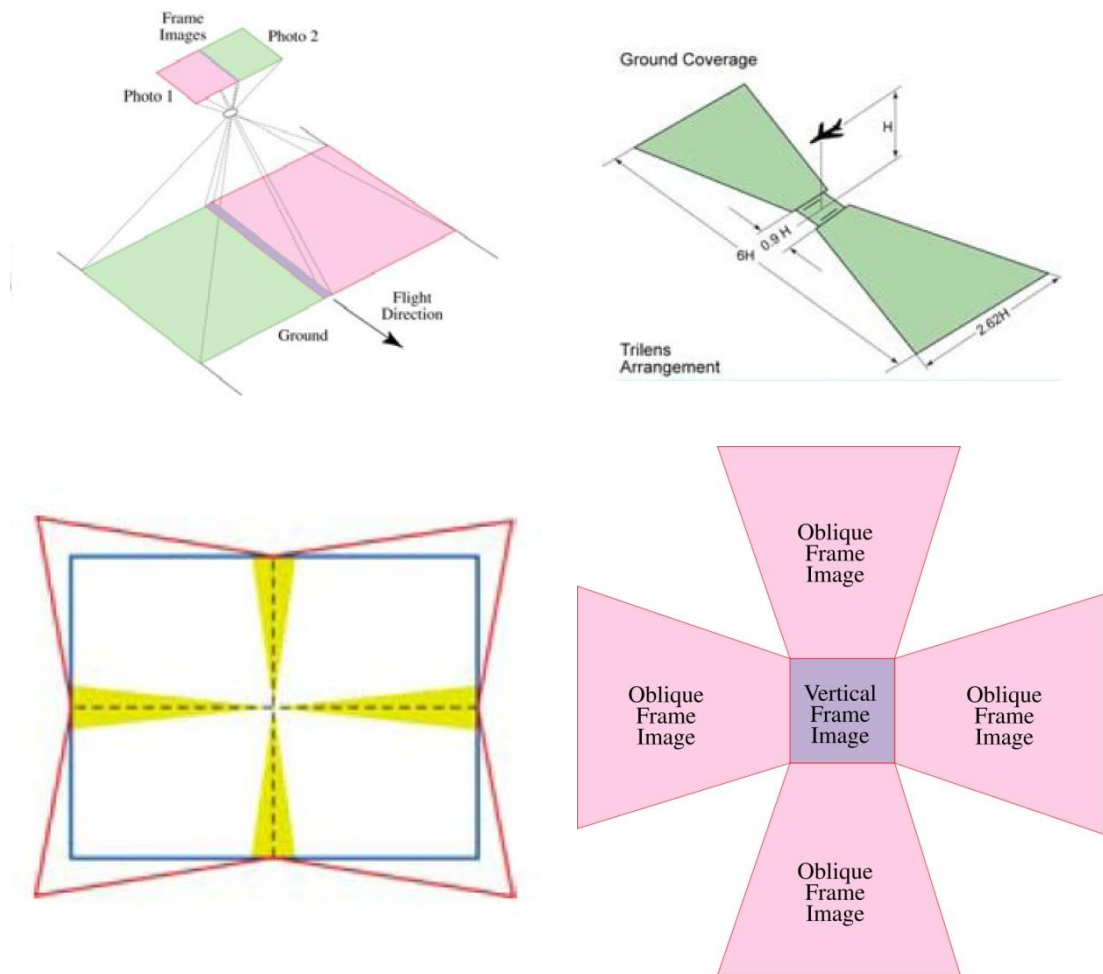


Figure 24: Multiple cameras system geometries [Ref. (4), (8)]

3.1.2 Airborne Pushbroom Line Scanners

There are two main groups of airborne pushbroom line scanners:

- *Simple monochrome scanners* equipped with a single CCD linear array producing a continuous strip image of the terrain and mainly used for military reconnaissance; *simple colour scanners* utilize a tri-linear CCDs which are $3 \times N$ arrays, in which different filter are reported for each line (R, G and B);
- *Three-line scanners* that generate overlapping forward-pointing, nadir-pointing and backward-pointing strip images that allow the production of three-dimensional stereo models, DEMs and ortho-images for mapping purposes.

The most diffuse airborne Pushbroom Line Scanner is the Leica ADS40. In this system each of the three lines consists of a pair of linear CCD arrays linked together in parallel, with each of the arrays being shifted laterally by half a pixel with respect to the other. In the same focal plane are mounted four additional single 12000 pixel linear CCD arrays that records the ground images in the individual RGB and nIR spectral bands. A beam splitter ensures that the radiation from the ground passing through the main lens of the ADS40 reaches the appropriate linear array. The ADS40 is supplied with a pneumatic stabilized mount and an high grade IMU and GPS receiver for direct georeferencing purposes [Ref. (13)].

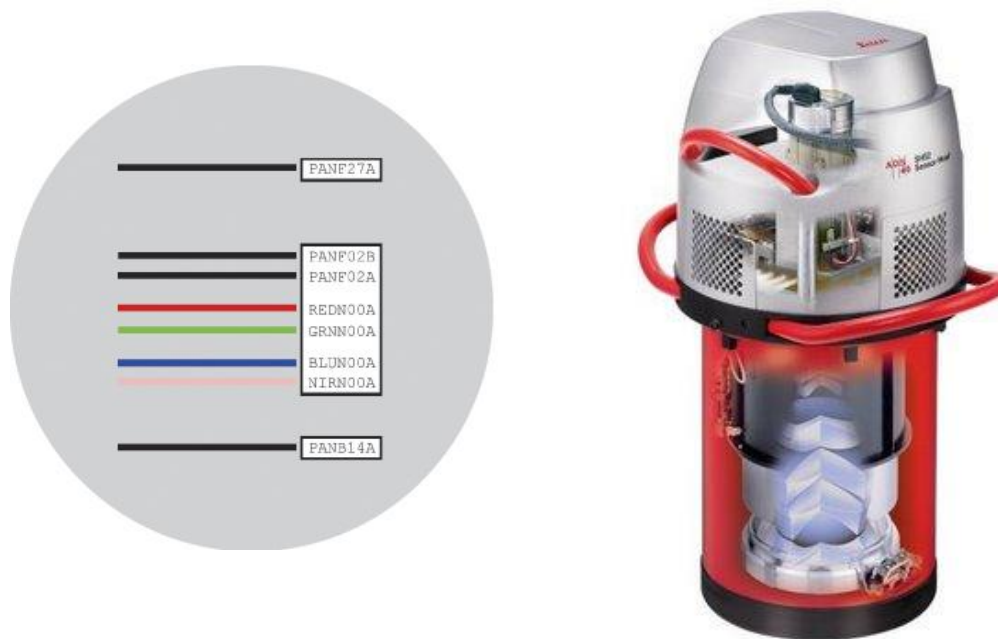


Figure 25: Leica ADS40 sensor head and assembly [

Chapter 4. FASTER

The review of the state of the art technologies presented in Chapter 3, allowed a better understanding of the major issues related to the photogrammetric field. In particular, it is clear that one of the most important innovations in this field was the introduction of the GPS and IMU sensors to determine, in a direct way, all parameters of the instrument external orientation¹. This solution is aimed at reducing the necessary number of ground control points always used in aerial triangulation (or resection), which is the process to retrieve the 6 external orientation parameters of the acquired images, without any other attitude or position sensors, using at least 3 ground control points for each image. Direct georeferencing systems, based on digital devices are also considerably less expensive than standard analogue systems and many steps of the photogrammetric production process can be skipped.

In this Chapter a fully digital, direct georeferencing system is proposed for both photogrammetric and remote sensing purposes. During the development, running costs have been considered so the result is a fully autonomous system, independent from the aerial platform, which is able to manage multiple acquisition instruments in order to achieve multispectral capabilities.

4.1 Underlying Idea

The project underlying idea was the development and realization of a direct georeferencing, photogrammetric system able to acquire high resolution images and fully independent from a specific aerial platform. Providing the system the possibility to be moved from an airplane to another, means that no further modifications have to be done to the aircraft structure, fuselage or avionic subsystem.

¹ The external, or extrinsic, parameters indeed, define location and orientation of the instrument reference frame with respect to the world frame, while internal, or intrinsic, parameters define pixel coordinates of image point with respect to coordinates in camera reference frame.

Very often, modified aircraft that can be equipped with photogrammetric instruments, are located in a limited number of airports and long transferring flights are needed to reach the area of interest. It often happens that the flight time required for the transfer equals that for the photogrammetric campaign. So if the instrument itself can be moved, these long transfer flights can be avoided and the nearest available aircraft to the operational area, can be used to perform the flight campaign reducing total costs.

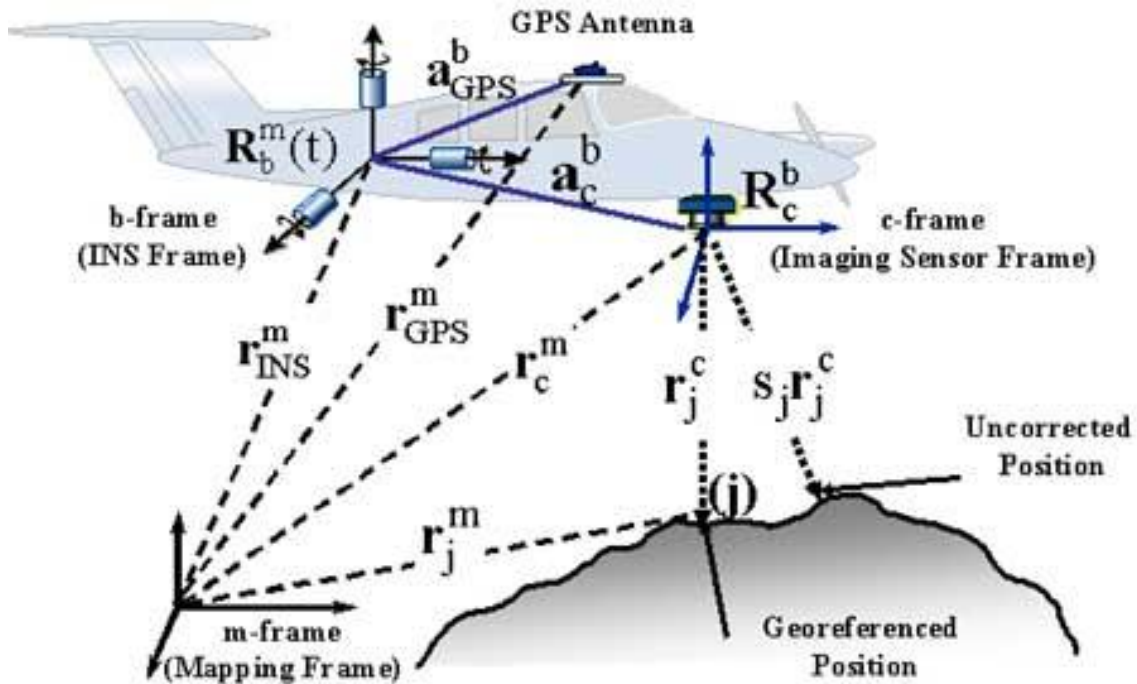


Figure 26: Direct Georeferencing System, reference frames [Ref. (3)]

Another important aspect that must be taken into account is the size of the area that has to be acquired. Large aircraft equipped with pushbroom line scanners are only suitable for very large land areas and cannot be used for a few square kilometers, but these are typical values for many applications like precision farming or coastal and urban monitoring.

During the development of the FASTER system two main objectives were pursued: the realization of a system which can be easily moved from an aircraft to another targeted for image acquisition on small areas.

4.2 Proposed Solution

Before proceeding to the realization phase a list of requirements, arising from the analysis of the state of the art technologies, was prepared and reported in the following Table. Each requirement has been commented to clarify how it could be implemented in the proposed solution.

Requirements		Comment
General Unit Requirements		
RE.G.01	FASTER shall be designed to be installed in a large variety of ULA and GA airplanes without any modifications to the a/c structure and avionics.	Several adapter will be studied to make the system compatible with different aircrafts aerodynamic configuration. For the purpose of this study only a support plate for high wing aircrafts will be developed.
Functional Requirements		
RE.F.01	The system shall have the capability to acquire high resolution Earth images over a large portion of the electromagnetic spectrum (ranging from visible to the thermal infrared interval, $0.3 \mu\text{m} < \lambda < 14 \mu\text{m}$)	In the FASTER system 2 colour CCD cameras and a third camera equipped with an nIR filter will be installed; onboard free space will be left where a microbolometer based TIR camera or a compact SWIR camera added later.
RE.F.02	The system shall be able to control and acquire more than one sensing device using different hardware interfaces	FASTER will use the GiGE Ethernet interface as a standard high data rate bus, USB will also be used to download images while RS232, 422, 485 will be available for camera timing and parameters setting.
RE.F.03	Given the target area, the system shall be able to generate an appropriate trajectory starting from the departure aerodrome to last selected waypoint	A planning tool will be developed to rapidly generate flight trajectories given departure and arrival airfield; the planning tool is discussed in Chapter 5.
RE.F.04	The system shall be able to guide the pilot through the previously planned flight	A visual guidance interface has been developed and presented in Section 6.6.
RE.F.05	The system shall be able to acquire images of the selected area only	Position information given by the GPS receiver will be compared to the target area coordinates and image acquisition will be automatically started in order to optimize data acquisition.

FASTER

RE.F.06	Images shall be acquired so that image mosaicing can be successfully accomplished during both real time processing or postprocessing operations	The planning tool will take into account the selected along track and cross track overlap percentage as stated in Section 5.4. For the purpose of this work mosaicing operations will be done in a postprocessing phase.
RE.F.07	Images and final mosaic shall be georeferenced during both real time or post-processing operations	Ancillary data to determine image external parameters will be acquired via the GPS receiver and the IMU. For the purpose of this work data will be saved in a flight log where each frame is referenced.
RE.F.08	The system shall be able to acquire a DEM of the target area in order to generate orthophotos	DEM extraction will be possible installing a stereo imager. At present DEM extraction feature will not be implemented, so existing DEMs will be used to generate orthophotos.
RE.F.09	All the acquired data must be stored in order to be available at a later time	FASTER will be equipped with Solid State Disks in order to store all the acquired images.
RE.F.10	The pilot shall be able to interact with the system in order to make any changes to the preloaded flight plan	Pilot interaction with the system will be possible through the guidance interface that has been provided with control buttons as stated in Section 6.6.
RE.F.11	The system shall have a totally independent power source	FASTER will have an independent power supply made up by a Pb battery.
Performance Requirements		
RE.P.01	The system shall ensure a GSD < 10 cm from the typical flight altitude of general aviation or very light aircrafts	Given the flight altitude a set of interchangeable lens can be used to keep the GSD below the 10 cm threshold; SWIR and TIR detectors will have a reduced GSD due to the bigger pixel pitch (25 to 30 μm)
RE.P.02	DEM resolution shall be in the same order of the GSD	Whereas DEM extraction is not implemented, the existing DEM used to generate the orthophoto will need to have a compatible resolution.
RE.P.03	The system shall guarantee blur free images in each particular flight condition	Although no Forward Motion Compensation will be implemented, the cameras pixel pitch (9 μm) has been selected in order to guarantee a short exposure time in order to avoid blur effects.
RE.P.04	Camera systems must be calibrated in order to correct distortion effects due to selected optical frontend	Each camera will be calibrated to retrieve internal orientation parameters via an image-processing based algorithm. Lens distortion polynomial coefficients are also determined by the same procedure.

FASTER

RE.P.05	Georeferencing accuracy shall be in the same order of the GSD	At present this requirement cannot be fulfilled, neither applying postprocessed GPS differential corrections. Further developments will be focused to make the system compliant.
RE.P.06	The system shall be able to guarantee a 3 fps acquisition	Selected cameras have a maximum frame rate of 5 fps allowing higher flight speed at equal along-track overlap percentage.
RE.P.07	The system shall be able to collect at least 20 GByte/hour	The system will be equipped with 3 256 Gbyte SSD disks allowing more than 3 hours of image acquisition at the maximum frame rate.
RE.P.08	Total autonomy of the system must be equal to that of the airplane on which the system is mounted	FASTER battery is sized to power the system for about 4 hours which is the typical ULAs flight endurance.
Interface Requirements		
RE.I.01	The system shall have standard RS232 serial ports in order to use different set of sensors (G.P.S, I.M.U, magnetometer and pressure sensors)	Each camera will be connected to a single PC/104 board, equipped with 2 programmable serial ports, which can be used for camera control or digital sensors acquisition
RE.I.02	Acquired images must be saved in a standard format (JPEG, JPEG2000, TIFF or GEOTIFF)	Images will be acquired in RAW format from the cameras and then converted, in realtime, in a compatible format
RE.I.03	In order to allow a fast download of the acquired data the system shall be equipped with a GBit Ethernet connection	Selected cameras use a standard GiGE high speed connection to download acquired data
RE.I.04	The system shall be compatible with standard aircrafts electric bus (12 V, regulated or unregulated) to allow battery recharge where possible	FASTER will be equipped with an external power connection to charge the battery. The same solution will be implemented in the FASTER EM as shown in section 6.2.
RE.I.05	The system shall be equipped with a DC-DC converter able to generate typical digital device voltage references (12, 8, 5, 3.3, etc)	FASTER will be equipped with a compatible DC-DC converter. See Section 6.2.

Table 2: FASTER system requirements

4.3 FASTER Cameras Geometry

In order to define the acquisition system geometry, some considerations regarding the different layout possibilities shown in Figure 24 and Figure 25 must be made:

- The upper right layout of Figure 24 shows an array matrix of 2 adjacent detectors sharing the same lens assembly; this solution was used when only small sized devices were available, so an array of detectors can be used on the same focal plane in combination with a standard photographic lens (36 x 24 mm format) or a large format lens (60 x 40 mm); to take advantage of modern full format digital sensors a custom lens must be made making this solution expensive;
- The upper left layout of Figure 24 shows a 3 cameras system arranged to obtain a very large swath width on the ground; image geometry must be carefully taken into account because of the tilt angle used between the two lateral cameras, in addition shadows effects may be relevant and cause problem during orthophoto reconstruction; this system is not suitable for remote sensing purposes because others bands may be difficult to add;
- In the bottom left layout of Figure 24 a 4 cameras system, using 4 different optical heads, is shown; such a system offers the same advantages of a two separate cameras system in terms of swath width but with a larger image side in the along-track direction, reducing the total number of images used to cover the same target area and thus the mosaicing time;
- The bottom right layout of Figure 24 shows an “oblique photography” system made up by five separate cameras; these system are suitable for 3D reconstruction but cannot be used for remote sensing purposes;
- The layout shown in Figure 25 represents a pushbroom line scanner; this solution implies the use of a very expensive custom focal plane assembly; it must be used from a very stable platform in order to obtain a correct image reconstruction (lines have to be merged together in order to generate the final image which is a process that requires an high computational load); it is suitable for very large areas because reduces the mosaicing operations;

In order to maintain multispectral capabilities (offering the red, green, blue and nIR bands) but maintaining a large swath width on the ground, thus reducing the total flight time, a three cameras system has been selected and it is shown in Figure 27.

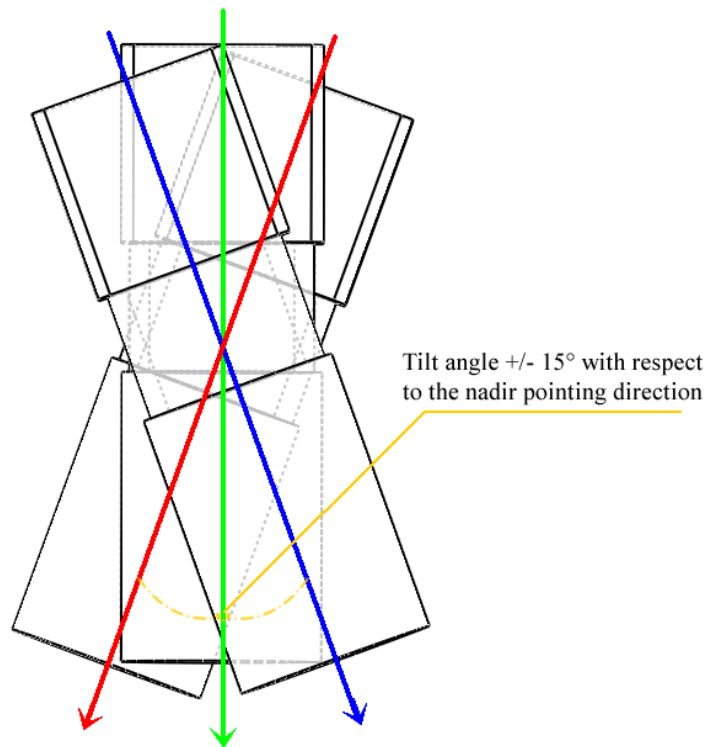


Figure 27: FASTER selected cameras system geometry

Cameras are arranged in line, with the first camera tilted 15° on the right side and last one tilted 15° on the left side. The first and third cameras are equipped with a Bayer filter mosaic to obtain colored images while the central monochrome camera is equipped with a nIR filter with $720 < \lambda < 850$ nm. Cameras are Prosilica GE4000, equipped with a full frame Kodak KAI-11002 CCD detector with 4008×2672 pixels and are described in the following section, together with two selected lenses which are the Zeiss Distagon 28 mm F/2.8 coupled with the colour cameras and the Zeiss Distagon 21 mm F/2.8 for the central nIR camera.

The ground projections of the three cameras are shown in Figure 28; when used for photogrammetric campaign such a system guarantees a maximum swath width, normalized with respect to the flight height, of about 1.47 times the flight height (220 m at 150 m of altitude). If also the nIR camera is used for remote sensing purposes (for example to retrieve the NDVI index) the swath width decreases to 1.3 times the flight height. The black dotted rectangle is the projection of the actual Canon EOS 450D APS-C detector (Section 6.1.3) which uses a 28 mm lens; in this case the acquired area is 1.66 times smaller with respect to a full frame sensor.

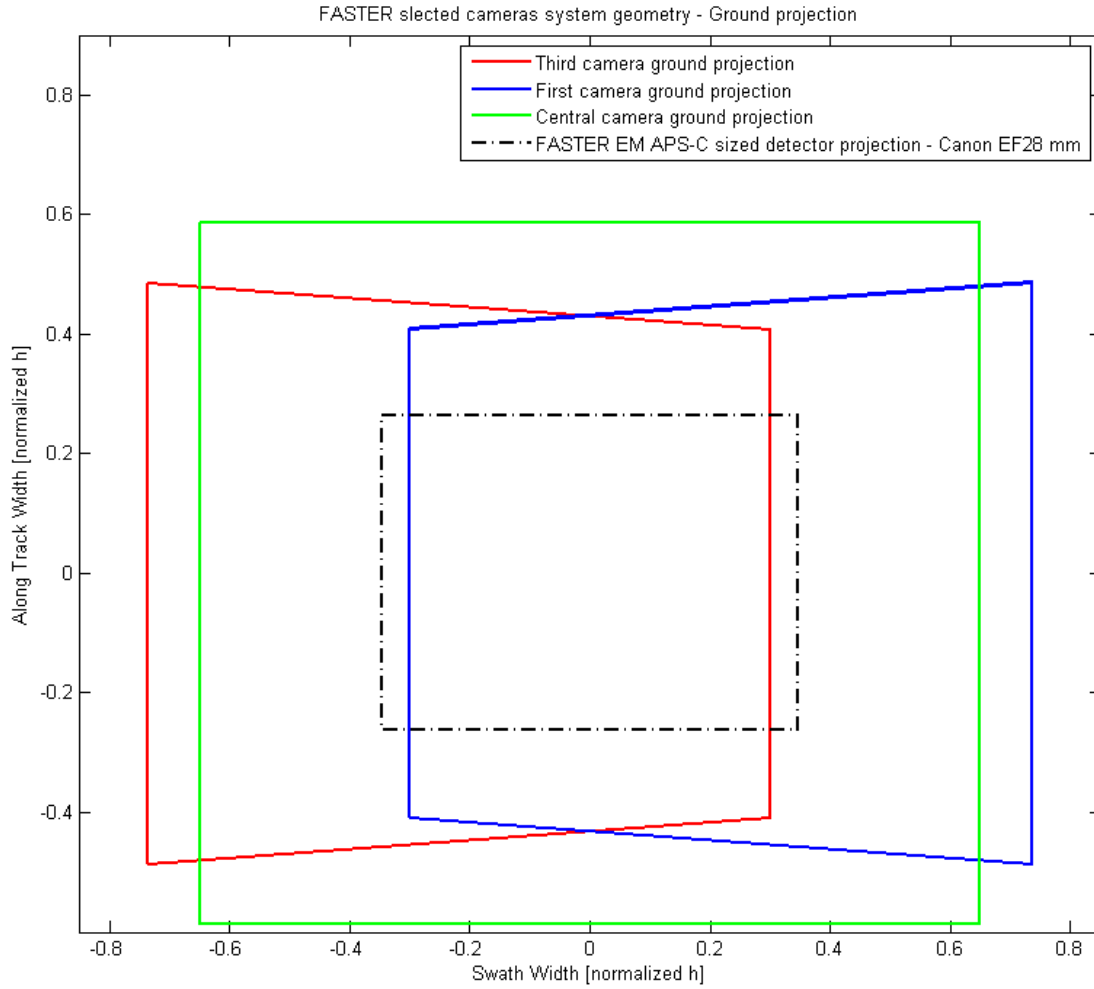


Figure 28: FASTER camera ground projections

The Ground Sampling Distance (*GSD*) defined as [Ref. (14), (15)]:

$$GSD = h \frac{\text{Pixel Pitch}}{f}$$

where h is the flight height and f is the focal length, at a flight height of 150 m the *GSD* for the colour cameras, with the 28 mm lens, varies between 4.8 cm at the Nadir direction and 7.13 cm at the maximum swath width. The corresponding *GSD* for the nIR camera, equipped with a 21 mm lens, varies between 6.4 cm and 8.5 cm. Values are compliant RE.P.01.

4.4 FASTER components

The FASTER system is made up of three main parts:

- The Ground Segment infrastructure
- The Airborne internal management and computing segment
- The Airborne external POD, equipped with the sensing devices

A detailed description of each unit is given in Chapter 6 where the FASTER Engineering Model is described. The major differences between the final system and the EM are the sensing device, and the positioning of the Inertial Measurement Unit and the GPS receiver. For safety reasons, they have been installed inside the airborne internal management and computing unit in the EM, instead of being mounted and referenced inside the external POD. Having the EM reduced functionalities, a single small frame camera has been used instead of the three cameras system.

The three cameras selected for the FASTER final system, the Prosilica GE4000 model, have already been employed in aerial photography. The CCD matrix has a pixel pitch of $9\ \mu\text{m}$ which is almost twice the size of standard cameras. It also has an electronic global shutter, which avoids image smear due to different exposure time between the first and the last row of the matrix [Ref (16)]. The camera fulfills RE.P.06 having a maximum frame of 5 fps at full resolution. It is powered by a 12 V bus and has a maximum power consumption of 6 W (18 W total for three cameras during acquisition); cameras weight 400 g each. Images are downloaded via a gigabit Ethernet connection which is able to withstand the high camera throughput. The Prosilica GE4000 has an F-mount lens mount which is used to connects the Zeiss Distagon lens. The Zeiss Distagon 28 mm F/2.8 [Ref. (17)] and 21 mm F/2.8 [Ref. (18)] guarantee respectively a 90° FOV and a 99° FOV. The 28 mm with the F-mount lens mount weights 620 g while the 21 mm 430 g (Figure 29).



Figure 29: Prosilica GE4000 [Ref. (19)] and the Zeiss Distagon 28 mm F/2.8 [Ref.(20)]

The FASTER final system will be provided with the same Crossbow NAV420 IMU used in the EM but this time in full nav mode in order to avoid the use of an external GPS receiver.

A complete 3D model of the FASTER external POD has been virtually assembled using Solidworks (Figure 30, Figure 31 and Figure 32); the CAD model is used to retrieve the relative distances between the camera reference systems and that of the IMU and between the IMU reference system and the GPS antenna phase center. In Table 3 the characteristics of the final model versus those of the Engineering Model described in Chapter 6.

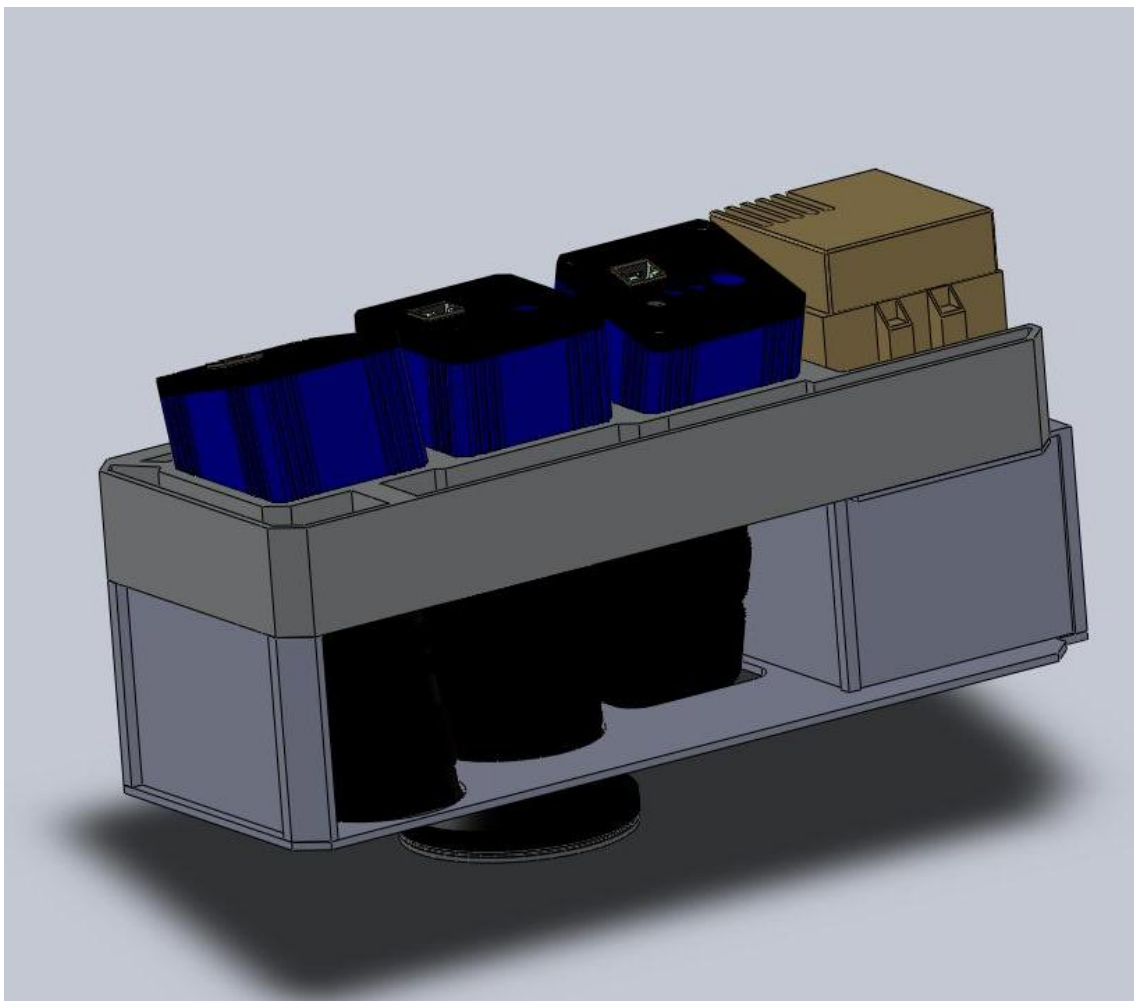


Figure 30: FASTER 3D model assembly

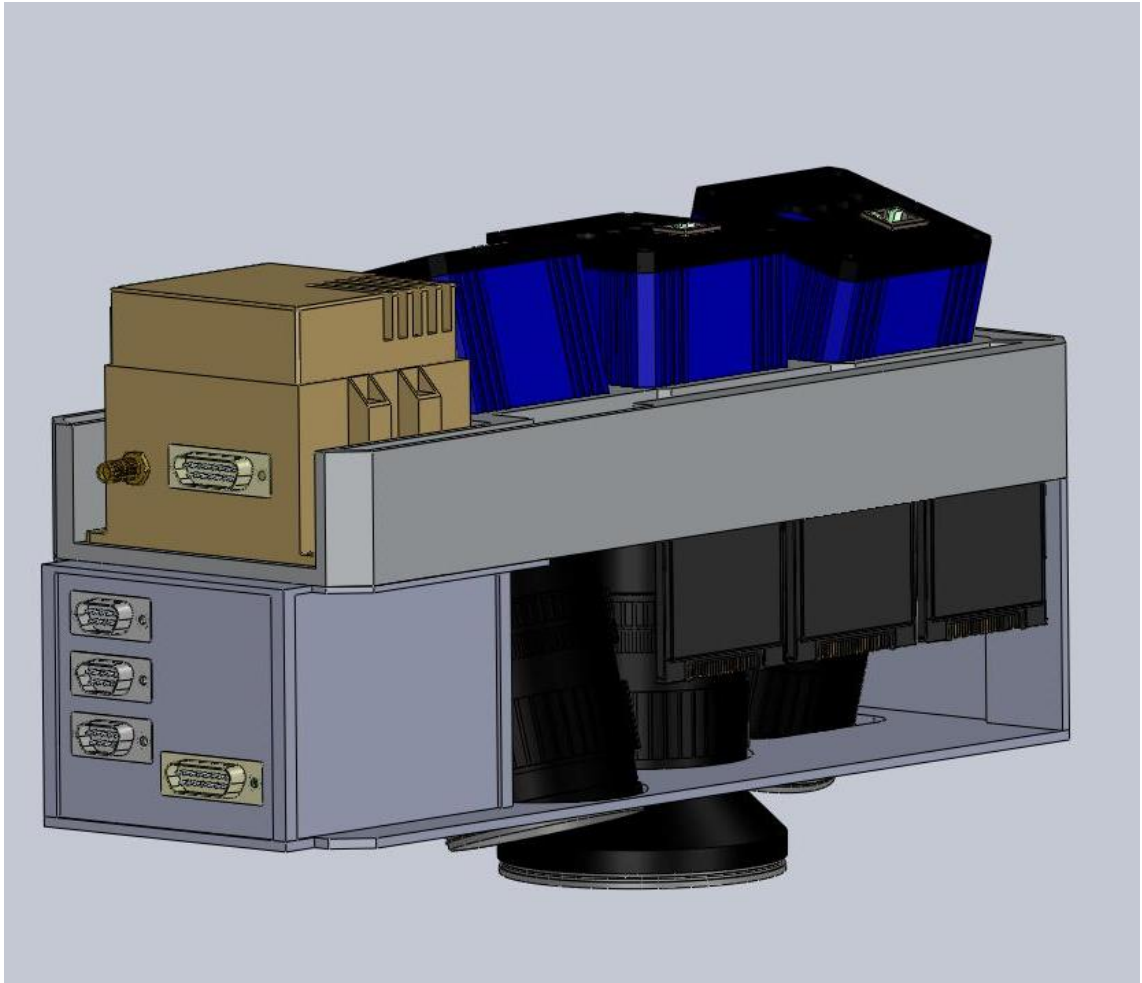


Figure 31: FASTER 3D model assembly, pc-box and SSDs mount

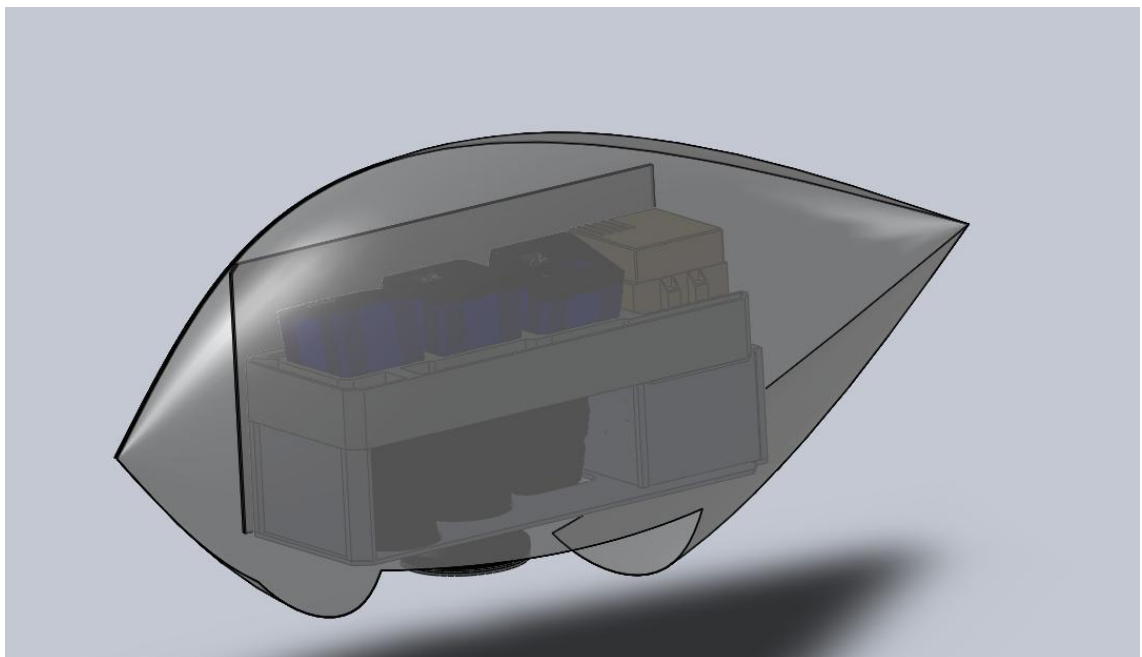


Figure 32: FASTER 3D model canopy

FASTER

	Engineering Model	Final Layout
Description	1 DSLR Canon EOS 450, CMOS sensor, controlled via USB interface	Simultaneous acquisition of 3 frames (2 colour + 1 NIR), CCD sensor, controlled via Gigabit Ethernet and RS232 interfaces
Image Area	4272 x 2848 Pixels (3:2 form format)	4008 x 2672 Pixels (3:2 form factor)
Pixel Size (pitch)	5.2 μm	9 μm
Detector Size	APS-C (22.2 x 14.8 mm ²)	35 mm (36 x 24 mm ²)
Field of View (FOV)	40° cross track 29° along track	65° cross track 46° along track
Lens	28 mm f/# 2.8	28 mm f/# 2
Radiometric Resolution	12 bit	14 bit
Maximum Frame Rate	3 fps	5 fps
Estimated power consumption	4 W	< 30 W

Table 3:FASTER final model vs Engineering Model characteristics

Chapter 5. FASTER Planning Software

5.1 Photogrammetric Aerial Mission

Purpose of a photogrammetric aerial mission is systematically cover a portion of the Earth's surface. Flights are arranged in parallel strips allowing a sufficient overlap of imaged areas, both in the across-track and along-track directions:

- Along-track direction, an overlap between 60 and 80% is generally selected, so that an overlapping pair of photos may permit the location of any photo point in at least two frames;
- Across-track direction, an overlap between 20 and 30% is selected because of the need to build strong geometric interconnection between adjacent image sequences;

Aerial campaigns typically require an accurate flight planning, whose general scheme is presented in Figure 33 [Ref (21)]. In this scheme a' is referred to the camera sensor size; depending on how the camera is mounted may corresponds to the sensor base or height; a is the projection of a' on the ground, supposing a flat Earth. h is the flight height with respect to the ground or another reference surface like WGS84 ellipsoid. Given a' , a can be found as follow:

$$a = \frac{h}{f} a' \quad \text{Eq.1}$$

where f is the lens focal length. Generally f is expressed with respect to the 35 mm format but in most cases digital sensors have different size if the camera is not a full frame camera. So Eq.1 becomes:

$$a = \frac{h}{cf} a' \quad \text{Eq.2}$$

where c is a crop factor which takes into account the ratio between the 35 mm format and actual sensor diagonal. The effect is an apparent longer focal length (if $c > 1$) that must be considered because directly effects the ground resolution (thus a).

The base between two subsequent images in the same strip is expressed by Eq.3:

$$b = a \left(1 - \frac{o}{100}\right) \quad \text{Eq.3}$$

in which o is the selected along-track overlap.

The across-track overlap p defines the distance on the ground between two consecutive stripes q :

$$q = a \left(1 - \frac{p}{100}\right) \quad \text{Eq.4}$$

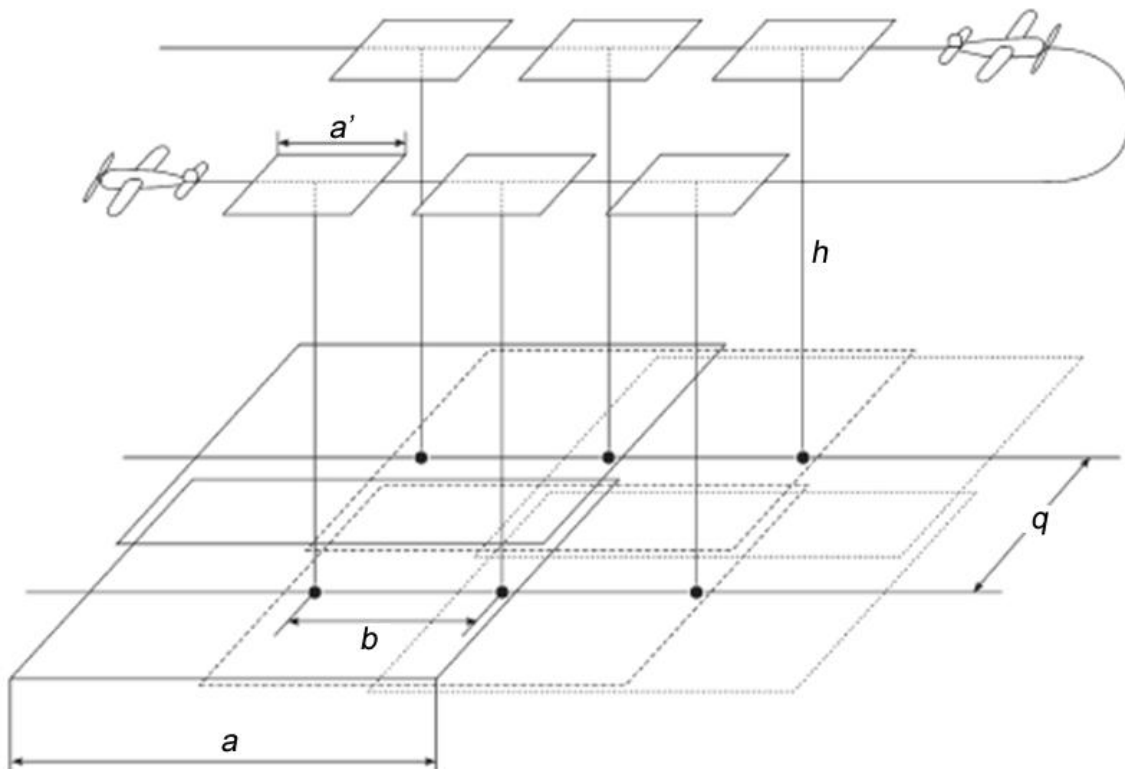


Figure 33: Flight plan scheme [Ref. (22)]

The image scale factor is given by the ratio h/f . For the purposes of this study flying height is limited to 500 ft (152.4 m) over the highest obstacle in a 3000 m range, because of the Italian regulation on Very Light Aircrafts flight. Low altitude makes a photogrammetric instrument more sensitive to scale factor variations; if the flight is conducted in a mountainous area there may be percentage variations of the scale factor in the order of 300/400% as experienced in the last FASTER EM flight campaign presented in Chapter 7. Once defined a' , f , o and p the total number of acquired images is a function of the target area dimensions. The minimum required time interval between two acquisition is defined as follows:

$$\Delta t_{min} = \frac{h_{min}}{v} \frac{a'}{f} \left(1 - \frac{q}{100}\right) \quad \text{Eq.5}$$

where v is the ground speed velocity measured by the G.P.S receiver which is different from IAS (*Indicated Air Speed*) shown by a standard anemometer installed onboard the aircraft.

Aerial flight can only be made in clear, cloudless weather conditions, carefully taking into account wind direction in the over flight area. If the photogrammetric system is not able to apply corrections to remove the crab angle (namely the sideslip angle β , as shown in Figure 34) via electric or pneumatic control systems, wind direction should be known and its effects must be planned [Ref. (22)].

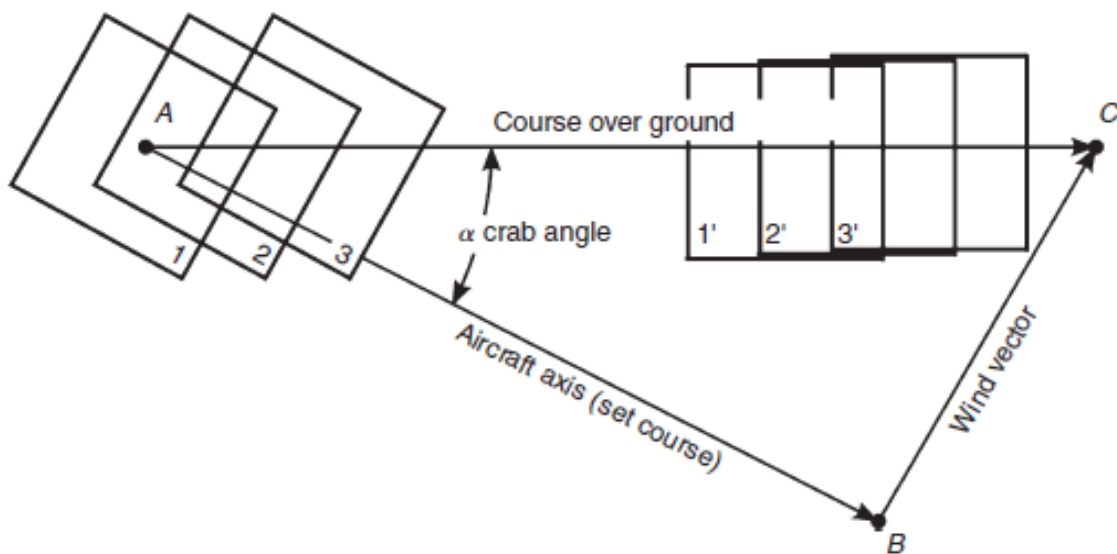


Figure 34: Crab angle representation [Ref. (22)]

5.2 FASTER planning software layout

In the following diagram the FASTER planning software block diagram is presented. The idea is to use a standard platform, easy and quick to use, to define the target area. At present, different tools are available which use a three-dimensional representation of the Earth globe to access for example, satellite and aerial imagery [Ref (23)]. They are known as geographical browsers or geobrowsers and have many features:

- Display satellite and aerial imagery available from several database all around the world constantly updated; high resolution imagery is available for a wide range of country (Ikonos and Quikbird satellite data with a GSD ≤ 1 m);
- Layers can be used to display proprietary information over the standard database and third party data can be displayed too;
- Users can create and save georeferenced paths or markers to identify interest areas;
- Tools are available to create new data that can be exported or imported using standard formats;

In particular, the capability to import/export data combined with the possibility to create georeferenced paths or markers creates an useful interface with many other software environments.

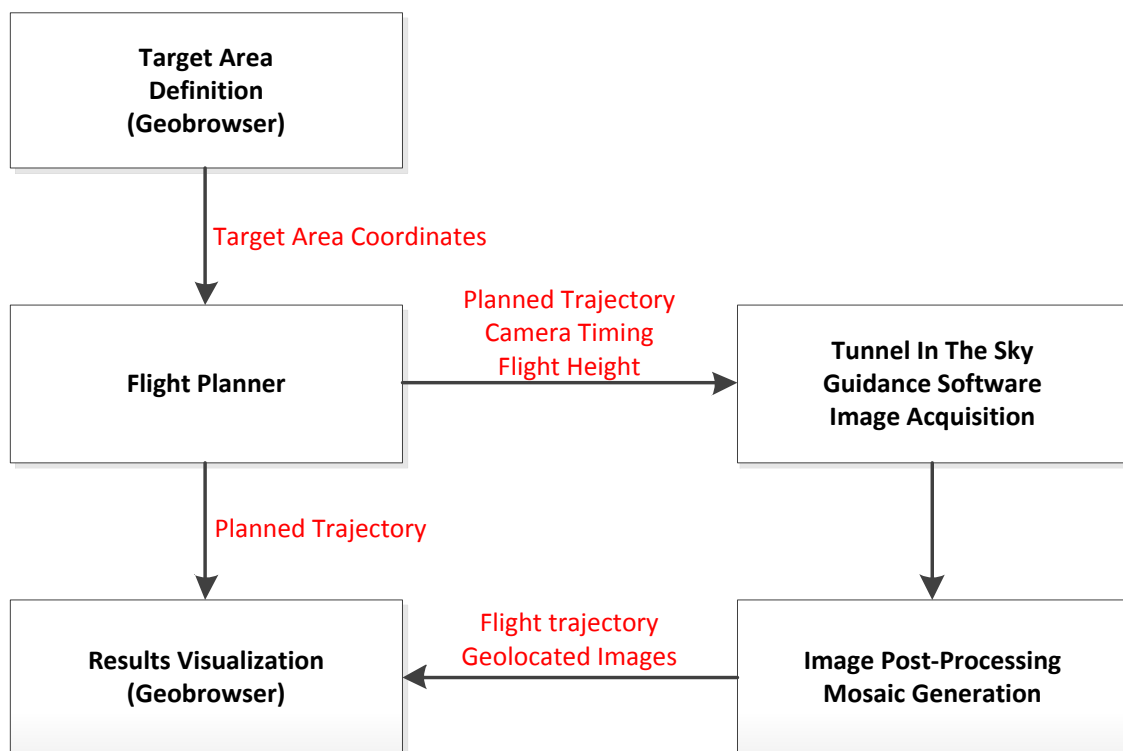


Figure 35: FASTER planning software block diagram

The planning software has been divided into five different blocks and two of them are implemented using geobrowser features. It has been found that this solution is particularly suitable when the use of maps can be helpful to speed up the target area selection process and to better understand the obtained results. One of the most widely available solutions for geobrowsing is Google Earth; it has over 100 million users and all the characteristics listed above. It uses the kml/kmz exchange format which is based on the xml 1.0 standard; it is well documented and can be implemented inside the Matlab environment, used to develop the flight planner block.

5.3 Google Earth Geobrowsing Solution

In this section the Google Earth geobrowser is presented describing how is possible to use it in combination with others software blocks.

As stated in the previous section Google Earth is a virtual globe, map and geographic information program which maps the Earth by the superimposition of images obtained from satellite imagery, aerial photography and GIS (*Ground Information Services*) 3D globe. It allows users to search places entering they geographical coordinates or simply search them using an input device, like a mouse. Google Earth uses DEM (*Digital Elevation Model*) data collected by NASA's SRTM (*Shuttle Radar Topography Mission*) to display an accurate model of the Earth surface, shown in Figure 37. SRTM has an absolute horizontal accuracy (with respect to the WGS 84 model) of less than 50 *m* and an absolute vertical accuracy (with respect to the EGM 1996) of less than 30 *m* [Ref (24)].

Most land areas are covered in satellite imagery with a resolution of about 15 *m*/pixel (multispectral Landsat which is pansharpened with the 15 *m* panchromatic Landsat imagery) and, where available, with 2.5 *m* SPOT imagery or < 1 *m* Geoeye or aerial products. Highest resolution images (up to 0.1 *m*) are concentrated in some specific areas like some German cities.

One of the most important features of the software are Google Earth layers, which provide access to all kinds of other data including, for example, real-time weather or thermal imagery. This functionality enables the possibility to show proprietary material on the 3D Earth globe almost instantaneously. In order to do this data must be accurately prepared and georefernced. Layers can also be completed with additional information relative to the acquisition campaign to better organize the output result.

The user GUI (*Graphical User Interface*) is shown in Figure 36, in the left frame address box, places and levels enabler are present.

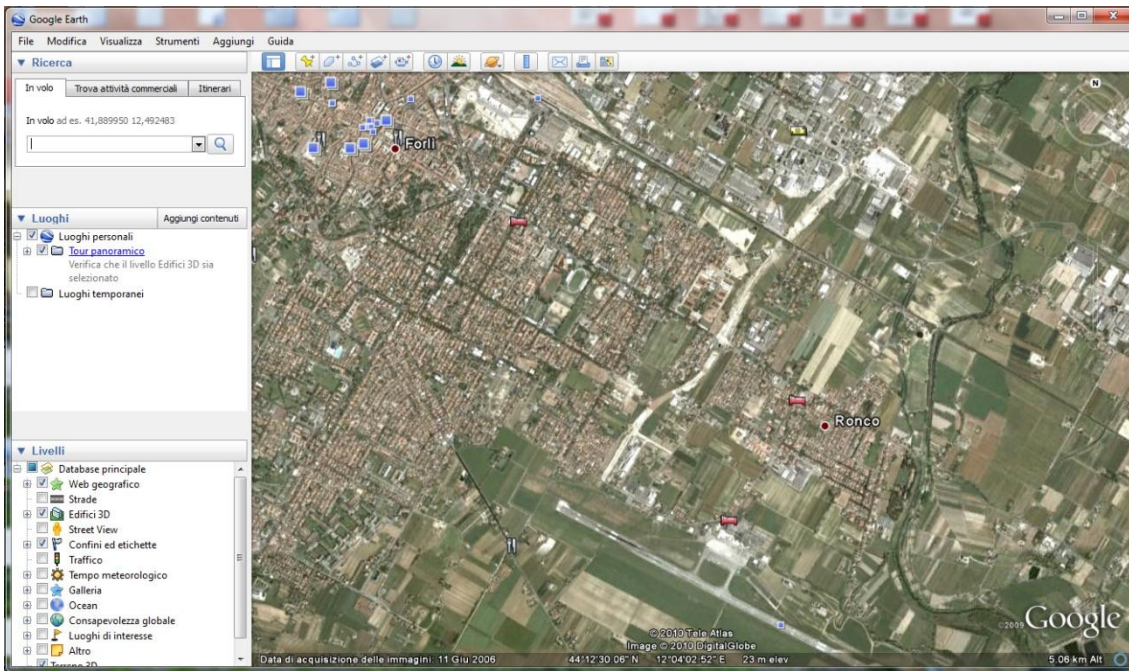


Figure 36: Google Earth geobrowser GUI

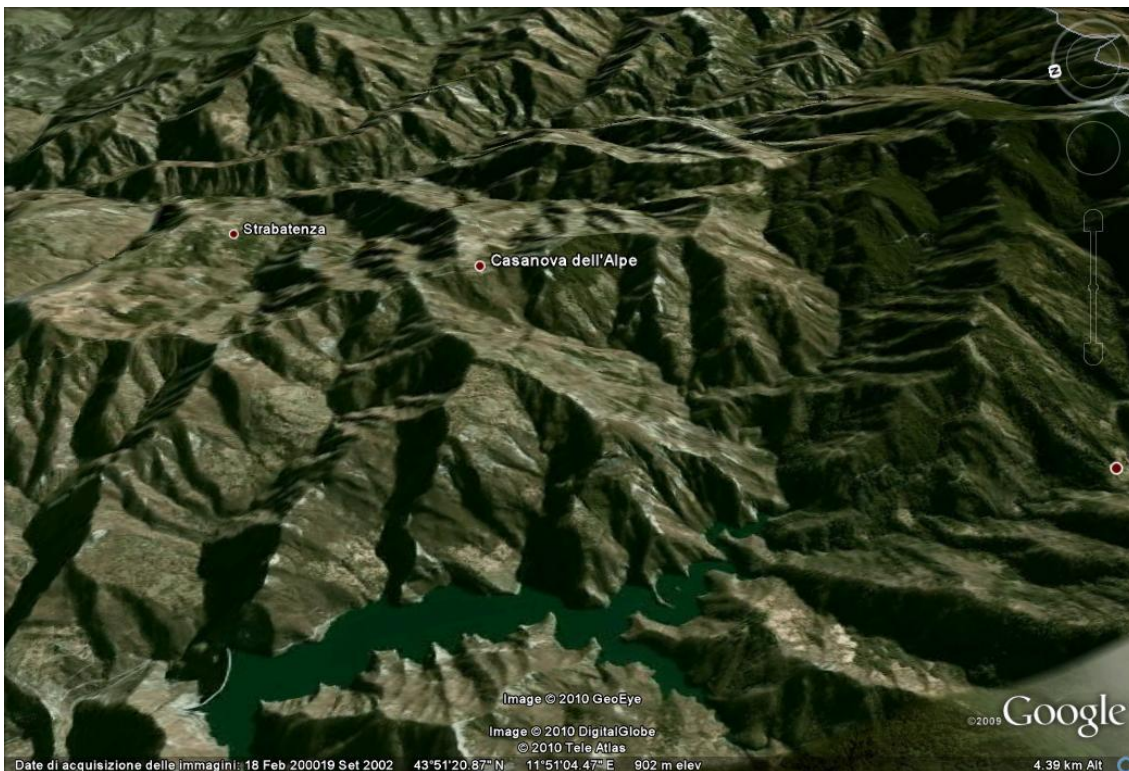


Figure 37: Google Earth SRTM DEM implementation

With the toolbar buttons, over the graphical window, is possible to draw paths or polygon over the Earth surface, carry out measurements, add images or placemarks for specific locations. Placemarks and polygons can be exported in the KML/KMZ format.

5.3.1 KML/KMZ Exchange Format

KML stands for Keyhole Markup Language, is an XML-based language schema for expressing geographic annotation and visualization on geographical browser and is an international standard of the Open Geospatial Consortium.

The KML file specifies a set of features (placemark, images, polygons, 3D models, textual descriptions, etc) for display in Google Earth or any other 3D geobrowser implementing the KML encoding. Each place is always described by at least two parameters: Latitude and Longitude. Other data can make the view more specific, such as tilt, heading and altitude. KML files are very often distributed in the KMZ format, which are compressed (ZIP) files with a .kmz extension. For its reference system, KML uses 3D geographical coordinates in this order: Longitude, Latitude and Altitude. These components are defined by the WGS84 (World Geodetic System of 1984) while the vertical component is measured from the WGS84 EGM96 Geoid vertical datum [Ref (25)]. Altitude can be omitted from the coordinate string, in this case the default value of 0 (approximately sea level) is assumed for the altitude component.

5.3.2 Reading KML/KMZ in Matlab

In Section 5.2 it has been pointed out that the capability of Google Earth to draw placemark and polygons is the function that enables data exchange between different environments. Every object drawn can be exported in an exchange format and being known the KML file structure (see previous section) it has been possible to create a Matlab script able to open and read KML or KMZ files.

The “*read_kml.m*” Matlab script directly opens KML files and searches for the *<coordinates>* tag that specifies the geographical coordinates for every *fix point*. Values are read and stored into a Matlab array, until the *</coordinates>* tag is found, and can be successively processed by the *FASTER_planner.m* script.

Placemarks are individual entity inside the KML file so the Matlab script will found a *<coordinates>* tags for each *fix point*; thus they are read as single 3 dimensional vectors and their linear interpolation defines target area boundaries. Otherwise polygons are

defined by a group of points in the space and their relative coordinates are reported in the same *<coordinates>* tag line in a repetitive sequence: *<coordinates> longitude₁,latitude₁,altitude₁ longitude₂,latitude₂,altitude₂... longitude_n,latitude_n,altitude_n </coordinates>*.

Polygons, are stored in a Nx3 array, where N is the number of points that constitute the polygon. Multiple polygons can be exported in the same KML file and imported in the Matlab at the same time, the script will assign an incremental numeric suffix to the array name. Other information contained in the KML file are currently discharged.

As mentioned in Section 5.3.1, KMZ are compressed files that can contain, in addition to the KML (always named *doc.kml*), external data as 3D models or images. In this case the Matlab script is able to extract the compressed data using the embedded ZIP format support and saving the *doc.kml* file in a temporary directory.

In the following example a 12-sided polygon has been drawn around the Forlì Ridolfi Airport (Figure 38) and then the file was exported in the KMZ format. The following string is extracted the encapsulated *doc.kml* file:

```
<coordinates> 12.04265484177943,44.18194756379602,0
12.06452048492158,44.17378303727157,0 12.10144169014094,44.17388037539627,0
12.1016006647769,44.18904683677211,0 12.0963112161245,44.20111856050828,0
12.09032069989327,44.20745768947005,0 12.07665277771444,44.21201734614615,0
12.0629961781692,44.21370752958197,0 12.04273941015088,44.21211257716238,0
12.03349310501469,44.20395888702259,0 12.03745912564322,44.1908753366266,0
12.04265484177943,44.18194756379602,0 </coordinates>
```



Figure 38: Example of polygon surrounding the Forlì Ridolfi Airport

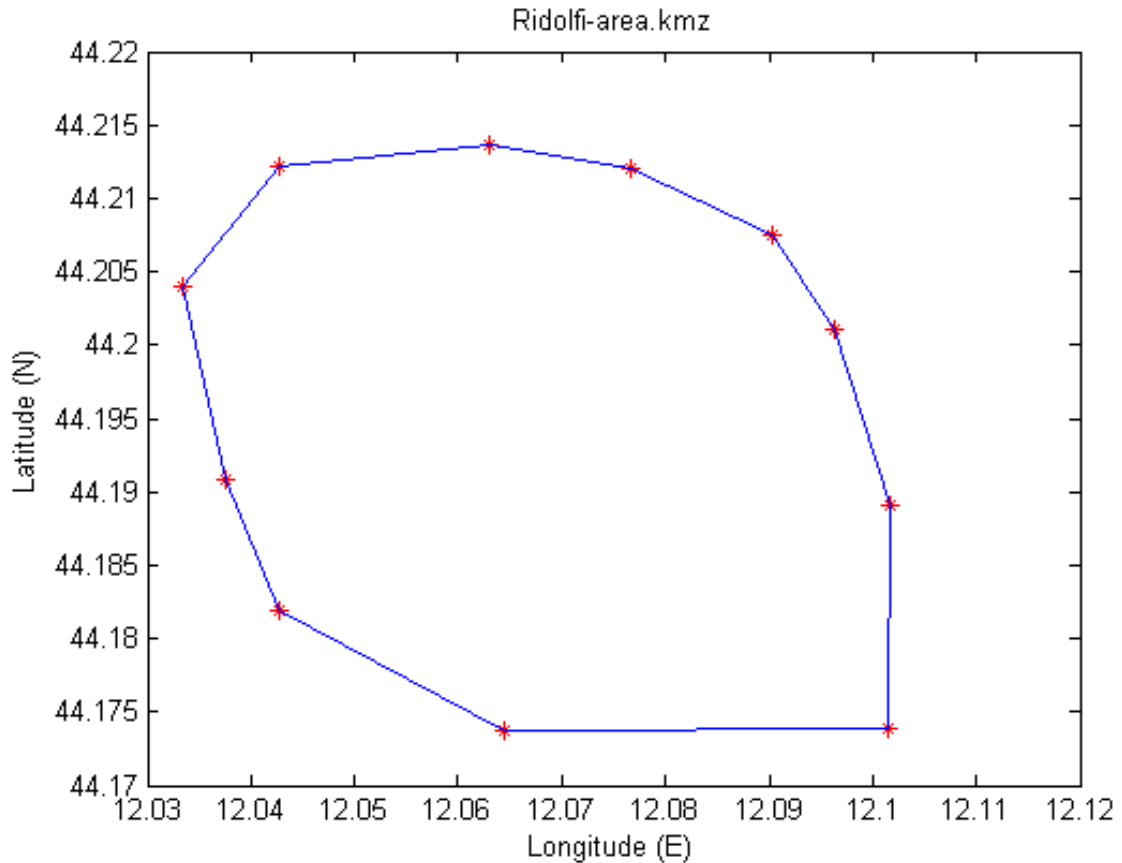


Figure 39: Imported KMZ in the Matlab environment

Figure 39 is a plot of the *Area_ridolfi* array created by the *read_kml.m* script. Once the array is created in the Matlab workspace the *FASTER_planner.m* script is recalled.

5.4 FASTER Flight Planner

The *flight planner* block shown in Figure 35 was also built in the Matlab environment and includes several scripts:

- *read_kml.m*, already described in Section 5.3.2;
- *FASTER_planner.m*, processes the target area to build the flight trajectory used in the tunnel in the sky interface, it also computes the flight height, camera timing intervals, the estimated elapsed time for the campaign and the total number of frames to be acquired. *FASTER_planner.m* recalls also some other Matlab function which have been developed for this project, *turn45.m* which calculates and draws turns between two consecutive stripes, *GEOtoUTM.m* and *UTMtoGEO.m* which changes the map representation from geographical coordinates to UTM coordinates and vice versa,

DEM_extraction.m which searches inside the ASTER DEM database and extracts the selected area altimetry data from a compressed archive;

- *KML_export.m*, produces a planned trajectory KML file.

Once imported inside Matlab, the array corresponding to the area defined in Google Earth maintains the same reference system used by the KML standard, and geographical coordinates are still used. In geographical coordinate system the distance covered by a degree of longitude differs moving towards the poles and only equals the distance covered by a degree of latitude only at the equator. Although longitude and latitude can locate exact positions on the surface of the globe, they are not uniform units of measure.

For measurement and trajectory planning purposes a more adequate mapping solution of the Earth surface must be adopted. A suitable map representation is the UTM (Universal Transverse Mercator) coordinate system which is a grid-based method of specifying locations on the Earth surface that is a practical application of a 2-dimensional Cartesian coordinate system.

5.4.1 Universal Transverse Mercator Coordinate System

The UTM is the ellipsoidal Transverse Mercator, which is a modified Transverse Mercator projection which, in general, has the following characteristics [Ref (26)]:

- It is a Cylindrical (transverse), conformal² projection;
- Central meridian (each meridian 90° from central meridian) and Equator are straight lines;
- Other meridians and parallels are complex curve
- Scale is true along central meridian, or along two straight lines equidistant from and parallel to central meridian (in case of the ellipsoidal Transverse Mercator lines are almost straight)
- Scale becomes infinite on sphere 90° from central meridian.

The Earth, between latitudes 84°N and 80°S, is divided into 60 zones, each generally 6° wide in longitude. Zones are numbered from 1 to 60 proceeding east from the 180th meridian from Greenwich with minor exceptions. There are letter designations from south to north (see Figure 40) and each of these quadrangles is further subdivided into grid squares 10⁵ m on a side with double letter designations, including partial squares at the grid boundaries.

² Conformal map projections preserve angles locally

One of the advantages of the UTM projection is that geographic location are given in x and y coordinates in meters, using the meridian halfway between the two bounding meridians as the central meridian, and reducing its scale to 0.996 of true scale (point 4 of the previous list). This reduction was chosen to minimize scale variation in a given zone and the amount of distortion is held below 1/1000 inside each zone. Distortion of scale increases in each UTM zones as the boundaries between two zones are reached. To define a position in the UTM system three value must be specified: *UTM zone and easting and nothing coordinate pair*.

The *easting* is the projected distance of the position from the central meridian, while the *northing* is the projected distance of the point the equator. I order to avoid negative numbers, to the central meridian of each zone is given a false easting value of $5 \cdot 10^5$ m.

In the northern hemisphere, positions are measured northward from the equator, which has an initial *northing* value of 0 m and a maximum northing value of approximately $9.328 \cdot 10^5$ m at the 84th parallel. In the southern hemisphere, *northings* decrease going southward from the equator, which has a false northing of 10^6 m so that no point within the zone has a negative value. As an example the Forlì Ridolfi Airport is located at [44°11'42'' N, 12°04'11'' E] in geographical coordinates which corresponds to [33T, 265835.35, 4897707.58] in UTM coordinates.

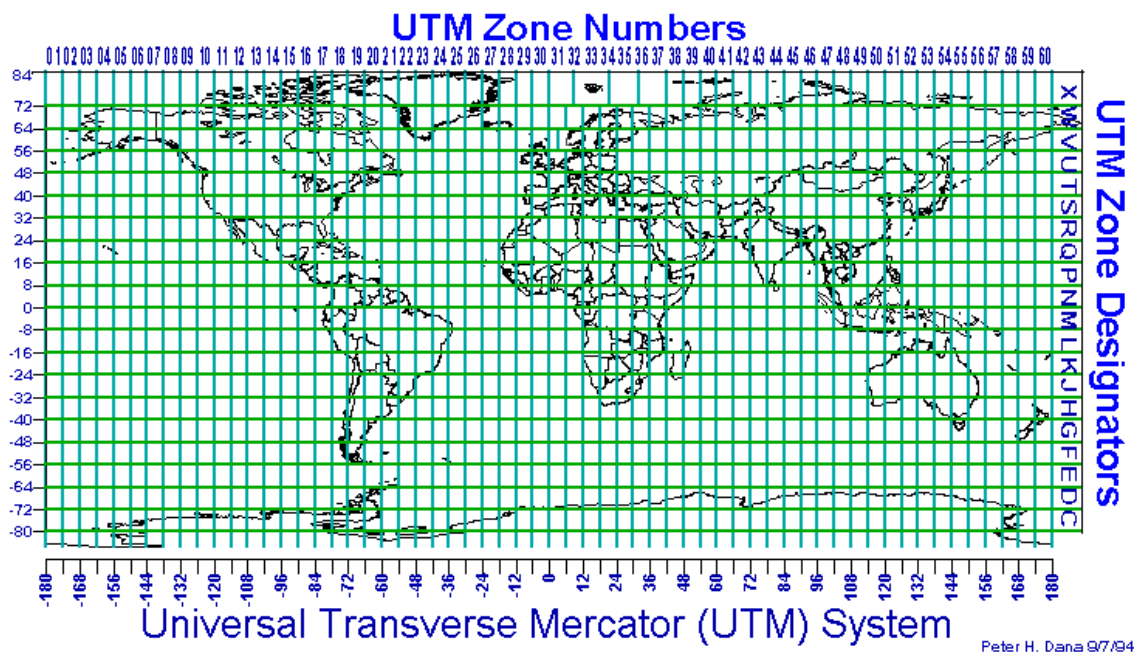


Figure 40: UTM System [Ref. (27)]

The ellipsoidal Earth is used throughout the UTM projection system, but the reference ellipsoid changes with the particular region of the Earth. A list of reference ellipsoids (datum) is presented in Table 4.

Datum	Equatorial Radius [m] (a)	Polar Radius [m] (b)	Flattening (a-b)/a	Use
NAD83/WGS84	6378137	6356752.3142	1/298.257223563	Global
GRS 80	6378137	6356752.3141	1/298.257222101	US
WGS72	6378135	6356750.5	1/298.26	NASA, DOD
International (1924)	6378388	6356911.9	1/297	Global
Clarke 1866	6378206.4	6356583.8	1/294.98	North America

Table 4: Datum

The mathematical formulation to convert geographical coordinates to UTM and vice versa are presented in Appendix 1 showing how *GEOtoUTM.m* and *UTMtoGEO.m* scripts work. In the following picture the polygon drawn in Figure 39 is plotted using UTM coordinates.

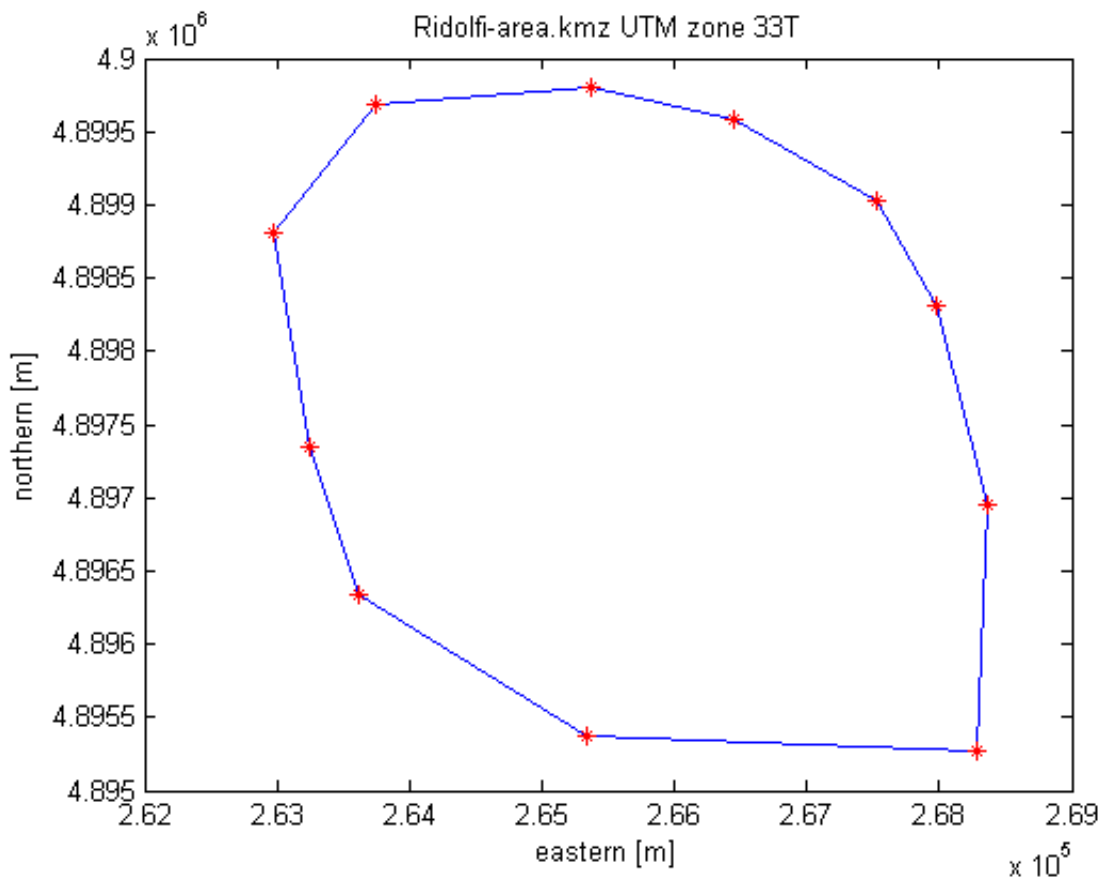


Figure 41:Ridolfi-area.kmz converted in UTM coordinates

5.4.2 Trajectory Determination

The *FASTER_planner.m* script is responsible of the trajectory determination. This script requires the following entries:

- Target area UTM coordinates, coming from the *GEOtoUTM.m* script;
- Surrounding area offset in m , is a squared surrounding area applied to target area in order to take into account errors;
- Quality, this variable tells the software how many waypoints have to be used in order to generate the trajectory; settings are *low*, *medium*, *high*
- Optical parameters, inputs are the focal length f , the lens field of view with respect to diagonal FOV , the horizontal field of view $hFOV$ and the vertical field of view $vFOV$ (if the sensor is squared $hFOV$ must be set equal to the $vFOV$); optical parameters are pre-calculated using *FASTER_geometry.m* script, described in Chapter 4.
- Overlap; along- and across-track overlap percentage must be declared
- Flight parameters, expected ground speed v and turn rate ω must also be inserted

Given these inputs the preliminary operations are calculation of the square surrounding area and the definition of the flight height using the digital elevation model of the target area. Latitude and longitude boundaries are retrieved and the square surrounding area is applied (see Figure 42). From the surrounding area center, the 3 km range is applied (Section 5.1), where the highest obstacle must be determined in order to find the appropriate flight height as shown in Figure 43 (Brisighella surrounding area DEM) and Figure 44 with the computed flight height.

The selected DEM database is the ASTER (*Advanced Spaceborne Thermal Emission and Reflection Radiometer*) global digital elevation model (Version 1) developed jointly by Japan METI and NASA. The ASTER GDEM covers land surfaces between 83° N and 83° S and is comprised of 22600 1° by 1° tiles. It is in GeoTIFF format with geographic latitude/longitude coordinates and 1 *arcsecond* (approximately 30 m) grid. It is referenced to the WGS84/EGM96 geoid. Its estimated accuracies are 20 m at 95% confidence for vertical data and 30 m at 95% confidence for horizontal data [Ref (28)]. The names of individual data tiles refer to the latitude and longitude at the geometric center of the lower-left corner pixel, example presented in Figure 43 and Figure 44 use the *ASTGTM_N44E011.zip* file.

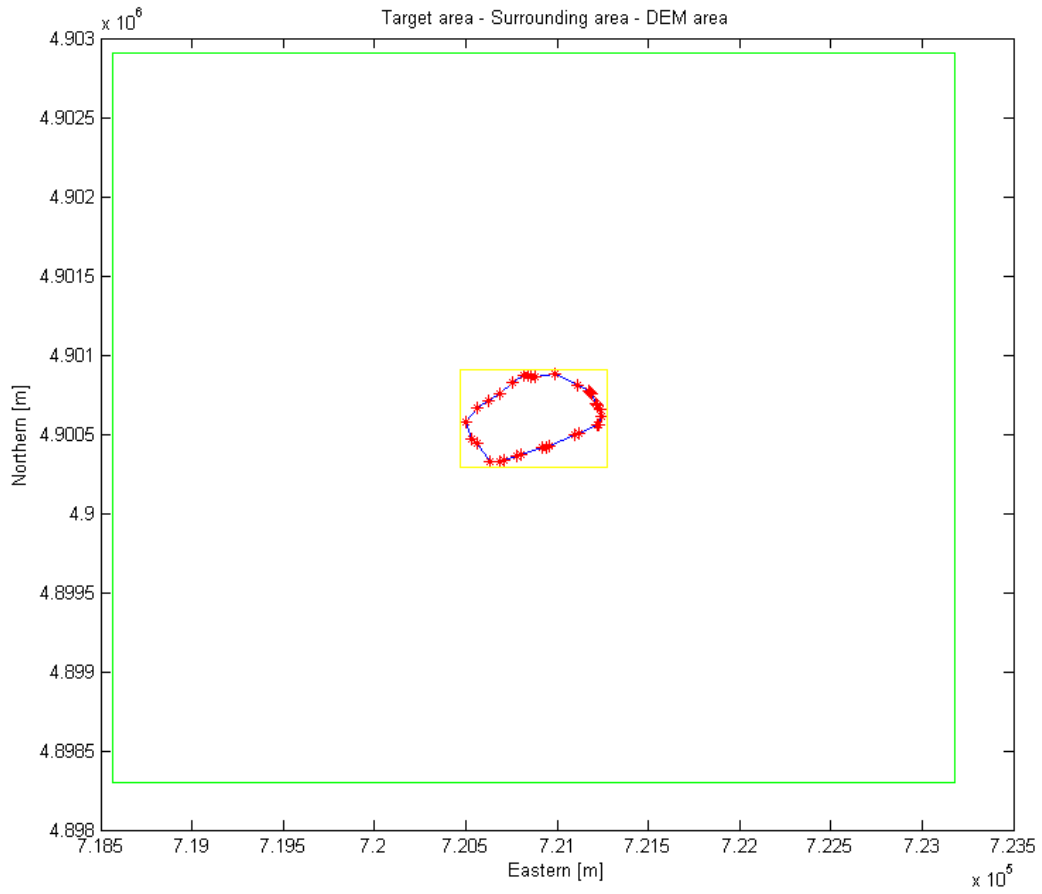


Figure 42: Example of plotting: target area, surrounding square area, DEM area

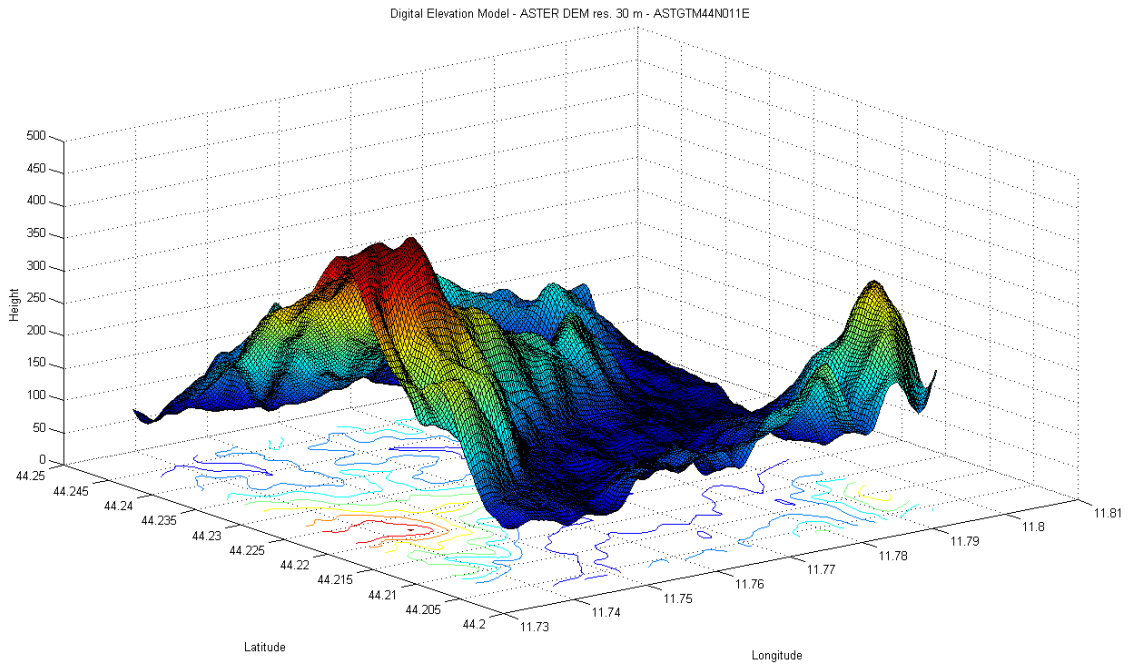


Figure 43: DEM extraction from the ASTER database, tile ASTGTM44N011E

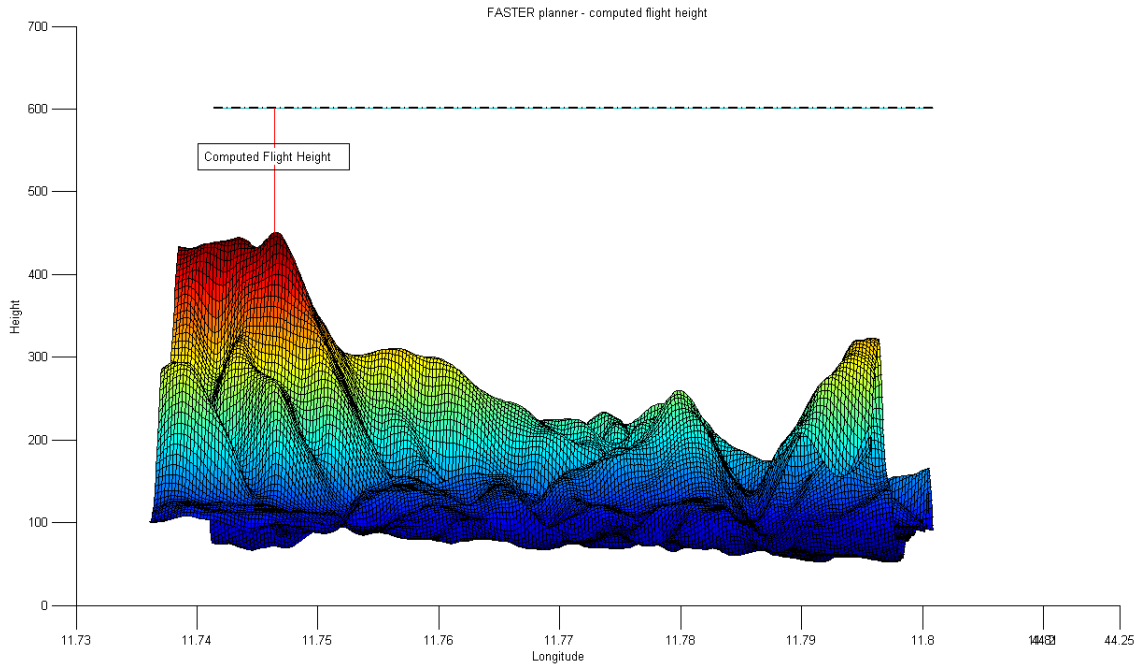


Figure 44: FASTER flight planner - computed flight height [m]

To use the ASTER DEM database the *DEM_extraction.m* script has been created. It takes as input the DEM area coordinates generated by the *FASTER_planner.m* script.

Longitude and latitude boundaries are evaluated in order to determine if all the DEM area corners belong to the same tile. Then tile file name is reconstructed using the ASTGTM_ prefix adding the coordinates already found. Once the file name is built the corresponding ZIP file is extracted and the GeoTIFF image is imported in the Matlab workspace using the *geotiffread.m* script (data is then converted to “double”). Each tile is managed as a 3601x3601 array (the first row and the last column overlap the adjacent tiles). Then the DEM area is searched inside the array and the highest value is selected as the highest obstacle in the 3000 m range expected by the aeronautical regulation. In the previous example a 215x155 subset matrix of the ASTGTM_N44E011 tile was used. The flying altitude is stored and the procedure continues with the successive step.

At this time optical parameters are necessary to compute the image sensor projection on the ground, using equations 1 to 5. A database of possible sensor solutions was created in which is possible, selecting a particular instrument, to retrieve corresponding values for the optical parameters. The database is accessed via the *FASTER_geometry.m* script where Matlab structures are used to store information. Acquisition sensors can be coupled

to different lens in order to have the same ground resolution when relative distance to ground varies.

When along-track, o , and across-track overlap, p , are introduced a and q values can be calculated and the trajectory can be finally determined. The flight trajectory is a sum of different parts: acquisition stripes, re-alignment turns and the acquisition area entrance maneuver. Exposure stations (where the image is effectively acquired) constitute the stripe waypoints while re-alignment turns must be adapted according to q .

Re-alignment turns are based on the *Standard 45/180 procedure turn* which has been modified in order to connect two consecutive stripes. The original maneuver is designed to reverse course, passing two times over the same fix point (Figure 45); the turn rate is fixed at $\omega_t = 3^\circ/\text{s}$. The maneuver has three straight legs and two turns, the first one is a 45° turn while the second one is 225° . The 60 s final straight leg allows the pilot to correct re-align the airplane before entering the acquisition stripe. This is fundamental, especially when dealing with small aircrafts which are particularly sensitive to meteorological conditions. The 38 s leg, called the *extension leg*, can be modified according to q in order to return to a fix which is translated with respect to its original position; the turning radius $r = \frac{v_{gs}}{\omega_t}$ can be used to express the extension leg length (supposing the x-axis parallel to the 60 s leg): $e_{leg} = r \cos(45) - q$ and $t_{e_{leg}} = \frac{\sqrt{2e_{leg}}}{v_{gs}}$.

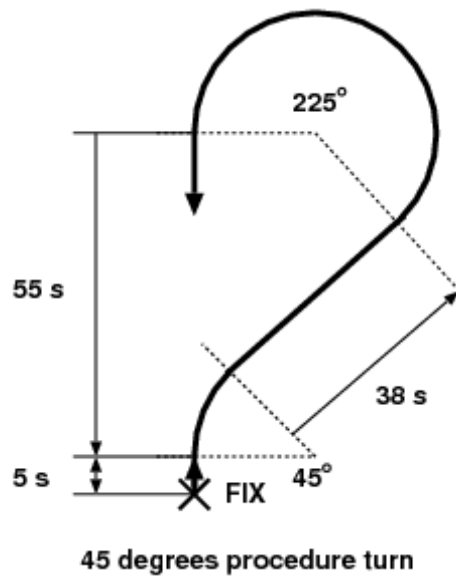


Figure 45: Standard 45/180 procedure turn [Ref. (29)]

The *turn45.m* script is recalled between each stripe calculation and waypoints and turns time are added during the iterations performed to cover the entire target area.

In Figure 46 an example of planned trajectory where the green line is the waypoints (red dots) interpolation. Stripes are typically directed East-West or West-East because of illumination effects and flights, when possible, should be conducted with the sun near to its zenithal position to minimize shadow effects and to reduce the exposure time (longer exposure may cause blurring).

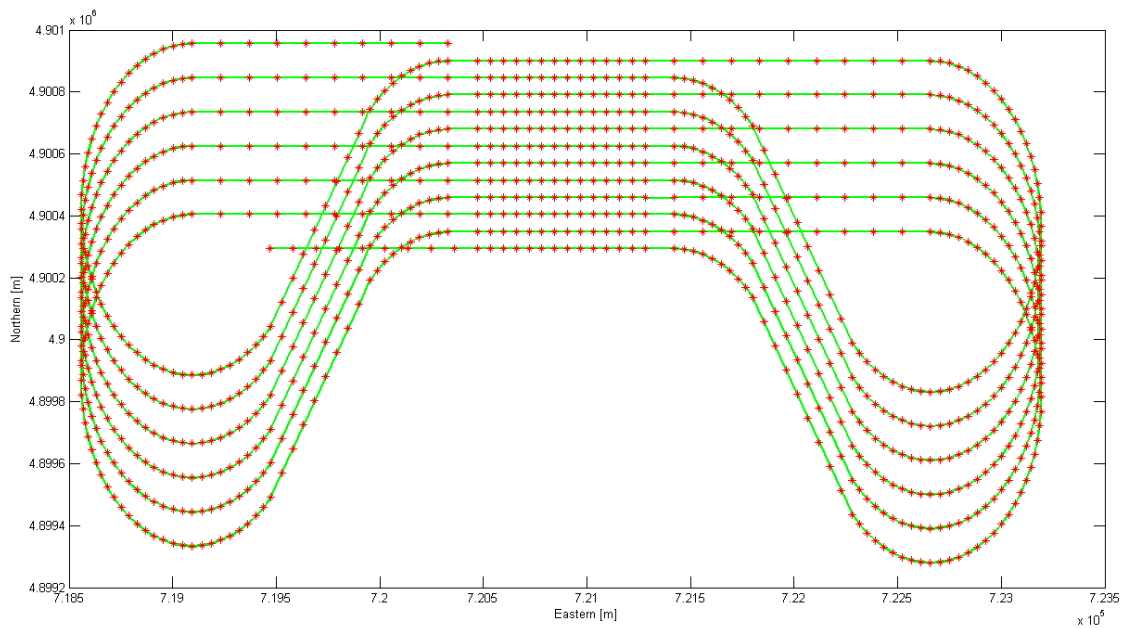


Figure 46: Planned trajectory

Figure 47 represents a standard output of the script, in green the flight trajectory, in blue the contours of the target area and in black the surrounding squared area. Red rectangles are the image projections (supposing a flat Earth surface) which in Figure 48 have been colored differently (first three stripes).

Each frame is tagged with its geographical and UTM coordinates so comparisons can be done between planned and real frame. As shown in Figure 35 diagram, the flight trajectory is exported in the KML format and can be visualized inside the Google Earth graphical window (Figure 49). This step is important because it is possible to take a look at the whole mission before takeoff, choosing the best transfer route between the aerodrome and the entrance leg of the planned trajectory. The flight can also be simulated using the advanced features of Google Earth.

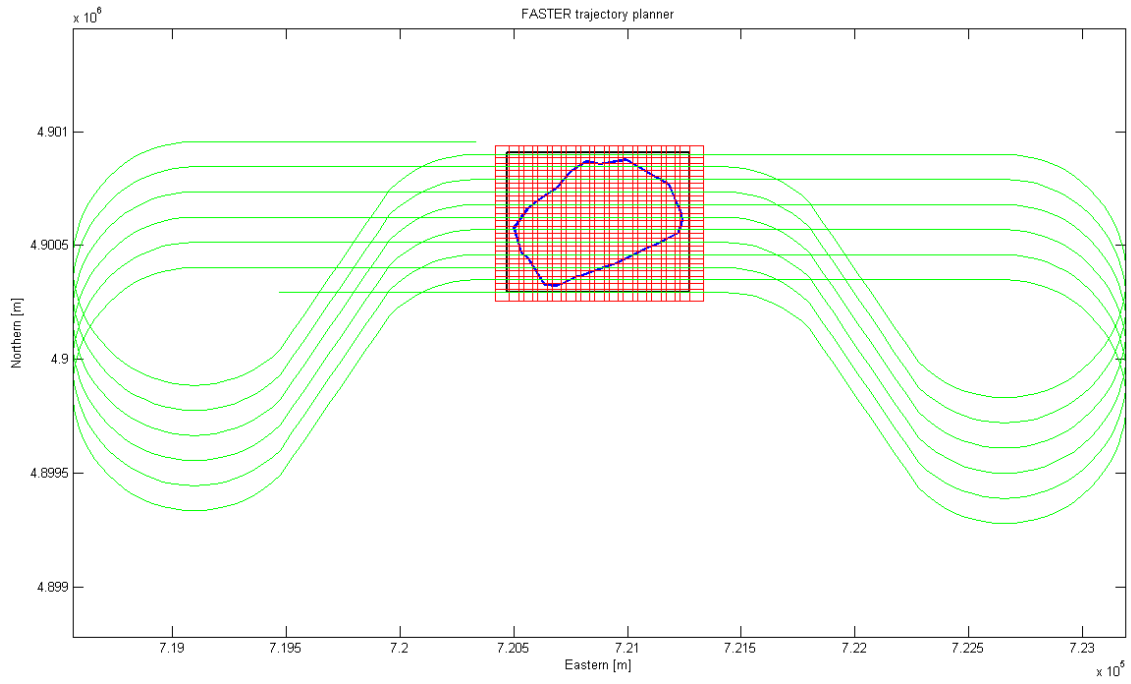


Figure 47: *FASTER_planner.m* script output

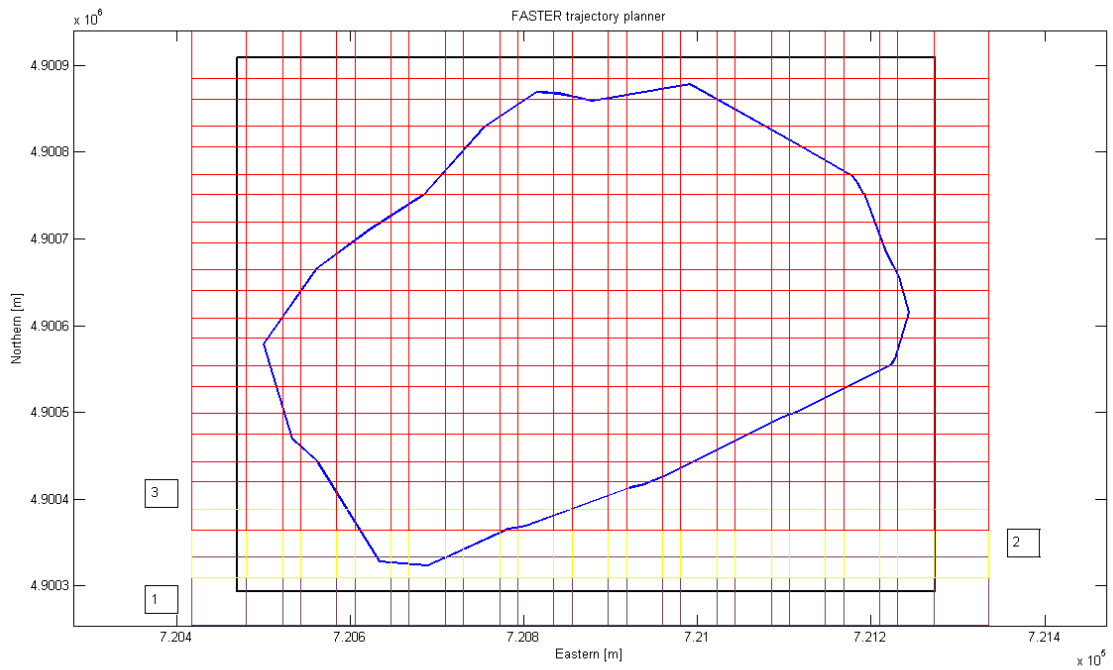


Figure 48: Particular of the target area

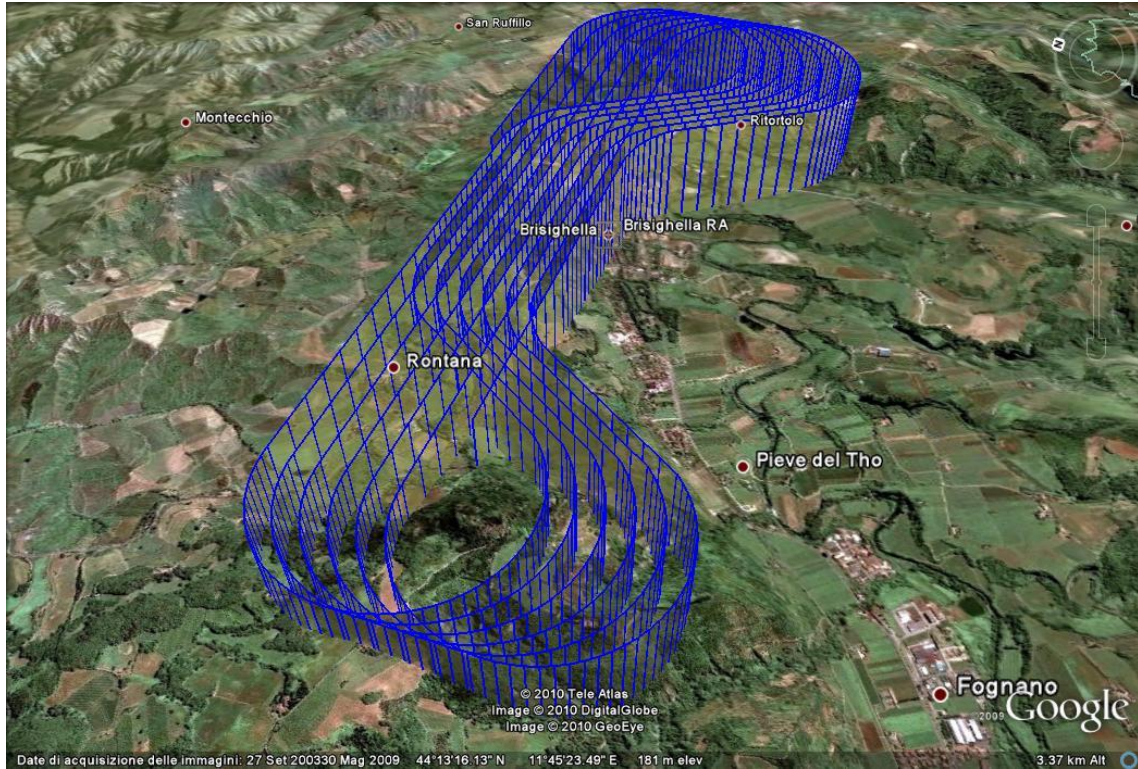


Figure 49: Planned trajectory exported in a KML file and visualized inside Google Earth

The final trajectory is saved in a *trajectory.mat* file that will be used in the FASTER Airborne internal management and computing unit to generate the guidance tunnel that will be displayed to the pilot during flight operations. Computed parameters are printed in a text file, values corresponding to the example used in the previous figures are summarized in the following table.

<i>FASTER_planner.m</i> outputs				
Inputs	Camera Δt_l [s]	A.T exposures	Stripes	Images
Surrounding area offset = 30 m; $V_{gs} = 28.5$ m/s; Camera sensor size = APS-C, (22.2x14.8 mm); Crop factor = 1.66 X; $f = 28.5$ mm; $FOV = 74^\circ$ (65°/46°); $o = 40$ %; $p = 30$ %;	2.23 (0.45 fps)	13	13	169
	Computed Flight Height			
	615 m			
	Estimated data size			
	2.2 Gbytes			
	Estimated over flight time			
	39 min			
	Total number of waypoints			
1126				

Table 5:FASTER_planner.m computed flight parameters

Multiple areas can be managed inside the same flight plan but transfers between each areas are actually not computed by script. This because of the specific ULA regulation which doesn't allow these aircrafts to over flight densely populated areas or enter a controlled airspace. All these constraints are very difficult to implement in the planning software, so navigation outside the target area is currently a pilot responsibility.

Chapter 6. FASTER Engineering Model

As seen in the previous chapter, the FASTER EM includes three main parts:

- The Ground Segment infrastructure
- The Airborne internal management and computing segment
- The Airborne external POD, equipped with the sensing devices

In this section a complete description of the internal management and computing segment, which is the most important and crucial part of the entire FASTER EM system will be given, describing how the functional requirements, presented in Chapter 4, were met in the development of the FASTER Engineering Model. In Table 6 functional requirements are again presented and for each of them their relative status of implementation reached in the EM (*I= Implemented; PI=Partially Implemented, NI=Not implemented*).

name	Requirements	EM Implementation
Functional Requirements		
RE.F.01	The system shall have the capability to acquire high resolution Earth images over a large portion of the electromagnetic spectrum (ranging from visible to the thermal infrared interval, $0.3 \mu\text{m} < \lambda < 14 \mu\text{m}$)	PI
RE.F.02	The system shall be able to control and acquire more than one sensing device using different hardware interfaces	PI
RE.F.03	Given the target area, the system shall be able to generate an appropriate trajectory starting from the departure aerodrome to last selected waypoint	I
RE.F.04	The system shall be able to guide the pilot through the previously planned flight	I
RE.F.05	The system shall be able to acquire images of the selected area only; the system shall be able to know its position with respect to the target area	PI

	automatically enabling the acquisition process	
RE.F.06	Images shall be acquired so that image mosaicing can be successfully accomplished during both real time processing or postprocessing operations	PI
RE.F.07	Images and final mosaic shall be georeferenced during both real time or post-processing operations	PI
RE.F.08	The system shall be able to acquire a DEM of the target area in order to generate orthophotos	NI
RE.F.09	All the acquired data must be stored in order to be available at a later time	I
RE.F.10	The pilot shall be able to interact with the system in order to make any changes to the preloaded flight plan	PI
RE.F.11	The system shall have a totally independent power source	I

Table 6: FASTER functional requirements and some notes on their implementation on EM model

As shown in Table 6 , some of the requirements relative to the final FASTER system, are not completely fulfilled because the effort has been focused on the realization of a working system, with reduced functionalities, ready to be employed in a first test phase. Having to start from scratch RE.F.01, RE.F.02, RE.F.05, RE.F.06, RE.F.07 and RE.F.10 were only partially implemented:

- *RE.F.01/02*, a single camera (DSLR) working in the visible spectrum has been installed on the external POD while different hardware interfaces are available for sensor connections like USB and GiGE (Gigabit Ethernet protocol used for GIGE cameras)
- *RE.F.05*, at present the system is controlled by the pilot (or the system operator) which manually enables the acquisition phase once entering the target area for monitoring
- *RE.F.06*, no automatic mosaicing algorithms have been implemented, data is stored onboard and the mosaicing operation is performed off-line on the ground
- *RE.F.07*, images are stored sequentially according to the flight data log; on ground each image is associated with its ancillary data (state vector)
- *RE.F.10*, the flight plan cannot be changed during airborne operations
- *RE.F.08* is not implemented because of the need of at least two cameras in order to perform 3-Dimensional reconstruction of the acquired scene

Despite these requirement relaxations, the result is compliant with the initial idea of a functioning test bed able to guarantee sufficient performances in order gain experience in the process of realization of the final system.

In order to proceed to the definition of the system, a functional block diagram of the airborne internal management and computing system has been drawn and is shown in Figure 50. The unit is managed by the *Data Acquisition and Camera Timing* block which receives position and attitude data respectively from the G.P.S receiver and the Inertial Measurement Unit. The camera arm switch controls the image acquisition mode and is activated by the pilot once overflying the target area. If the camera switch is armed the unit sends to the acquisition devices an appropriate electric signal controlling the shooting mode. The entire flight plan (list of 3-Dimensional waypoints) is loaded before flight directly from the ground segment infrastructure, using the flight planner described in Chapter 4.

The flight plan is presented to the pilot using the “tunnel in the sky” visual interface, which through a geometrical interpolation of the reference waypoints, displays the pre-computed trajectory.

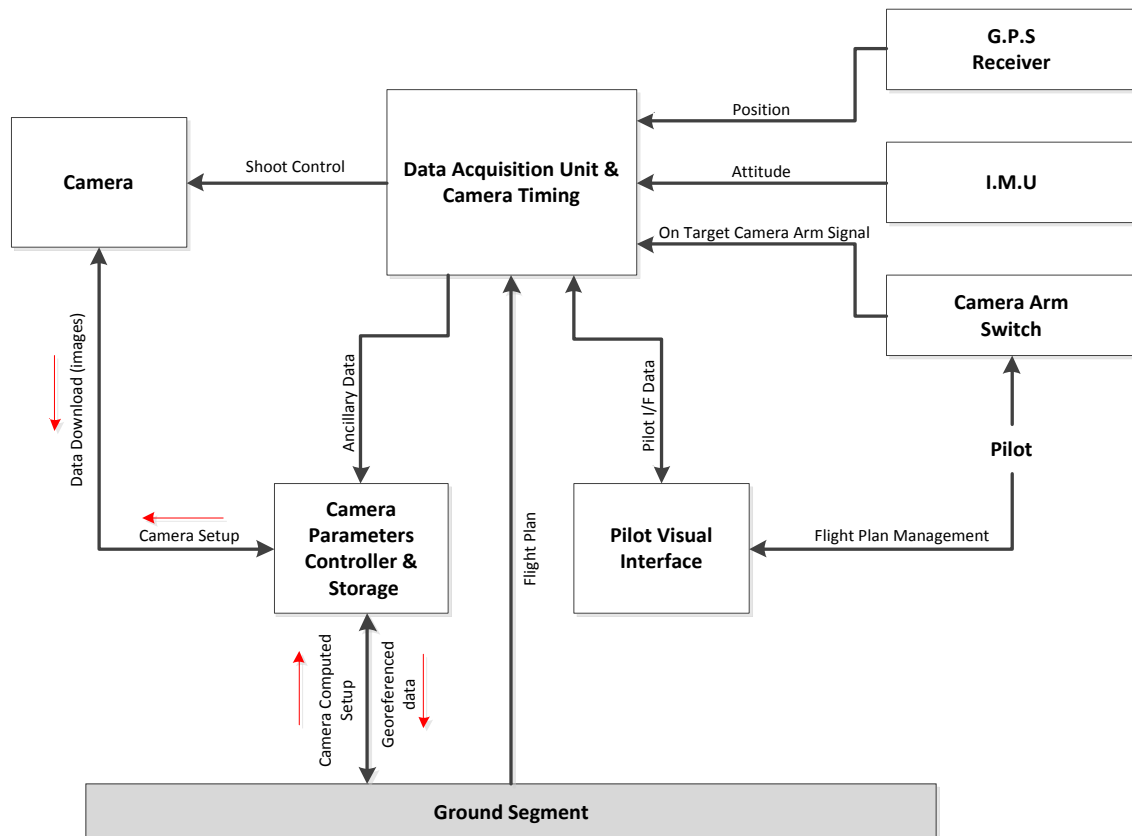


Figure 50: Airborne internal management and computing system functional layout

Acquisition devices configuration (i.e. aperture and exposure time) is setup via the *camera parameters controller and storage* block which also includes the support for image data saving and download to the G.S; camera parameters are passed to this unit from the ground equipment which selects the appropriate values for aperture and exposure time.

Starting from the layout shown in Figure 50 and thanks to previous experiences gained in previous projects involving sensor integration and data logging, it has been possible to compile a list of all the necessary hardware for the realization of the FASTER EM, which is mainly based on the integration of COTS (*Commercial Off The Shelf*) components. As a matter of fact, after a series of trade-off, it was decided to use PC boards both for sensors acquisition and camera control in order to concentrate only on developing the necessary software.

In the next section the hardware list and the proposed layout will be discussed describing all the selected components and their electronic and electric interconnections, while Section 6.5 will be focused on the design of the software environment which has been developed using the Matlab/Simulink package.

6.1 FASTER EM Hardware layout

The FASTER EM hardware layout is presented in Figure 51. All the components, except the Canon EOS 450 camera which is contained in the external pod, are installed inside a 19 inch, 2 unit aluminum rack box. In the diagram, boxes represent the physical instrumentation while arrows, in different colors depending on the connection type, show the connections between each subsystem:

- Red lines are used to identify power connections;
- Black lines for point to point RS232 serial connections;
- Green lines for high speed USBs (Universal Serial Bus);
- Violet lines for 100 Mbit/s Ethernet connections,
- Orange lines represent two G.P.I.O (General Purpose Input-Output) connected to a parallel port on the PC/104 board
- The blue line is the VGA connection between the Windows based VIA EPIA and the LCD screen

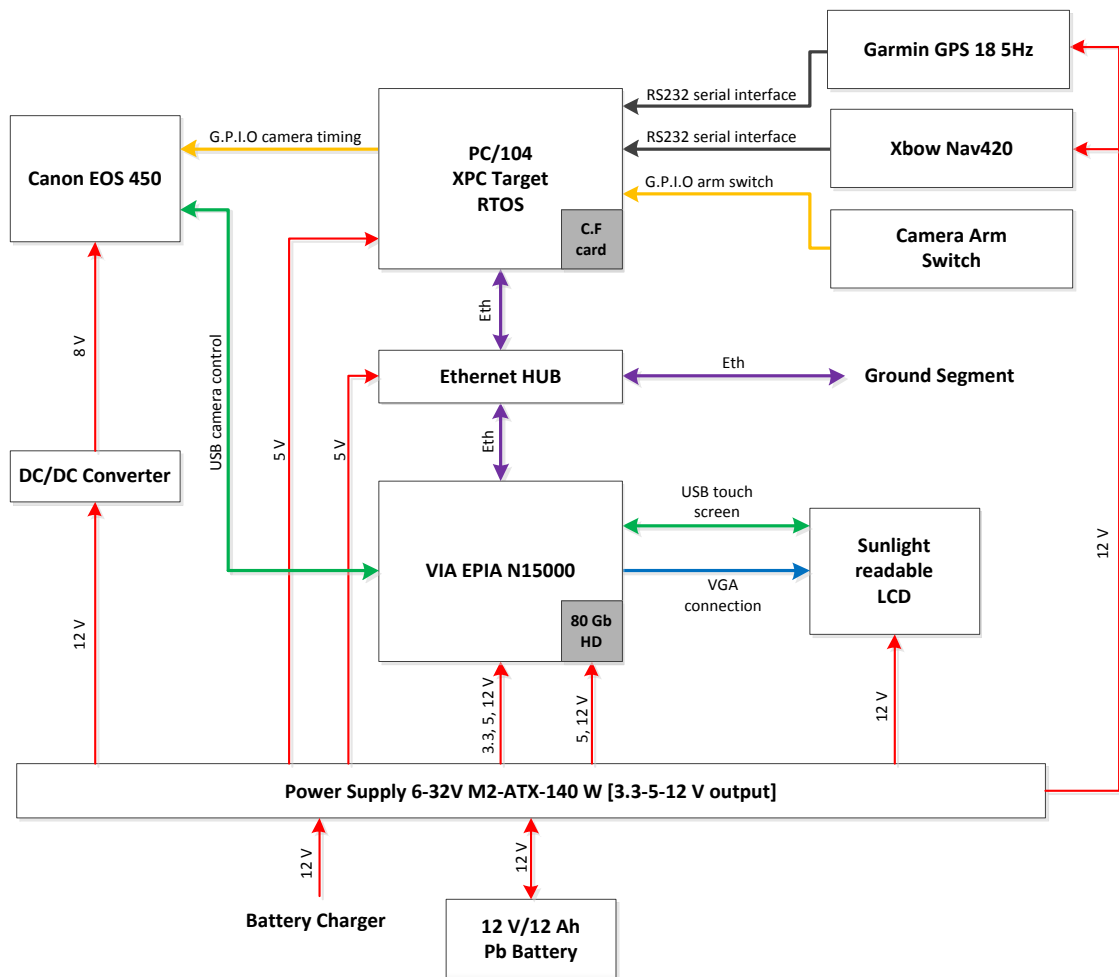


Figure 51: FASTER EM Hardware Layout

6.1.1 Sensors And Data Logger

The PC/104+ module (90 x 96 mm) act essentially as a data logger, collecting data from different sources; is made by Advantech and is equipped with an AMD LX800R fanless cpu (functioning at a maximum frequency of 500 MHz), a soldered module of 256 MByte of DDR RAM memory and a 10/100 PCI Ethernet interface. On board three RS232 port and one configurable RS232/422/485 are available, together with a parallel port which supports SPP/ECC/ECP modes [Ref (30)]. Apart from size, the PC/104+ format has several advantages with respect a standard PC ATX architecture: power consumption is considerably lower reducing or negating thermal management issues and they are built to function in harsh environment where vibrations and g-forces loading must be taken into account.

As shown in the previous picture, two RS232 ports are used to acquire position and attitude data from the Garmin GPS 18 receiver and the Crossbow I.M.U. The Ethernet

connections are used to send the state vector (which in addition to position and attitude data store also a reference time and the magnetic field components) to the EPIA EN15000 throughout the User Datagram Protocol (*UDP*). The UDP uses a simple transmission model and is often used in time-sensitive applications because dropping packets is preferable to waiting for delayed packets which may cause the system to not properly work.

Parallel port controls the camera shooting mode, sending an electric impulse which substitutes the pressure of the shutter button, and acquires the camera arm switch position which enables image acquisition. The XPC Target real time operative system is installed on a 512 Mb Compact Flash card on the back side of the board. A picture of the board with its mechanical drawing is shown on Figure 52.

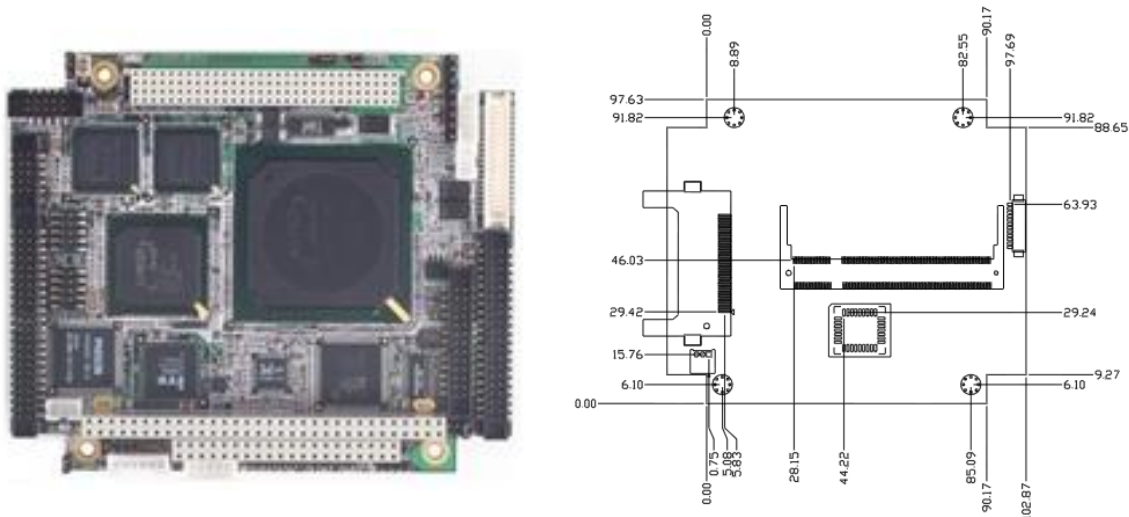


Figure 52: Advantech 3353 PC104+ board and mechanical drawing [Ref. (31)]

The GPS receiver is a Garmin 18x 5Hz (Figure 53), an OEM high-sensitivity GPS sensor for use in guidance applications where a more frequent update of position and velocity (instead of 1 Hz) can improve the measurement accuracy and trajectory reconstruction, especially when coupled with high frequency devices like the inertial units (100-500 Hz) in a Kalman filter estimator.

It has a 12-parallel-channel and is WAAS (*Wide Area Augmentation System*) enabled so it is possible to use in Europe the EGNOS (*European Geostationary Navigation Overlay Service*) differential correction in order to get a typical accuracy in position determination $< 3\text{ m}$ and of 0.1 kts RMS steady state [Ref (32)]. It is connected to the PC104+ data logger via a RS232 serial connection at 38400 bps (8 data bits, 1 stop bit, no

parity bit) using the NMEA (*National Marine Electronics Association*) 0183 ASCII interface specification (GPGGA, GPRMC, GPVTG and PGRMV sentences are currently used).



Figure 53: Garmin GPS 18x 5Hz and its mechanical drawing [Ref. (33)]

The Crossbow NAV420 is a combined GPS navigation and GPS-Aided Attitude & Heading Reference system (*AHRS*) that utilizes high stability MEMS-based inertial sensors. Internally A 16 bit A/D converter acquires data from several sensors: a tri-axial accelerometer, a tri-axial rate sensor, a tri-axial magnetometer and a temperature sensor; the digital output and the GPS data is computed by an high speed sampling&DSP which provides sensor compensation (factory calibration data, stored in an internal eeprom is used by the DSP to remove temperature bias, misalignment, scale factors errors and non-linearities from the sensor data) and applies a full-state Kalman filter algorithm resulting in a state vector composed by GPS position (x,y,z); Velocity (x,y,z); Acceleration (x,y,z); Roll, Pitch and Heading; 3-axis angular rate and the UTC time. The update rate is set to 100 Hz and under static conditions is possible to have fully stabilized data in about 60 seconds from power up [Ref (34)].

Due to some problems with the external GPS active antenna, for the purpose of this study, the “navigation mode” provided by the I.M.U has not been used. Instead of the “navigation mode”, the NAV420 has been utilized in “angle mode” acting as a complete attitude and heading reference system giving as output the stabilized pitch, roll and yaw angles together with the angular rates, accelerations along the 3 axis and the components of the magnetic field. In the “angle mode” the onboard EKF tracks the rate sensor bias and calculates the stabilized outputs. Accelerometers are used to correct for rate sensor drift in pitch and roll, while magnetometers to correct for rate sensor drift in the yaw angle.

Missing GPS data prevent magnetic declination determination so the computed heading coming from magnetometers is relative to the magnetic north direction instead of the true north direction; true heading is thus provided by the Garmin GPS receiver. NAV420 accuracy is reported in the following table.

NAV420 Accuracy		
Specification	GPS disabled	GPS enabled
X,Y Velocity [m/s rms]	N.S	< 0.4
Z velocity [m/s rms]	N.S	< 0.5
Attitude angles [° rms]	< 2.5	< 0.75
Bias: R,P,Y (EKF stabilized) [°/sec]	< ±0.1	< ±0.1

Table 7: Crossbow NAV420 measurement accuracy



Figure 54: Crossbow NAV420 and its mechanical drawing [Ref. (35)]

6.1.2 Visualization and data storage

The second PC based board is a mini-itx (170 x 170 mm) VIA EPIA EN15000, powered by a VIA C7 cpu running at 1.5 GHz and provided with a 1 Gbyte of DDR2 RAM memory, a Gigabit Ethernet interface and an integrated VIA UniChrome Pro AGP graphics card with up to 64 Mbyte of shared memory [Ref (36)]. The EPIA EN15000 has two SATA II ports, one of which is occupied by a 3.5” 80 Gbyte hard disk used to store the images coming from the Canon EOS camera; RS232 and VGA ports are available too. This kind of embedded PC solution has been selected because of the need to guarantee a sufficient graphical performance in 3D graphic, although another PC/104 board should represents a better choice in term of reliability.

The Canon EOS is connected to the EPIA via an USB port using the widely supported Picture Transfer Protocol (*PTP*) developed by the International Imaging Industry Association to allow the transfer of images from digital cameras to computers without the need of additional device drivers. In this case the protocol has been custom modified by Canon to fully support camera parameters control, replicating the same functions accessible from the hardware buttons on the camera. The second USB port is used by the touch screen interface installed on the LCD monitor (video signal passes through the VGA port).

The EPIA is not completely fanless due to the thermal requirements of the integrated modules, so a small 20 x 20 mm fan is mounted on the top of an aluminum heat sink (Figure 55).

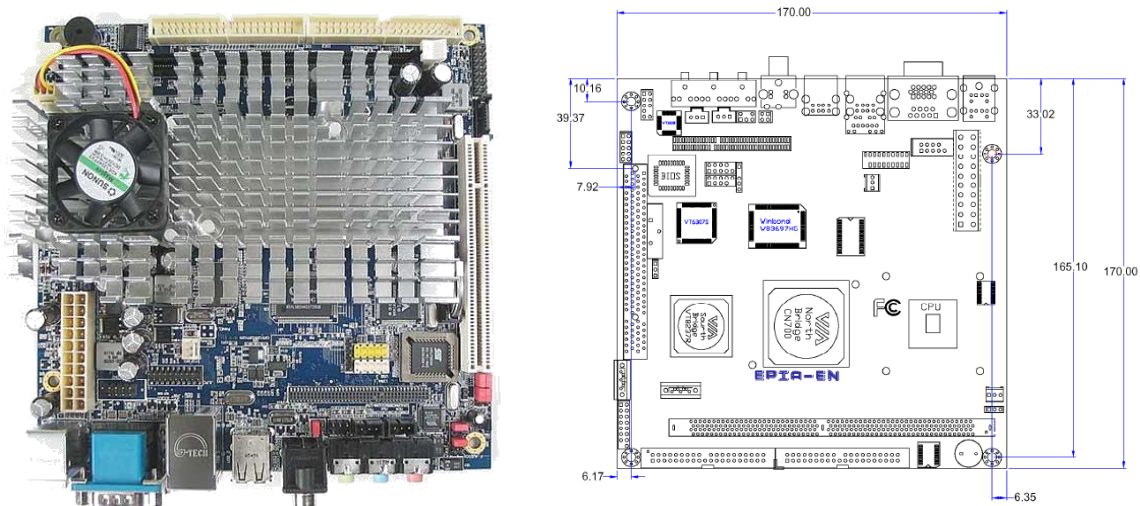


Figure 55: VIA EPIA EN15000 board and mechanical drawing [Ref.(37)]

Onboard is installed a Windows XP operative system needed to run the Dynaworlds simulation environment, the Canon camera control center and the java-based FASTER display, which constantly monitors the entire system status (GPS and I.M.U activity, signal quality, WAAS correction, number of received satellites, latitude, longitude, camera arm switch position and number of acquired frames).

To display the “tunnel in the sky” pilot interface an 8.4” high brightness (1000 nit) sunlight readable LCD is used. The open frame Litemax DLH0835 is equipped with a LED backlight and has been selected in order to solve visibility problems encountered inside the aircraft cockpit when incident light strikes the monitor surface (Figure 56). Screen resolution is 800x600 pixels and the optional 4 wire resistive touch screen film is

connected via a USB port to the EPIA EN15000. The LCD matrix is mounted on a fiberglass support jointly with the AD5621GA control board (VGA and power connector), the LI0610A inverter board and the LID08A LED driving board [Ref (38), (39), (40), (41)].

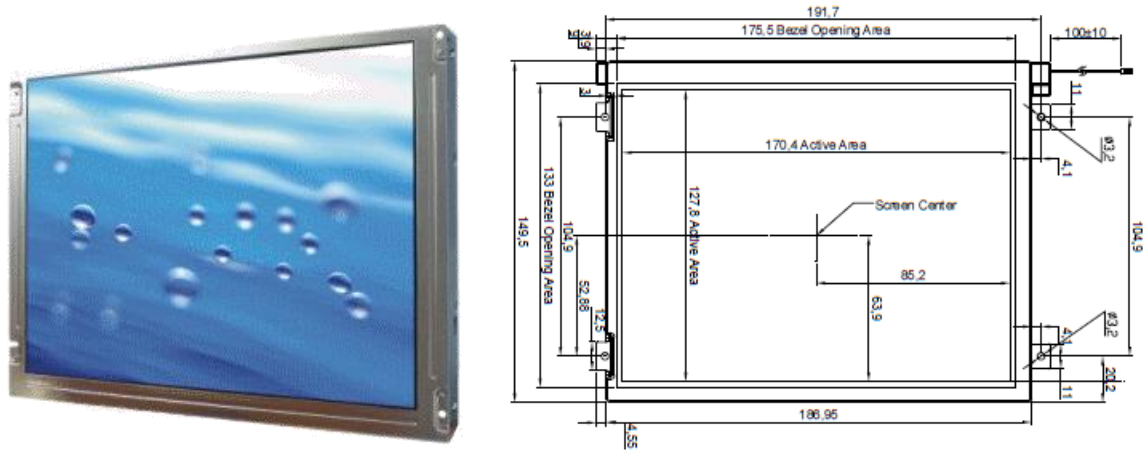


Figure 56: Litemax 8.4" high brightness LCD display and its mechanical drawing [Ref. (42)]

6.1.3 Sensing Device

The selected sensing device is a commercial DSLR (Digital Single Lens Reflex) camera, the Canon EOS 450 coupled with a fixed focal length 28 mm lens Canon EF28 f/2.8 (Figure 57). The EOS is equipped with a 22.2 x 14.8 mm CMOS sensor (APS-C format, 3:2 aspect ratio, 1.6x FOV crop) with a total amount of 12.2 million effective pixels (12.4 million total pixels considering also the dark area used for automatic sensor calibration). Sensor matrix is composed by 4272 columns and 2848 rows with a pixel pitch of 5.2 μm . In order to obtain the maximum image quality, images are saved in an uncompressed 14-bit RAW format [Ref. (43)].



Figure 57: Canon EOS 450 and Canon EF28 f/2.8 [Re.(6)]

The camera has an all plastic structure so it is therefore necessary an adequate protection when installed outside the aircraft.

It is fixed on a rapid prototyping plastic base which has been designed to perfect fit the lower part of the camera body, avoiding rotations once it is mounted. To realize the base, the EOS body has been digitalized through a three-dimensional scanner allowing the extraction of the lower surface; the surface has been subsequently extruded to create a printable solid. To achieve a better fixation the camera tripod mounting hole was used too; the plastic base is provided with four holes used to install the assembly inside the external pod. The supplied battery pack (Li-Ion, 7.4 V, 1050 mAh) usually in standard operations guarantees no more than 300 shots, so it has been replaced with a power supply adapter which permits a continuous power-on mode.

A built in SD card reader (with SDHC up to 32 Gbyte compatibility) is used only when high frequency (1-3 fps) acquisition is needed. This because of the low USB data transfer rate, which is suitable only for low frame rate (< 1 fps).



Figure 58: Canon EOS 450D fixed in the rapid prototyping base; lens focus ring has been blocked to avoid ring movements during flight

The camera is normally set to manual mode to permit an enhanced management of the acquisition parameters. Camera configuration is managed by a very light, custom

modified, C++ based remote camera control software available from the Canon SDK support.

6.2 Power Subsystem

As shown in Figure 51, the FASTER EM power subsystem includes the M2-ATX-140W automotive power supply, the 12 to 8 V DC-DC converter and the 12 Ah-12V lead battery. The power supply covers a wide range of input voltages, 6 to 32 V and provides the standard outputs for digital electronics: +3.3, +5, +5_{SB}, and ±12 V with maximum current values reported in Table 8.

A standard 24-wire ATX power cable is used to power the EPIA EN15000 but only a 2-wire 5 V cable is needed by the PC/104 [Ref. (44)]. All other devices are powered using the 12 V bus while for the Canon EOS has been necessary to develop a custom DC-DC converter in order to guarantee the same Li-Ion battery voltage (8 V, slightly higher with respect the nominal value of 7.4 V).

Maximum Power Characteristics		
Output [V]	Current (max continuative) [A]	Current Peak (< 60 s) [A]
3.3	6	8
5	6	8
5 _{SB}	1.5	2
12	7	8

Table 8: M2-ATX-140W maximum power characteristics

A lead acid battery has been selected because of its simple recharge circuit, which does not require special precautions, although Pb batteries have the lowest energy density (30-40 Wh/Kg) and a modest cycle durability (500-800 cycles). The FASTER EM can also be powered via a standard laboratory power supply or, if available, connected directly to a 12 V stabilized power source onboard the aircraft, bypassing the battery. Power consumption has been measured for each component using an amperometer connected to the M2-ATX power supply, so currents are so referred to the 12 V bus.

Results are shown in Table 9, the computed battery duration is about 2 hours and 40 minutes which is slightly better of what experienced during test campaigns. This is probably due to the cpu load variation of the EPIA EN15000 which has a maximum power consumption of about 50 W at full load.

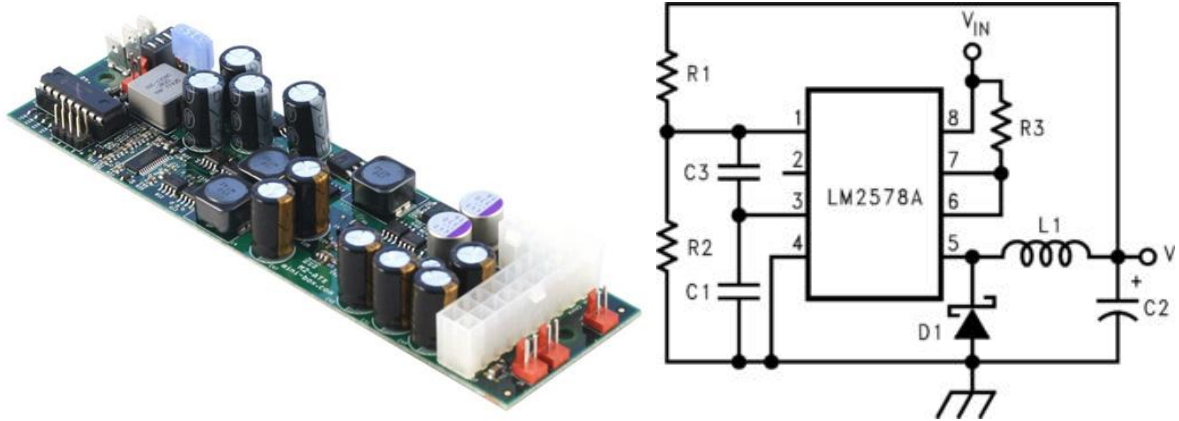


Figure 59: M2-ATX-140W power supply [Ref. (45)] (a) and the DC-DC converter used to power the camera (b)

FASTER EM measured power consumption				
Component	Status	Voltage	Current	Power
VIA EPIA EN15000/HD/Ethernet Hub	Stand by	12 V	0,12 A	1,44 W
	Startup	12 V	3 A	36 W
	Idle	12 V	1,65 A	19,8 W
	Medium load	12 V	2 A	24 W
Advantech PC/104+	On	12 V	0,8 A	9,6 W
Garmin GPS 18x 5Hz	On	12 V	0,05 A	0,6 W
Crossbow NAV420	On	12 V	0,35 A	4,2 W
Canon EOS 450D	On	12 V	0,1 A	1,2 W
	Shooting	12 V	0,4 A	4,8 W
Litemax 8,4" LCD	Stand by	12 V	0,08 A	0,96 W
	On	12 V	0,86 A	10,32 W
Total (during image acquisition)		12 V	4,46 A	53,52 W
Battery estimated duration (12 V, 12 Ah)		2h 40 min		

Table 9:FASTER EM measured power consumption

6.3 Airborne External POD Assembly

Sensing devices must be installed in specific areas of the aircraft clear of any possible obstacles that may create even a partial occlusions of the field of view and possibly not too far from aircraft center of gravity in order to minimize maneuver effects. Unfortunately it is often difficult to take advantage of these areas (depending on aircraft aerodynamic configuration, suitable zones are on the lower part of the fuselage, under the cockpit, or on fuselage sides) because typically, are very difficult to reach because of the lack of specific fixtures or the need to make major changes to the fuselage itself.

During the development of the FASTER EM we had the opportunity to have at our disposal a Tecnam P92, which is one of the most popular ULA (*Ultra Light Aircraft*) in Italy. It is a single-engine high-wing aircraft which employs a monocoque tail cone section with the forward fuselage using sheet aluminum over steel tubing [Ref. (46)].

After a careful inspection of the P92, the most suitable solution found was to fix an external POD, containing the camera, to the lower structure of the plane in the passenger door area, using a c-shaped bracket. This configuration allows also to pass all the necessary cable (power, usb and camera shooting) through the door, to reach the internal computing and management unit placed behind the two seats. The c-shaped bracket is made of folded aluminum, 5 mm thick to prevent door misalignment once it is closed and it is blocked to the airplane structure using two threaded bolt. Being very close to the engine mount, especially at high rpm, vibrations may have adverse effects on image quality (blur) so an insulating neoprene adhesive has been placed between the fuselage and the supporting bracket.

The bracket is then attached to a wood base on which is mounted the EOS camera through the plastic adaptor, described in section 5.1.3. 4 small silent blocks are placed between the plastic adaptor and the wood base. For security reasons iron wire is used as an emergency retain system in case of failure.

In order to protect the camera from relative wind and possible impacts during landing, an aerodynamic canopy has been designed and realized. For this purpose the three-dimensional model of the EOS camera, including also the plastic adapter and silent blocks, was used to identify a reference volume that has to be covered by the canopy and the final shape has been founded using a spline interpolation of 6 points.

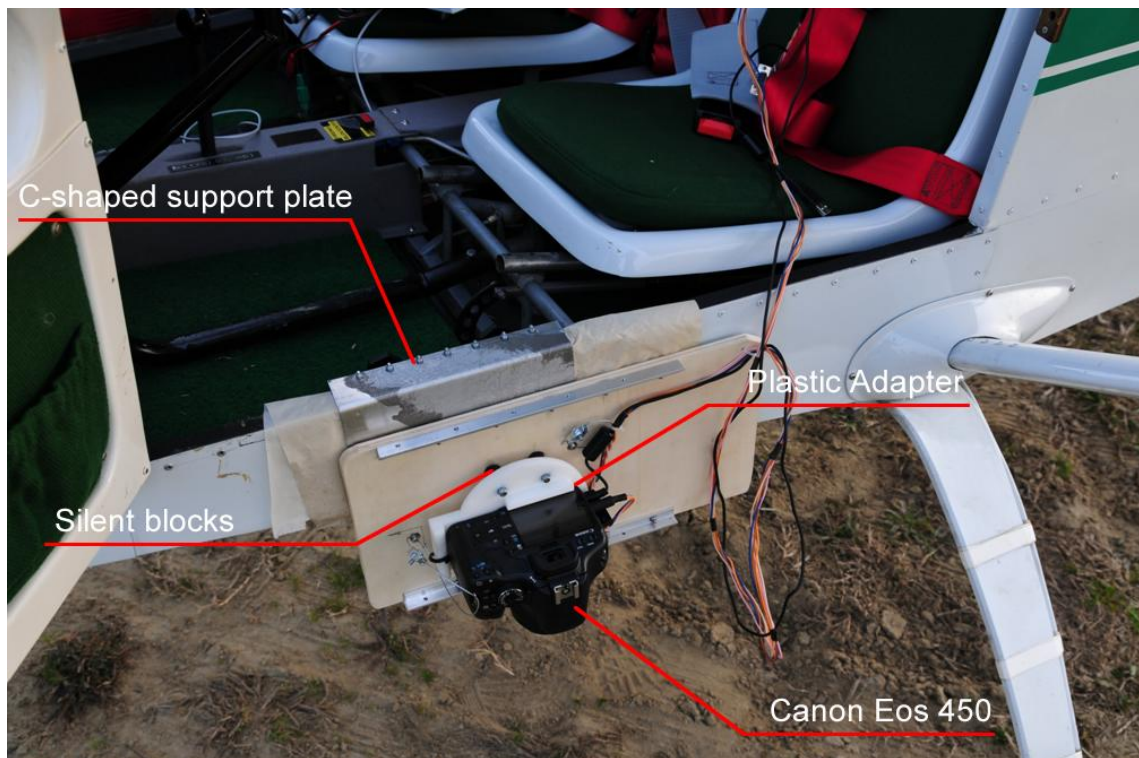


Figure 60: Tecnam P92 selected mounting area for the external POD

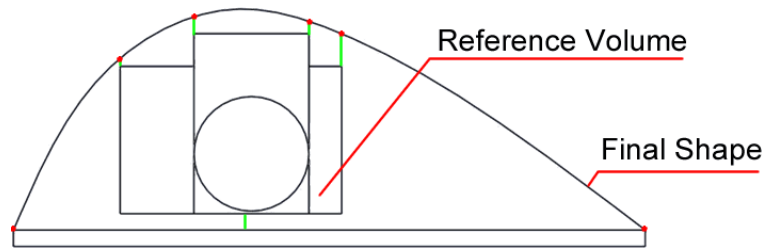


Figure 61: Canopy section

After the definition of the canopy section profile, it has been extruded along the whole wood base in order to create a reference polystyrene solid to be used as a mold for fiberglass drafting. Once the fiberglass canopy model has been realized it has been refined and painted in order to obtain a smooth surface; a 70 mm diameter aperture was created on the lower surface for camera use and two series of 5 fixing holes have been made both in the upper and lower surfaces for the connection with the wood base.

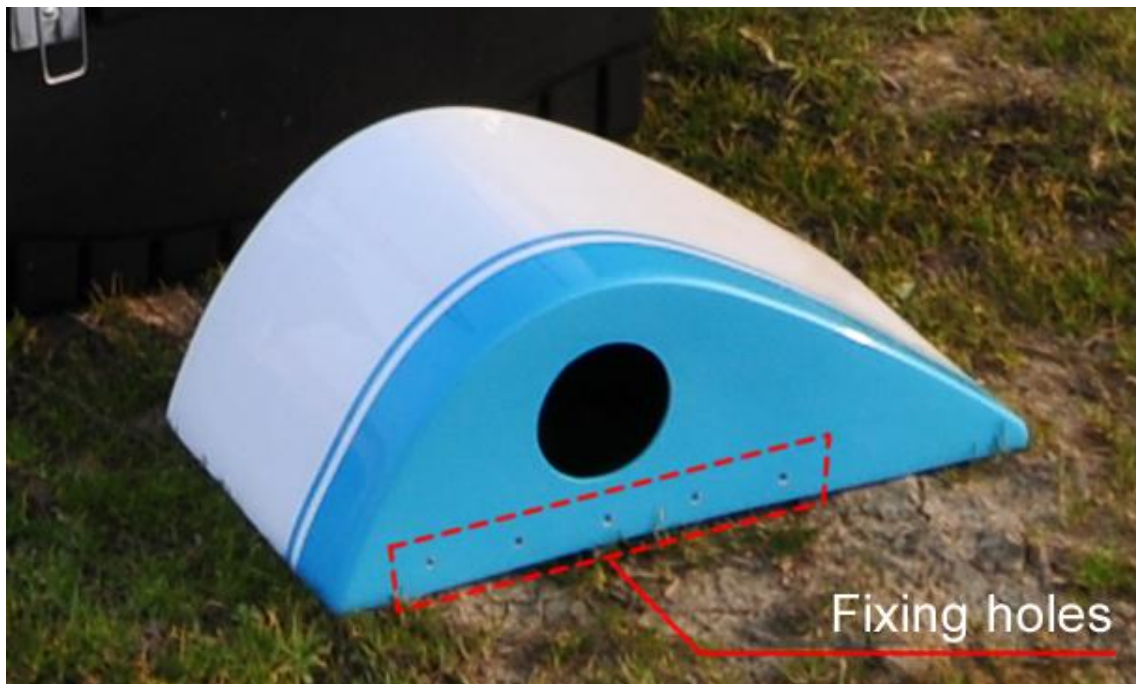


Figure 62: Canopy lower side features



Figure 63: FASTER EM fiberglass canopy installed on Tecnam P92 passenger side

6.4 Airborne Internal Management and Computing Unit Assembly

The airborne internal management unit is entirely fit inside a 19 inches, 2U custom modified rack aluminum rack enclosure. Being the prototype an engineering model, there are some differences between this and the final FASTER system that will be compliant to all the requirements specified in Chapter 4. One of the main difference is the hardware positioning; for direct georeferencing purposes the origin of the reference systems of GPS antenna, I.M.U and camera sensor must be know and compensated in order to maintain the predicted accuracy during the frame georeferencing process, otherwise errors may arise due to fact that position and attitude are referred to different reference systems.

During the first test campaigns, however, was preferred to leave both the I.M.U and the GPS receiver inside the aircraft because they are two of the most expensive FASTER components and it would be risky to put them inside the external pod when this had never been tested before. The I.M.U was installed inside the internal management and computing unit while for the GPS has been prepared an external DB15 connector; the antenna/receiver was typically placed on the dashboard to improve reception.

Port layout is shown in Figure 64 and as it can be seen, two DB15, 12V powered connectors are available and just one is used to power the LCD display. Camera shooting signal and the 8V bus are put together in a DB9 connector while only 3 pin of the DB25

are currently enabled to connect the camera arm switch, others can be employed to driver LEDs or to pilot an external alphanumeric display to monitor the system functioning status. At present there is no possibility to power off or reset single components in case of failure, but this function will be implemented in the upcoming version. The battery charger works only when the master switch is turned off; an external power supply can be used

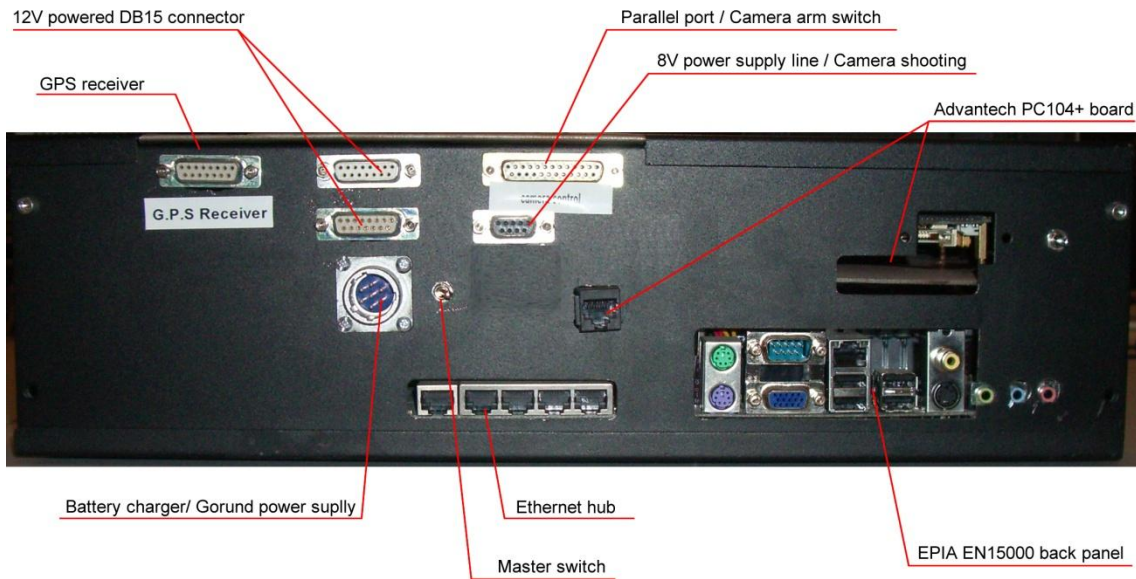


Figure 64: FASTER airborne internal and computing unit front panel



Figure 65: FASTER airborne internal and computing unit installed onboard the Tecnam P92



Figure 66: FASTER airborne internal and computing unit inside view of the rack box

6.5 FASTER EM Software Description

To allow the proper functioning of all hardware components was necessary to develop appropriate software algorithms. In particular, because many of the Windows-based applications for the tunnel in the sky visualization and camera control, only needed to be fine tuned, most of the efforts were spent on the realization of the Real Time Operating System that equips the Advantech PC104+ board. This was the most critical application indeed, because of its key role in the entire processing chain: except for images, all the other data is collected by this processing unit.

To speed up the development process, the model was made in the Matlab/Simulink environment, using many of the functions that the suite provides, like the xPC Target solution. This toolbox offers some advantages for prototyping, testing and deploying real-time systems using standard PC hardware. The target application is designed and built on a Matlab workstation and could be based on a Simulink model; the same model can also be run in nonreal-time for debugging purposes. Then an executable target application can

be created using the Real-Time Workshop and a C compiler; this will run on a compatible target PC in real-time mode using the same initial parameters from the Simulink model that were available at the time of code generation [Ref. (47)].

The target PC is booted using an xPC Target boot disk (or from a network boot image) that loads the xPC Target real-time kernel and then the target application can be downloaded from the host machine. xPC Target software uses the real-time resources on the target PC hardware and based on the selected sample rate it uses interrupts to step the model at the proper rate. With each new interrupt, the target application computes all the block outputs from the model. In some cases the xPC Target Embedded option can be useful because allows the standalone operational mode, in which target application and real-time kernel are combined and booted together on the target PC, from an hard drive or a flash memory. The target application can be provided with the same scopes used in the Simulink model, so if the target PC has a display connection, system status can be continuously monitored; otherwise signal data can be stored in RAM or log files can be written on a mass memory.

The xPC Target module has an extensive block library which supports the most common I/O functions(48), including:

- Analog input and output;
- Digital input and output;
- RS232/422/485 support for serial communication with external devices;
- UDP support for communications with other systems using the standard UDP/IP network protocol;

xPC Target also supports a wide range of PC and I/O boards including, especially, the Advantech PC/104+ board used for the FASTER engineering model. In this case, the embedded option was used because the system works all time as a standalone application and tuning of the internal parameters is possible only before the system startup, modifying directly the source files stored on the Compact Flash support.

The Simulink model is shown in Figure 67 and it is composed by six main parts: the GPS acquisition block; the IMU acquisition block; an external magnetometer (currently not in use) acquisition block; the Tunnel In The Sky management block; the EOS 450 shot control and camera arm switch acquisition block, the data log management block and a block that sends data to the FASTER system monitor. In the following paragraphs a detailed description of each block will be given.

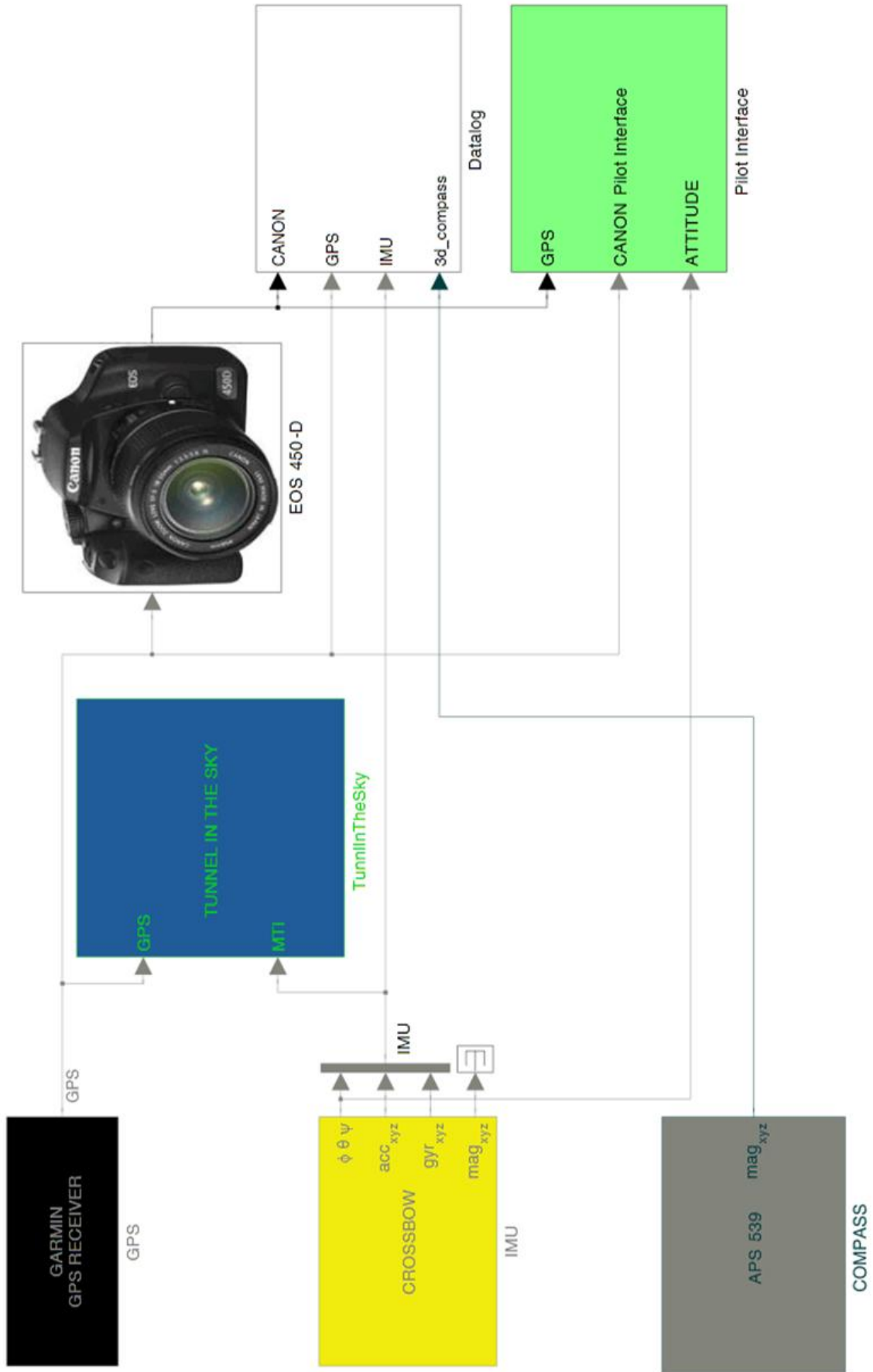


Figure 67: FASTER EM Simulink model

6.5.1 Garmin GPS 18 5Hz Acquisition Block

The Garmin GPS 18 5Hz block acquires data packets from the receiver decoding each sentence and the corresponding Simulink model is shown in Figure 68. For this specific application only the following sentences were enabled:

- GP-GGA, described in Table 10
- GP-VTG, described in Table 11
- GP-RMC, described in Table 12
- GP-RMV, described in Table 13

The GP suffix indicates that sentences are compliant to the NMEA 0183 standard [Ref. (49)] but via a proprietary implementation. The transmission time of the entire subset of enabled sentences, with a 38400 bps serial connection, is 61.18 ms, far below the maximum allowed time, which at a 5 Hz of refresh rate, is 200 ms.

The *Baseboard RS232 Send-Receive FIFO* out block is used to get data from one of the two serial ports and with a First In First Out logic the incoming data is passed to a FIFO headers reading block which separates the different sentences. Each sentence has a dedicated decoding block in which the data is read, split into single variables and converted in double numerical values. Not all the information contained in the sentences are used thus some are discharged using a terminal block. A cyclic redundancy check is performed in each decoding block and prevent corrupted data to be propagated inside the model; in this case decoded data is tagged as not updated and the previous output is maintained.

A final multiplexer packets the variables in a single GPS vector which constitutes the block output.

Global Positioning System Fix Data (GGA)		Used
Syntax	\$GPGGA, <1>, <2>, <3>, <4>, <5>, <6>, <7>, <8>, <9>, M, <10>, M, <11>, <12>, *hh<CR><LF>	
<1>	UTC time of position fix, hhmmss.s format	Y
<2>	Latitude, ddmm.mmmmm (leading zeros will be transmitted)	Y
<3>	Latitude hemisphere, N or S	Y
<4>	Longitude, dddmm.mmmmm (leading zeros will be transmitted)	Y
<5>	Longitude hemisphere, E o W	Y
<6>	GPS quality indication, 0 = fix not available, 1 = Non-differential GPS fix available, 2 = Differential GPS (WAAS) fix available, 6 = Estimated	Y
<7>	Number of satellites in use, 00 to 12 (leading zeros will be transmitted)	Y
<8>	Horizontal dilution of precision, 0.5 to 99.9	N
<9>	Antenna height above/below mean sea level, -9999.9 to 99999.9	Y

	meters	
<10>	Geoidal height, -999.9 to 9999.9 meters	N
<11>	Null (Differential GPS)	N
<12>	Null (Differential Reference Station ID)	N

Table 10: GPGGA sentence structure

Track Made Good and Ground Speed (VTG)		Used
Syntax	\$GPVTG, <1>,T, <2>,M, <3>,N, <4>,K, <5>*hh<CR><LF>	
<1>	True course over ground, 000.0 to 359.0 degrees (leading zeros will be transmitted)	N
<2>	Magnetic course over ground, 000.0 to 359.0 degrees (leading zeros will be transmitted)	N
<3>	Speed over ground, 000.00 to 999.99 Knots (leading zeros will be transmitted)	N
<4>	Speed over ground, 0000.00 to 1851.89 Km/h (leading zeros will be transmitted)	Y
<5>	Mode indicator: A = Autonomous, D = Differential, E = Estimated, N = Data not valid	N

Table 11: GPVTG sentence structure

Recommended Minimum Specific GPS/TRANSIT Data (RMC)		Used
Syntax	\$GPRMC, <1>,<2>,<3>,<4>,<5>,<6>,<7>,<8>,<9>, <10>, <11>,<12>,*hh<CR><LF>	
<1>	UTC time of position fix, hhmmss.s format	N
<2>	Status, A = Valid position, V = NAV receiver warning	N
<3>	Latitude, ddm.mmmmm (leading zeros will be transmitted)	N
<4>	Latitude hemisphere, N or S	N
<5>	Longitude, dddmm.mmmmm (leading zeros will be transmitted)	N
<6>	Longitude hemisphere, E or W	N
<7>	Speed over ground, 000.00 to 999.99 Knots (leading zeros will be transmitted)	N
<8>	True course over ground, 000.0 to 359.0 degrees (leading zeros will be transmitted)	Y
<9>	UTC date of position fix, ddmmyy format	Y
<10>	Magnetic variation, 000.0 to 180.0 degrees (leading zeros will be transmitted)	N
<11>	Magnetic variation direction, E or W (westerly variation adds to true course)	N
<12>	Mode indicator: A = Autonomous, D = Differential, E = Estimated, N = Data not valid	N

Table 12: GPRMC sentence structure

3D Velocity Information (GPTMV)		Used
Syntax	\$PGRMV, <1>,<2>,<3>*hh<CR><LF>	
<1>	True east velocity, -514.44 to 514.44 m/s	Y
<2>	True north velocity, -514.44 to 514.44 m/s	Y
<3>	Up velocity, -999.99 to 999.99 m/s	Y

Table 13: GPTMV sentence structure

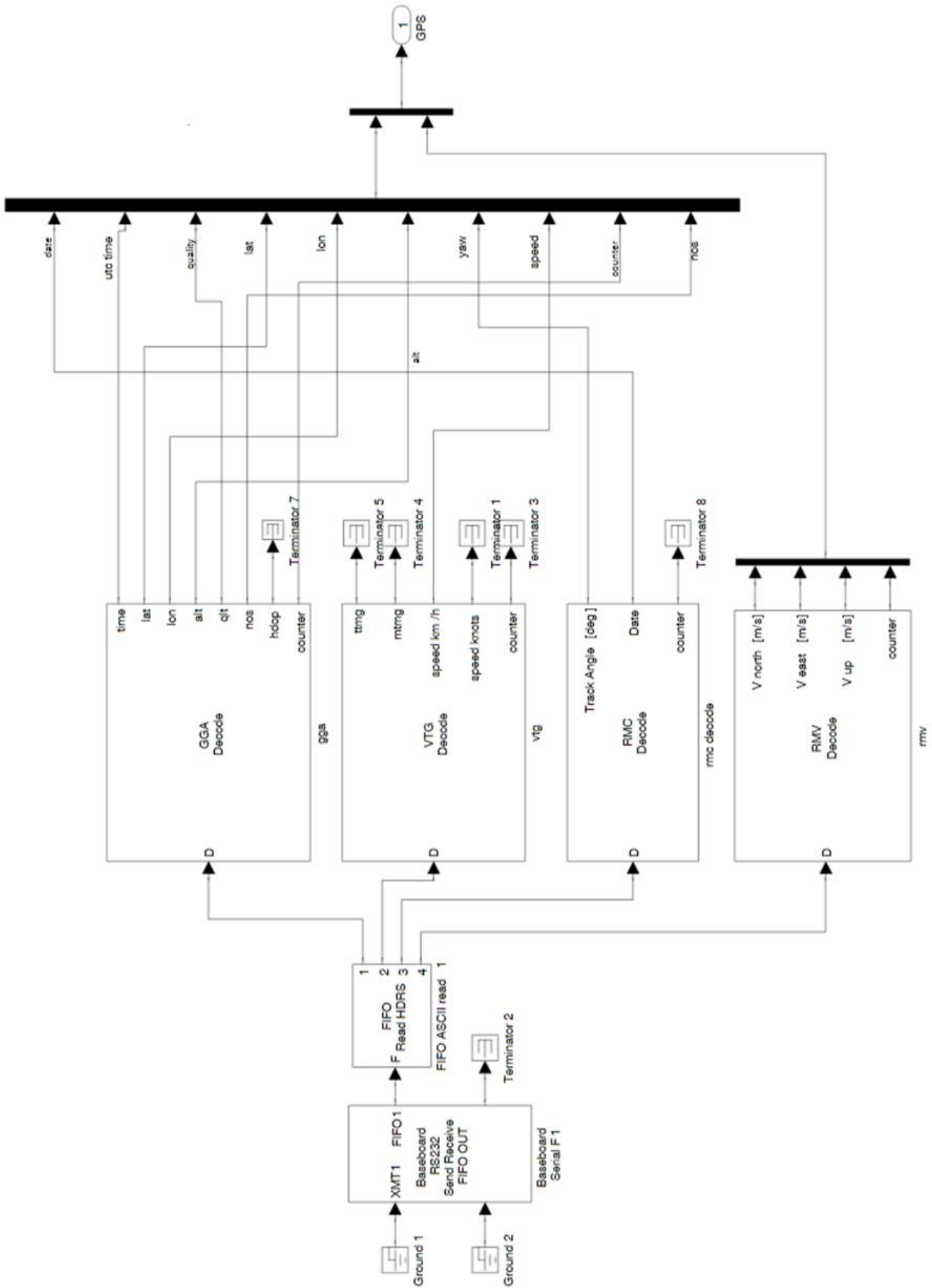


Figure 68: Garmin GPS 18 5Hz acquisition block scheme

6.5.2 Crossbow NAV420 Acquisition Block

The same structure used in the previous section has been adopted for the NAV420 acquisition block shown in Figure 69. While in the GPS acquisition block no commands can be sent to receiver , in this case configuration data can be transmitted using the bi-directional RS232 connection to set one of the three *Data Packet Mode*: Scaled Sensor Packet, Angle Packet and NAV Packet.

As stated in Section 6.1.1, due to several problems with the external active antenna the unit has been used in Angle mode. The unit outputs the stabilized pitch, roll and yaw angles along with the angular rate, acceleration and magnetic field information. Being GPS information not available the Kalman filter operates using an AHRS type filter tracking the rate sensor bias and calculating stabilized roll, pitch and yaw angles. Angular rate sensors are used to integrate over the aircraft rotational motion finding the actual pitch, roll and yaw angles.

Accelerometers correct for rate sensor drift in the pitch and roll angles while magnetometers correct for rate sensor drift in the yaw angle. Accelerometers are also used to provide long term stability keeping the rate gyro drift continuously within acceptable boundaries. Data is streamed at 100 Hz and to convert the digital data to angle the following relation is used:

$$angle = data * \frac{180}{2^{15}}$$

where *angle* is the actual angle in degrees and *data* is the signed integer data output in the data packet. Pitch angle is defined as $-90^\circ < \theta < +90^\circ$. Other relations are used to convert accelerations, angular rates, magnetic field components and temperature:

$$accel = data * \frac{10}{2^{15}}$$

$$rate = data * \frac{630}{2^{15}}$$

$$mag = data * \frac{1}{2^{15}}$$

$$temp = data * \frac{100}{2^{15}}$$

Accelerations are measured in *G*'s (actual measurement range is ± 4 G), angular rates in *deg/s* (actual measurement range is ± 200 deg/s), magnetic field components in *Gauss* and temperature in $^{\circ}\text{C}$. The digital data representing each measurement is sent as a 16-bit number (data list in Table 14) and starts with a 2 byte header followed by the selected functioning mode. At the end of each string a BIT message is present providing comprehensive information into system health; 2 bytes checksum information is available too. The BIT message definition is reported in Table 15 because during preliminary the correct functioning of the unit has been verified using the proprietary software NAV-VIEW, showing an error in the EEPROM integrity (bit 10) [Ref. (34)]. It seems that EEPROM calibration data is corrupted, but the effects of this malfunction are not easily measurable. Further investigation will be carried out in the future to solve the problem.

In the Simulink model a *FIFO binary read* block is used to transfer the acquired data to the decoder where it is split and converted to numerical double values. Some of the variables need to be converted before use.

Angle Mode Packet			
Bytes	Description	Range	Units
0,1	Header		
2	'A'		
3,4	Roll angle	[-180,180]	deg
5,6	Pitch angle	[-180,180]	deg
7,8	Heading angle (mag north)	[-180,180]	Deg
9,10	Roll angular rate	[-630,630]	Deg/s
11,12	Pitch angular rate	[-630,630]	Deg/s
13,14	Yaw angular rate	[-630,630]	Deg/s
15,16	X-axis acceleration	[-10,10]	G
17,18	Y-axis acceleration	[-10,10]	G
19,20	Z-axis acceleration	[-10,10]	G
21,22	X-axis magnetic field	[-1,1]	Gauss
23,24	Y-axis magnetic field	[-1,1]	Gauss
25,26	Z-axis magnetic field	[-1,1]	Gauss
27,28	Temperature	[-100,100]	$^{\circ}\text{C}$
31,32	BIT		
33,34	Checksum		

Table 14: NAV420 Angle Mode Packet list

BIT Message Definition		
3	Turn detect	0: Yaw rate magnitude < 0.4 deg/s; 1: Unit is executing a turn
4	Comm Transit Error	0: No serial port transmit communication failure has been detected; 1: A serial port transmit communications failure has been detected such as overrun, parity
5	Startup Rate Bias Check	0: Angular rate bias estimates are below 0.8 deg/s and normal operation can proceed; 1: Angular rate bias estimates during system startup are above 0.8 deg/s. System will continue to operate in high gain mode until sensor bias stabilizes below this threshold
6	GPS status	0: GPS 3D solution is valid; 1: GPS unlocked or data packet not present
8	Algorithm Initialization	0: Initialization complete 1: Not ready, waiting for power-up, and initialization completion
9	1 PPS Signal Lock	0: GPS 1 PPS signal locked; 1: GPS 1 PPS signal not locked
10	EEPROM integrity	0: EEPROM calibration data is valid 1: EEPROM calibration data is corrupted
11	Magnetometer Calibration Valid	0: Magnetometer hardiron/softiron calibration valid 1: Magnetometer hardiron/softiron calibration invalid
12	User Port Comm Receive Error	0: No user port receive communication failure has been detected; 1: A user port receive communications failure has been detected
14 15	Algorithm Accuracy	00-GPS available, full accuracy NAV; 01-low accuracy NAV/high accuracy AHRS, 02-low accuracy AHRS, 03-AHRS initialization

Table 15: NAV420 BIT message definition

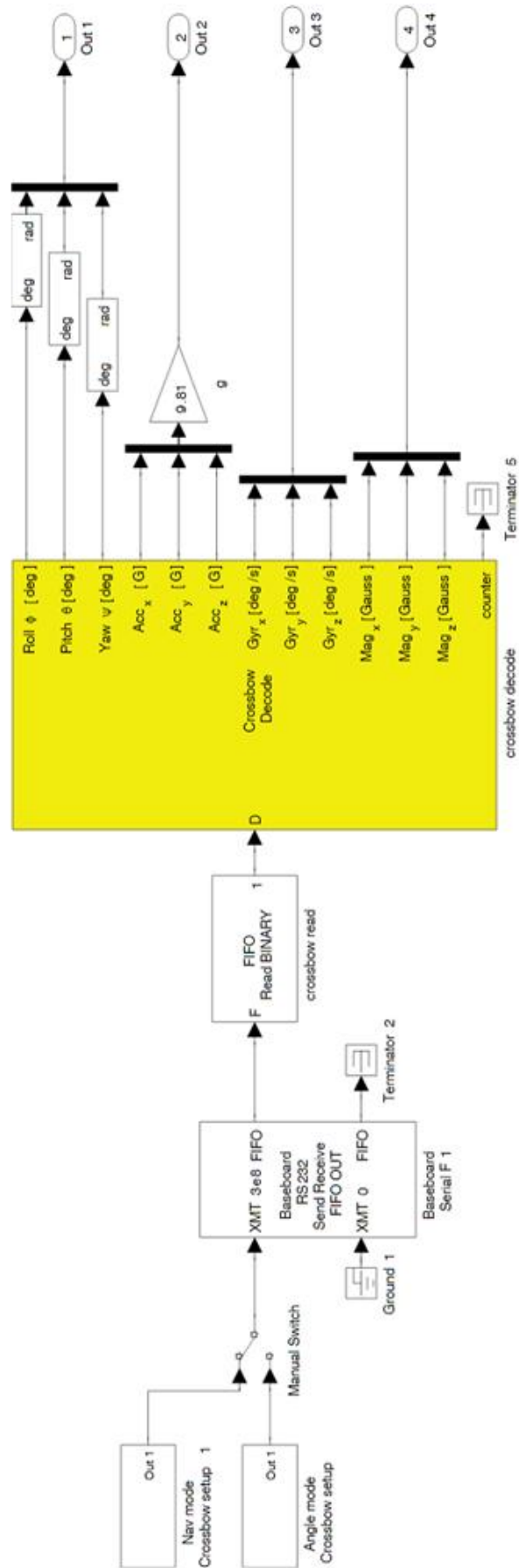


Figure 69: Crossbow NAV420 acquisition block scheme

6.5.3 Magnetometer acquisition block

This block was added because of the need to understand how the magnetic fields generated by the electronic equipment, placed near the I.M.U, can affect the integrated magnetometers measure. In order to do this a second 3-axial magnetometer (the same Applied Physics 539 used onboard ALMASat-1) will be placed on a boom fixed to the external POD, in order to be sufficiently far away from unwanted stray magnetic fields [Ref (50)].

At present, with the I.M.U installed in the internal management and computing unit, test revealed that despite the presence of an hard drive with its magnetic heads effects are almost negligible. In the final system the I.M.U will be placed as close as possible to the acquisition device, as seen in Chapter 4 and mechanical shutters tend to generate strong magnetic fields to move blades.

Block structure is similar to those used in previous sections for the GPS receiver and I.M.U unit, layout is depicted in

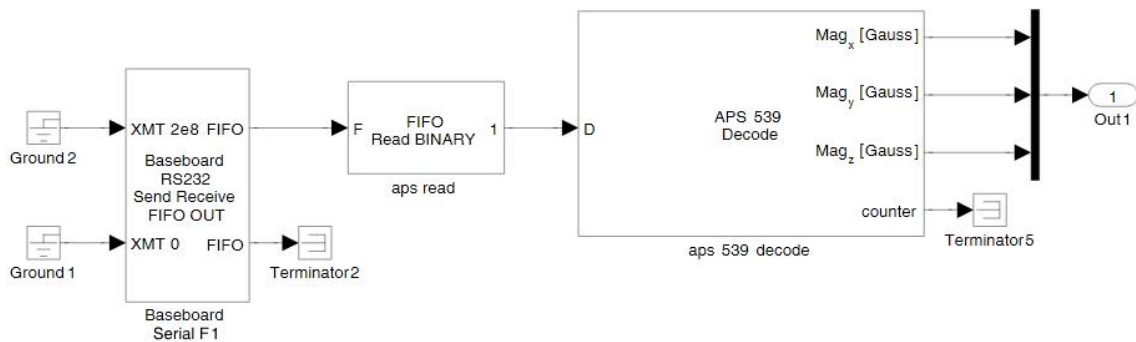


Figure 70: Magnetometer acquisition block scheme

6.5.4 Canon EOS 450D Management Block

Purpose of this block is the control of the camera shot using the GPS timing and the camera arm switch status acquisition. Inputs are taken from the GPS block, in particular the following variables: sentences counter, latitude, longitude and altitude (Figure 73).

Two modes of operation are implemented: the first one utilizes the camera arm switch position, manually controlled by the pilot or a system operator, to enable image acquisition while the second one, which at present has never been used during in flight campaigns, proposes a completely autonomous control strategy based on aircraft position.

In this case a surrounding quadrilateral or circular area is drawn around the selected target area, depending on the shape, and latitudinal and longitudinal boundaries are taken into account to define where the camera has to be enabled. In this case pilot doesn't interact with system at all. Values are calculated by the FASTER planning software described in the previous Chapter. More refined control strategies will be implemented in the future, utilizing also information about the aircraft heading, in order to better fit target areas with complex form.

The camera arm switch position is acquired reading signals from the parallel port register throughout a dedicated Simulink block. This value is used as an input for an AND block together with a timing system output which applies the pre-computed time interval between two images (Δt_I), coming from the planning software. If the two values are both "1" an impulse is generated and transmitted to a *Parallel Port Digital Output* block that shoots the camera and updates the *click* variable which counts the number of acquired images. The click number is used to associate the image to its ancillary data.

The timing subsystem is responsible to control the shot frequency applying the correct Δt_I . The implemented solution is the following:

- A block generates a base function

$$f(t) \begin{cases} 0 & \text{if } n\Delta t_I + s \leq t < (n+1)\Delta t_I \quad \forall n \in \mathbb{Z}^+ \\ 1 & \text{if } n\Delta t_I \leq t < n\Delta t_I + s \quad \forall n \in \mathbb{Z}^+ \end{cases}$$

where $s < \Delta t_I$.

- $f(t)$ is used as a reference timing function and is passed into a second logic AND block which compares it to the output of the GPS sequence counter. If a valid sequence is available the sequence counter value is 1 else is 0. So a shooting signal is generated only if both values are equal to 1. In this case the reference timing function is reset to 0 as shown in Figure 71.

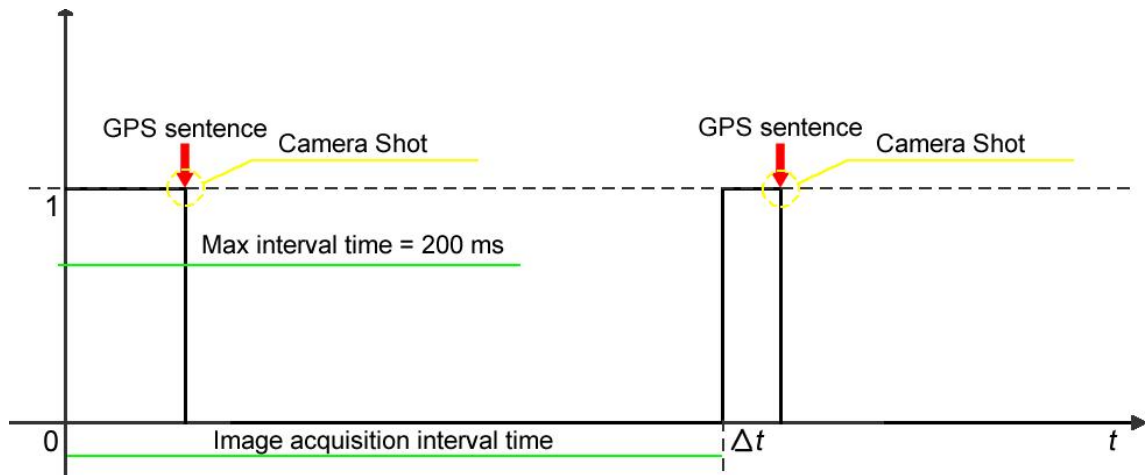


Figure 71: Camera shot signal generation

Before reaching the parallel port output the correct waveform to control the shutter button release is generated. The shutter button is typically hold down for 0.5 s for frame rate ≥ 1 . Greater frame rates could be reached simply keeping always down the shutter buttons; the camera enters the continuous driving mode and frame rates up to 3.5 fps can be achieved. At the highest frame rate images must be saved into the onboard Secure Digital memory card because the measurements reveals that the USB connection has a maximum transfer rate of about 52 Mbit/s (corresponding to about 0.5 fps); the EOS 450D connections panel is shown in Figure 72. A 40 ms delay must be considered between signal generation and effective shutter movement.



Figure 72: Canon EOS 450 remote connections panel

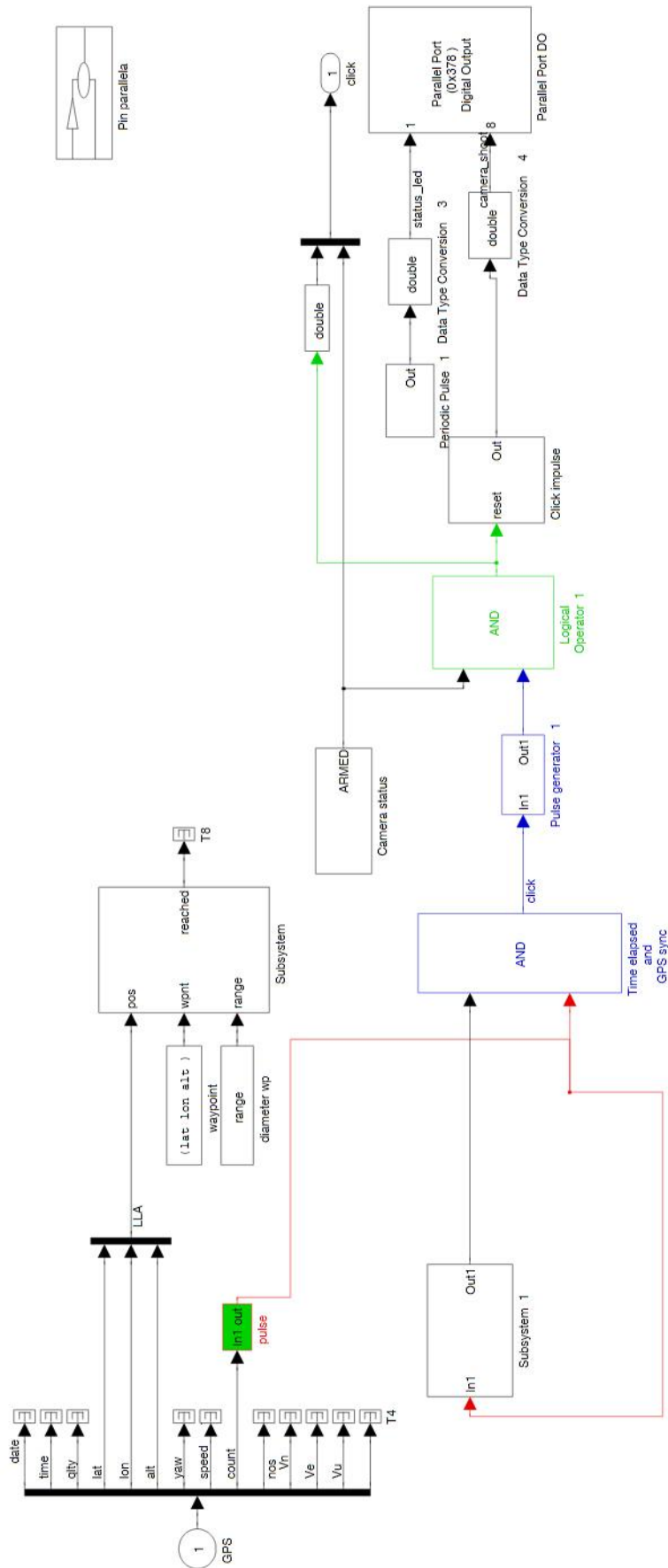


Figure 73: Canon EOS 450D Management Block Scheme

6.5.5 Tunnel in The Sky Management Block

The guidance tunnel is a critical tool for repeating the same planned trajectory during flight and constitutes one of the peculiarities of the FASTER EM. A complete description of the system is given in the next Chapter and here is presented only the Simulink block used for transmit all the state variables needed for attitude representation and the trajectory drawing.

The tunnel in the sky management block (Figure 74) is connected to both GPS and I.M.U blocks; these two blocks have different update rates: 100 Hz the I.M.U and 5 Hz the GPS one. The block itself must guarantee an adequate refresh rate to avoid “choppy” animations during tunnel representation, and it is actually set to 10 Hz. This value is the result of some trades off that involved also the graphical software running on the EPIA board, which has limited graphical performances, and it is not able to reach an higher video refresh rate.

Simulink is able to manage different block rate using *Rate Transition Blocks*. The block behavior is automatically selected and depends on the sample times of the ports to which the block connects, the priorities of the tasks for the source and destination sample times and whether the model specifies a fixed or variable-step solver [Ref. (51)].

Being periodic the sample times of the GPS and I.M.U blocks the following behavior are applied:

- GPS block outputs: $inTs > ouTs$ (5 to 10 Hz), the block acts as unit delay with data integrity and deterministic. The input is delayed and held by one sampling interval.
- I.M.U block outputs: $inTs < ouTs$ (100 to 10 Hz), the block acts as a Zero Order Hold with data integrity and deterministic. It samples and holds its input for the specified sample period.

Subsystem 1 & 4 operate a selection of the necessary variables while the small block on the right bottom substitutes the yaw angle measured by the I.M.U (magnetic course) with the yaw angle determined by the GPS receiver (true course). This “trick” solves a visualization problem that arise when flying with high sideslip angles that could make the tunnel impossible to be seen by the pilot. The *virtual tunnel* block is the processing block that prepares data before transmission and manages tunnel waypoints.

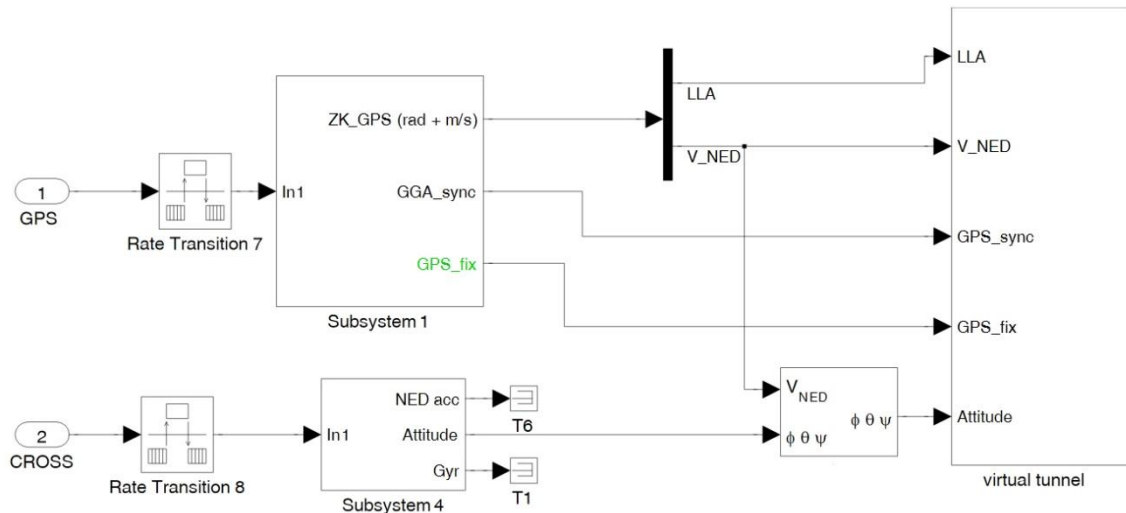


Figure 74: Tunnel in the sky management block scheme

6.5.6 Virtual Tunnel Block

The *virtual tunnel* block has been developed during a previous project aimed to realize an attitude visualization system for a remote piloted aircraft. The control and visualization system runs on a portable ground station and the pilot is able to control the aircraft even when the aircraft is not in sight. One of the problems encountered during the integration of this block inside the main project was its poor management of tunnel waypoints which was not reliable for many repeated parallel tracks used in photogrammetric flight campaigns.

In the original application all the waypoints were simultaneously loaded to build a unique tunnel visible until the end of the mission. When parallel track are too close from each other, typically tens of meters, tunnel intersections are present and small displacements from the planned trajectory may induce system errors. Additionally there were no information regarding the direction in which the tunnel was passed through, so if the pilot left the trajectory for any reason could re-enter in the wrong direction unconsciously.

Aware of these issues, most of the work was spent to achieve an enhanced management of the entire waypoints list trying to avoid any possible visualization problem during flight operations.

Changes were made to both the Simulink block and the Dynaworlds environment and the result is the actual configuration of the block presented in Figure 75:

- All waypoints are still stored in a unique file into the xPC target machine (that must be loaded into the Compact Flash memory before system boot and

currently can't be further modified) and read by the *virtual tunnel* block, but only a subset of 20 at a time is used to create a small portion of the trajectory which is transmitted via UDP connection to the Dynaworlds visualizer;

- Waypoints subset is refreshed every 5 seconds taking into account the actual GPS position. GPS fix is compared to the entire waypoint list selecting the nearest. Then the trajectory is generated using 13 waypoints in the front and 6 in the back, defining the 20 points subset, in order to avoid mistakes during the waypoint interpolation process performed by the Dynaworld visualizer. This solution avoid tunnel intersections in parallel tracks because the already completed trajectory part is no more considered defining a unique direction in which the tunnel can be pass through;
- The tunnel is forwarded only if the aircraft is within a range of 500 m from reference waypoint, otherwise the position is maintained; the pilot is not forced to exactly stay inside the guidance tunnel during course turnabouts or transfers to decrease the workload in long-duration mission;
- A 5 s position predictor has been added using an EKF which calculates future aircraft coordinates; this helps the pilot to maintain the aircraft inside the tunnel. Using the predictor tunnel section dimensions can be reduced improving the system effectiveness;
- Dynaworlds environment major changes are relative to the introduction of a “re-entry” tunnel. This is a secondary tunnel that brings back the aircraft on the trajectory defined by the main tunnel, every time it goes off the course exceeding a defined error. Furthermore maneuvers are limited to a maximum turn rate of 3 deg/s (standard turn rate); flight data (ground speed, altitude, true course and roll angle) is also presented to the pilot;

The capability to insert additional waypoints during flight has been evaluated together whit the possibility to select multiple trajectory, for example in case of more than a target area. The last one will be implemented in the final system.

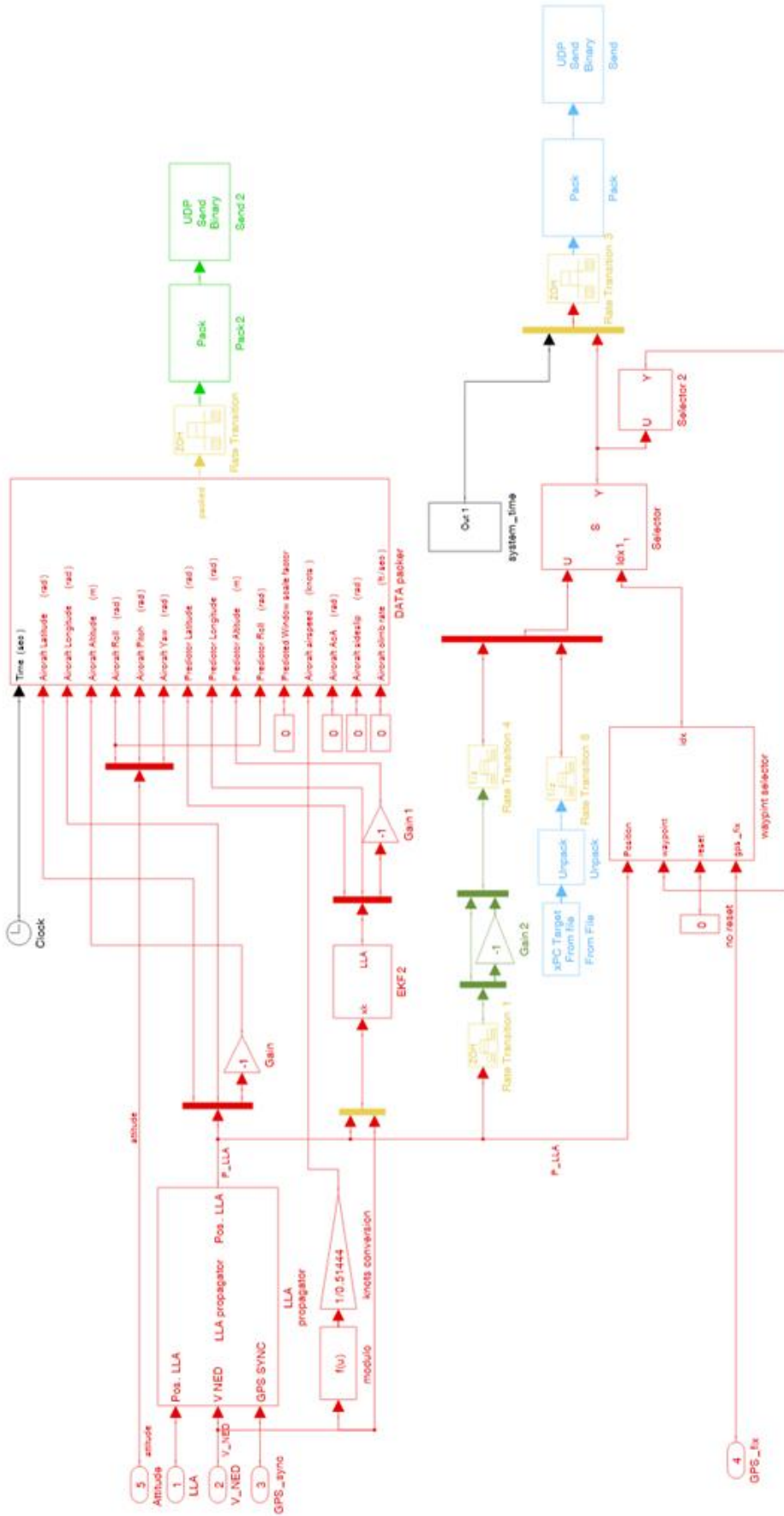


Figure 75: Virtual Tunnel block scheme

6.5.7 Datalog Block

The *datalog* block function is to save all the acquired information in a log file in which ancillary data for each image is contained (Figure 76). The log file structure is shown in the following table.

Log File Structure			
1	Click count	9	Altitude [m]
2	Date	10	GPS Yaw angle [deg, 0...360]
3	Hours	11	GPS Ground Speed [km/h]
4	Minutes	12	Roll angle [rad]
5	Seconds	13	Pitch angle [rad]
6	GPS quality [0,1,2]	14	Yaw angle [rad]
7	Latitude [deg]	15	Mag X [Gauss]
8	Longitude [deg]	16	Mag Y [Gauss]
		17	Mag Z [Gauss]

Table 16:Log file structure

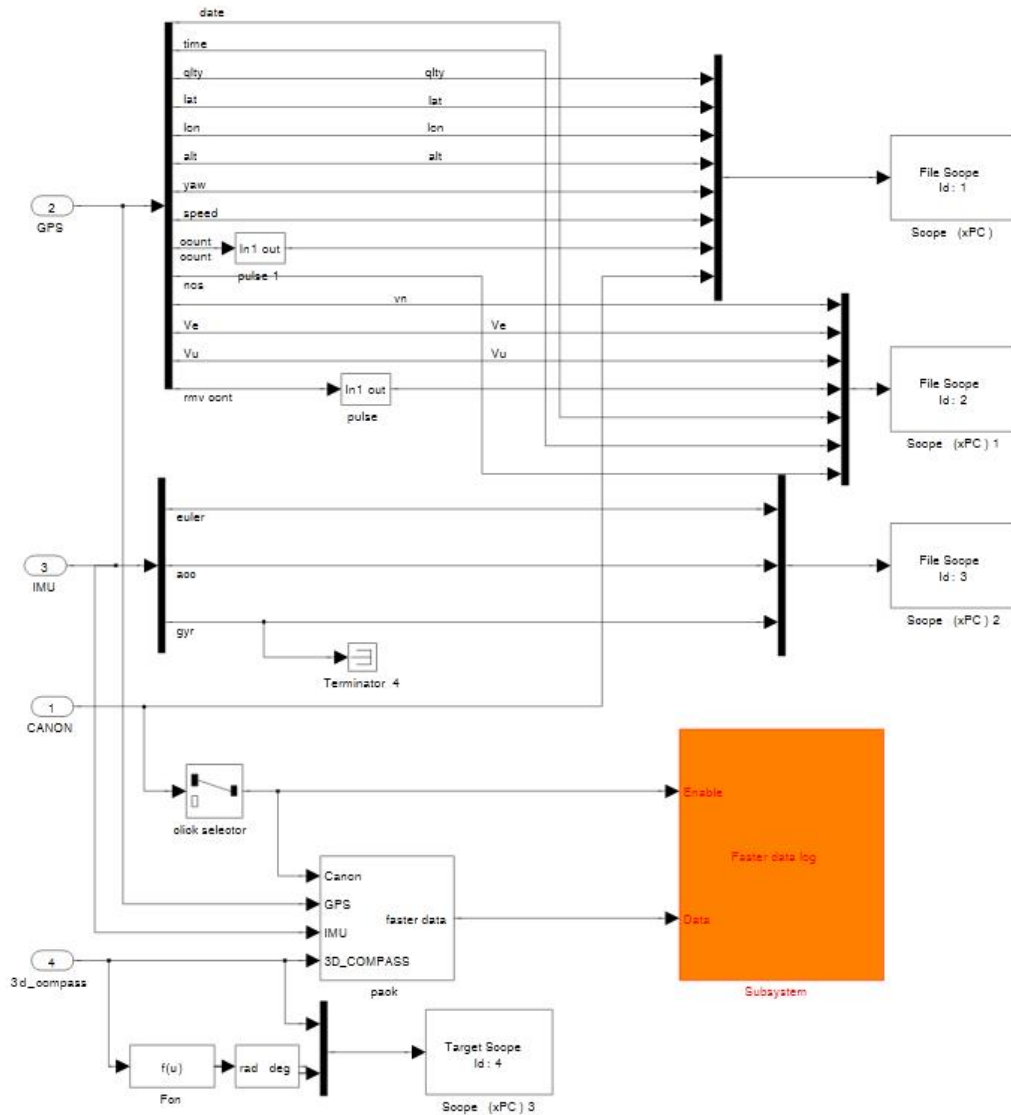


Figure 76:Datalog block scheme

6.5.8 Pilot Interface Block

The *pilot interface* block has been added to control the FASTER status monitor which is a Java-based software. This block collects a series of variables and send it via UDP connection to the EPIA EN15000 which runs the FASTER status monitor. The software displays a series of three lights and four numerical values:

- System Status, continuously scans the UDP port for packets, when the system is down (PC/104+ powered off) a red light is presented instead of green one;
- Acquisition Status, shows the camera arm switch position, green light means that the camera is enabled and ready to acquire images;
- GPS Status, reads the GPS sentence counter and shows a green light when GPS receiver is working correctly, in addition a numeric string inside the light shows the GPS quality value;
- Numerical displays show the aircraft position, altitude, speed and the number of acquired frames.

The block scheme is presented in Figure 77 and the FASTER system monitor in Figure 78.

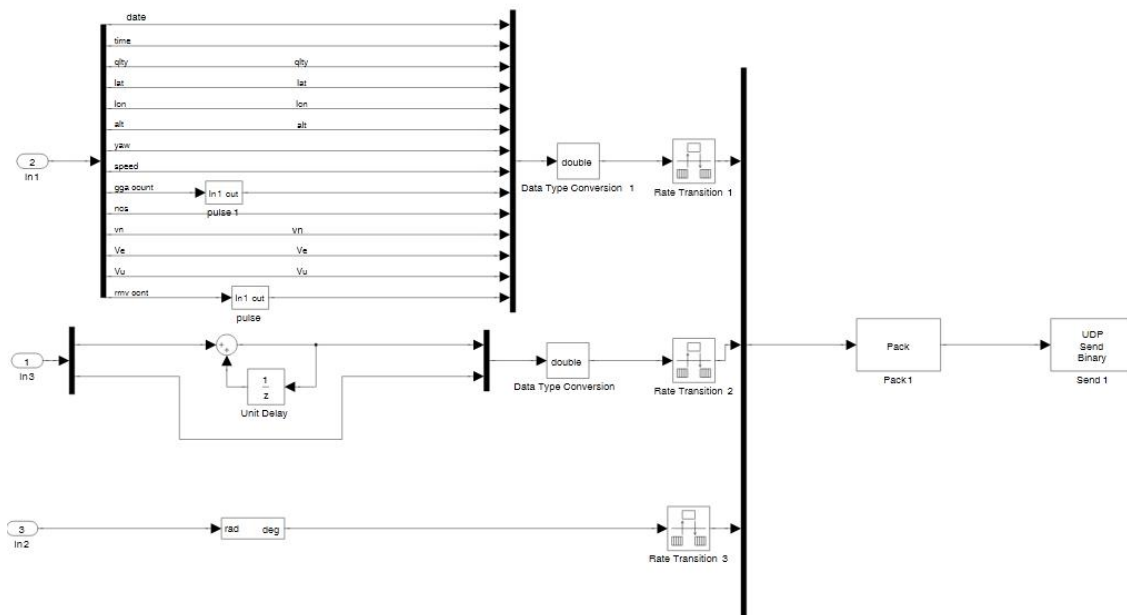


Figure 77: FASTER status monitor block scheme

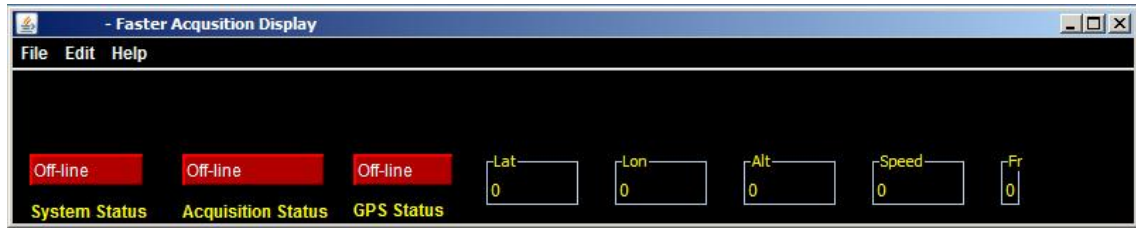


Figure 78: FASTER Acquisition Display

6.6 Tunnel In The Sky Visual Interface

The pilot visual interface is displayed on the LCD screen, which is placed over the cockpit dashboard in a central position not to obstructing pilot's view (Figure 79).



Figure 79: Pilot visual interface inside the Tecnam P92 cockpit

The solution that has been developed, inside the Dynaworlds environment, is a graphical interface that visualizes in perspective a 'tunnel of flight', made up by a series of segments joining several waypoints defining the reference trajectory. This trajectory can be overlapped to the external visual aid, or to a synthetically reconstructed scenario (which uses the same DEM utilized by the planning software), or to a fusion of the two, as in a conventional Head-Up Display (HUD). Together with the flight tunnel, the most important result of the filtering operation computed in the Simulink *virtual tunnel* block

are visualized by colored markers: in particular, it is shown the prediction of the future position of the aircraft by means of emphasized tunnel sectors that, in the future, will be interested by the effective trajectory. Experimental tests have shown that the combination of the visual information coming from the guide tunnel and from the predictions reduces the oscillations around the reference trajectory during the mission [Ref. (52)]. At present only the position prediction is used although the virtual tunnel block is able to estimate also future attitude.

The guidance tunnel is a critical tool for repeating the same planned trajectory or to flight throughout adjacent parallel stripes (i.e. for precision farming applications or air pollution monitoring where the same path must be repeated several time during the day).

Screenshots of the guidance tunnel are shown in Figure 80 and Figure 81. The first one shows the original interface developed for remote piloted aircraft. This early version was used only indoor and placed side by side to another monitor indicating the aircraft position and air data.

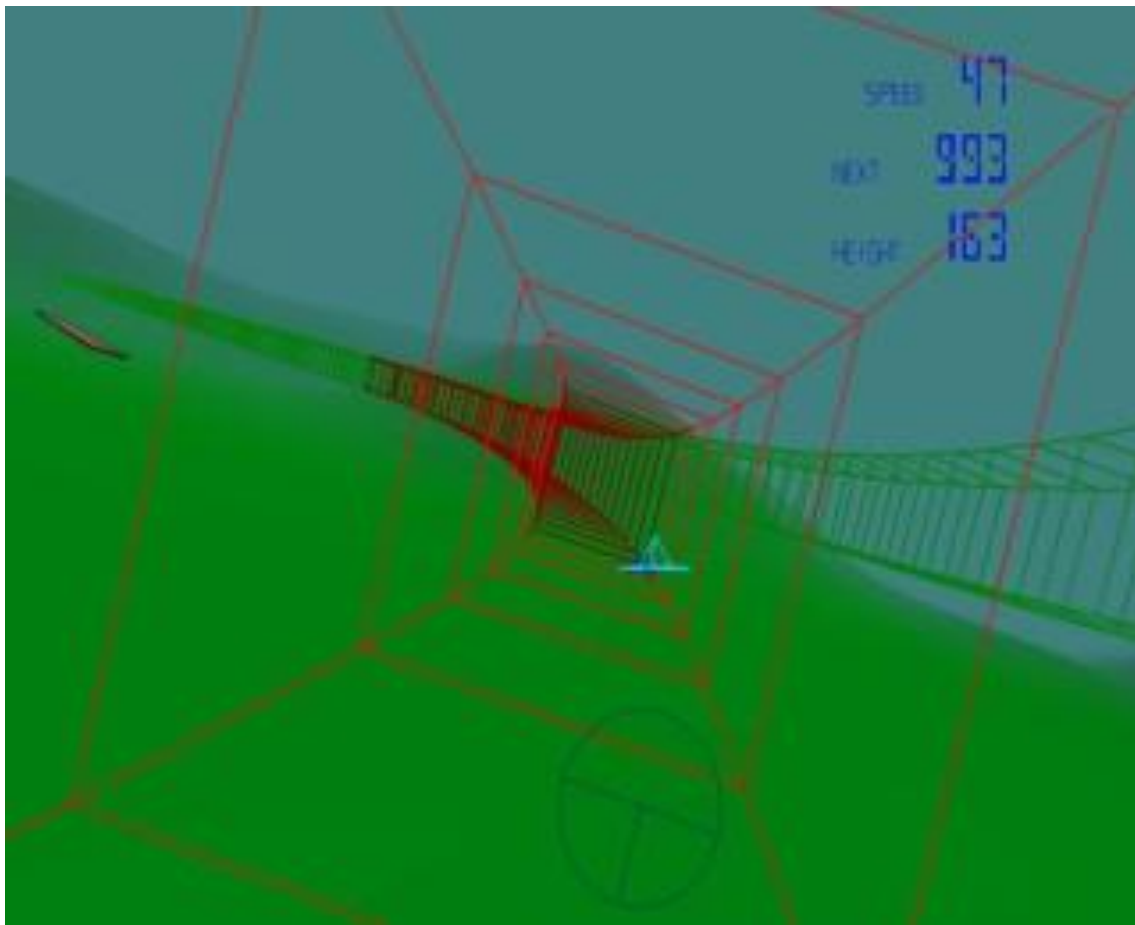


Figure 80: Guidance tunnel ver. 1

Visualization layout was fixed and a poor screen resolution was used. During flight operations this screen configuration showed its limitation because of the reduced visibility due to the selected color palette. Characters were barely readable too and the distance from the next waypoint shown between the ground speed indication and the flight height was misleading.

So an updated version of the guidance tunnel was built, taking into account also changes made to the Simulink model described in Section 6.5.6. Screen resolution has been increased, obtaining more readable fonts; image contrast is better and notwithstanding the brightness reduction, due the touch screen layer applied on the LCD screen, the new colour palette makes the guidance tunnel more distinguishable. Waypoint's distance has been deleted and the course indication (true heading) added. Now the layout is more similar to those provided by a modern aircraft Primary Flight Display showing attitude, speed, altitude and heading information. Altitude (*ft*) is on the left side while speed (v_{gs} , *km/h*) on the right. Other indications can be enabled before takeoff; options available are vertical speed and roll angle.

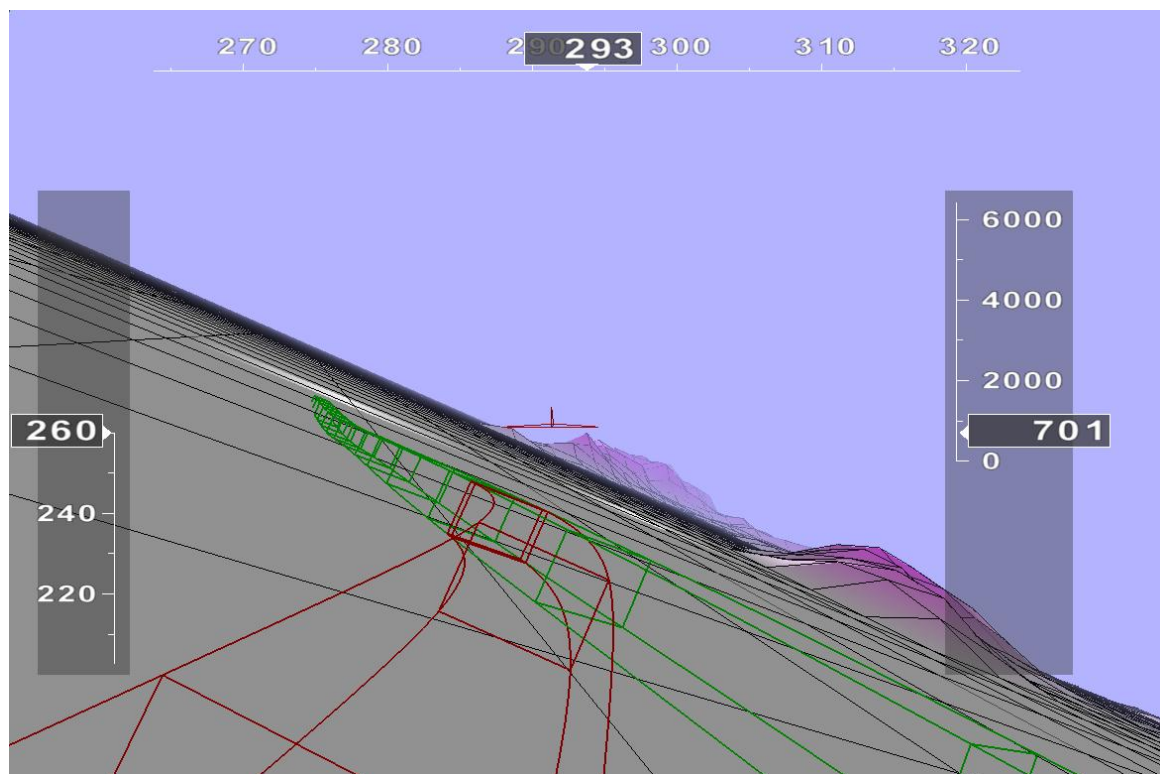


Figure 81: Guidance tunnel updated version

To increase the system effectiveness, another tool called 're-entry tunnel' has been introduced (red tunnel in the previous images). This is a secondary tunnel that brings back the aircraft, compatibly with its ability to maneuver (turn rate is limited to standard 3 °/s) on the trajectory defined by the main tunnel, every time it goes off the course exceeding a defined error. To enable pilot interaction with the system, a specific version of the virtual interface has been built and shown in Figure 82.

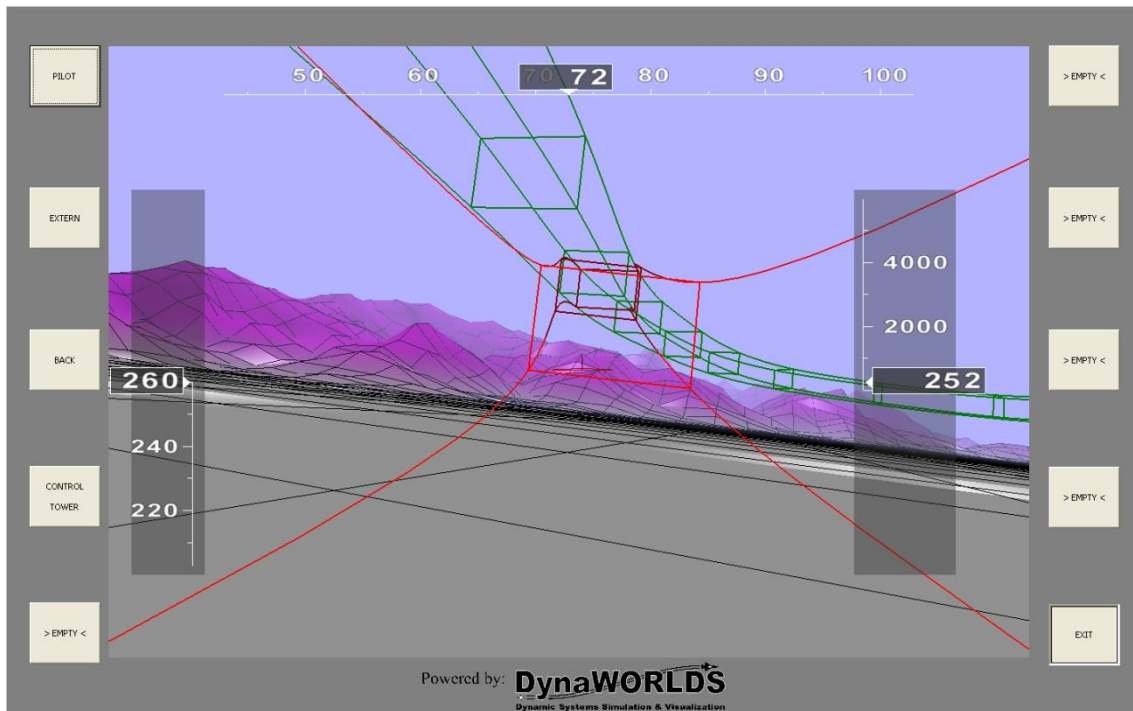


Figure 82:Guidance tunnel interface provided with interactive buttons

In this case, different functions can be assigned to the lateral buttons, for example the “go to home” function which stops the planned mission and design a re-entry tunnel that will fly the aircraft directly to the destination airport. Another important function that could be implemented is relative to the management of more than a target area. Buttons can be used to select target area number and a transfer guidance tunnel is drawn.

6.7 Canon Camera Control Software

To remote control the Eos 450D camera, Canon makes available through its SDK, a C++ script that once compiled, offers a complete control of the camera functions via the USB link. This solution has been preferred to the Canon EOS utility shipped with the camera itself which proved to be very unstable and high resource-demanding.

A screenshot of the camera control center software is provided in Figure 83.

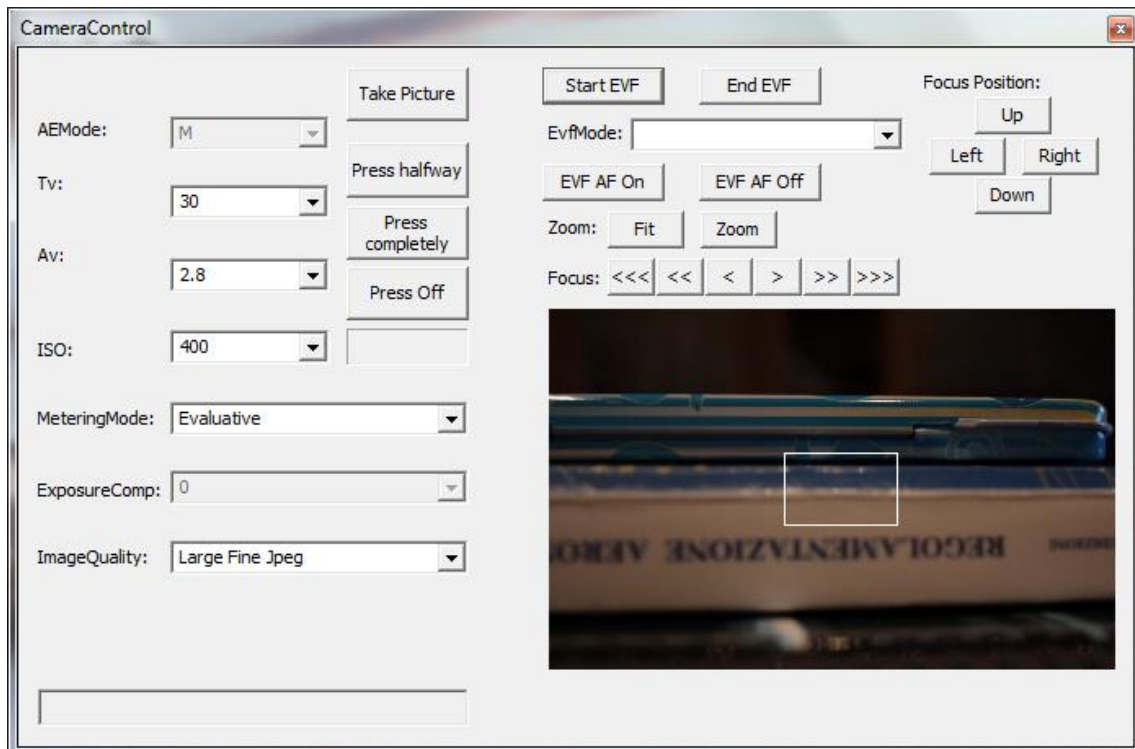


Figure 83: Camera control center screenshot

As it can be seen the accessible camera functions are:

- AEMode, is the Automatic Exposure mode and during acquisitions is always set to manual in order to avoid different exposure setting between frames; the AEMode must be physically set on the camera using the AEMode wheel;
- Tv, is the exposure time, it can be set between 10^5 s and $2.5 \cdot 10^{-4}$ s;
- Av, is the aperture value, its values depends on the mounted lens; for the Canon EF28 F/2.8 apertures varies from 2.8 to 22. The Aperture or F-number is $A = f/D$ where D is the lens exit pupil diameter (which only sometimes corresponds to diameter of the outside lens in the assembly) and gives a measure of the incoming light flux, the greater the F-number the less light per unit area reaches the image plane of the system. The amount of light transmitted to the detector decreases with the F-number squared;
- ISO, measures the sensitivity of the image sensor, change the ISO value equals to set a different gain to the output sensor signal. At higher ISO values noise may become clearly visible (artifacts) on the acquired image so the

optimal value must be carefully evaluated. ISO can be set between 100 and 1600 but for APS-C sized detectors, like the ones used in the EOS 450D, ISO values higher than 400 should be avoided;

- Metering Mode, this setting refers to the way in which a camera determines the exposure but it is not applicable in manual mode;
- ImageQuality, refers to how the image is saved to storage support. Options available are JPEG (low, medium and high quality) and RAW mode. In RAW mode images are not compressed and saved in a proprietary format (.cr2).

Chapter 7. Results of the test campaigns

After completing the realization of the FASTER EM, the system was subjected to a series of tests to verify its correct operations and performance. The tests were carried out both in laboratory and in flight.

7.1 Laboratory Tests

During the laboratory test phase each subsystem was thoroughly tested. Initially, PC-based boards were stressed to verify their limits in terms of cpu load and memory usage. Already in this first test, some problems were encountered with one of the two boards, the VIA EPIA nano-itx N10000. This board was originally selected because of its smaller form factor with respect the EPIA EN15000 mini-itx. Nano-itx boards are only slightly larger than a PC/104 board (120 x 120 *mm*) and have lower power consumption than a mini-itx board because of its architecture and the limited number of peripherals. However, this board, which was equipped with a VIA C7 processor running at 800 MHz in fanless mode and a slim 2,5" 40 GByte hard drive, was not able to run all necessary applications at the same time: the guidance tunnel interface, the camera control software and the java-based FASTER display. So it was necessary to replace the board with the one currently used, which proved to be sufficiently powerful to maintain a constant image download data rate from the camera (3 Mbyte/s) while running the two graphical applications (the more demanding in terms of computational resources). In order to avoid system slowdowns the tunnel in the sky refresh rate was set to 10 Hz without major effects on the 3D animation fluidity.

The Advantech PC/104+ board was tested with the acquired device attached one at a time so single software blocks could be debugged. Then parallel port connections were tested to check the camera arm switch functioning. Some precautions had been taken in case of power loss or board reset. In the first software release, the data log file, containing ancillary information, after a re-start was overwritten causing the loss of all previous data.

The problem was corrected applying a files check routine which changes the file name if it already contains data. This action was taken because it had been verified that when the battery is almost discharged, small voltage variations can cause some systems to restart before the full discharge of the battery.

Acquisition tests were conducted on the NAV420 and GPS receiver units, verifying expected data exchange rate. NAV420 magnetometers calibration procedure was applied before and after the installation inside the airborne internal management and computing rack box. Being the NAV420 installed near other electronics devices (as shown in Figure 66) the magnetic field was also measured during system operations with minor changes.

Tests on the GPS signal demonstrate that image acquisition was correctly enabled only if a valid GPS sentence is received and the camera arm switch is on the enable position. Ethernet connections were tested too; UDP packets are sent from the Advantech PC/104+ board (IP address 192.168.1.100) only to the EPIA EN15000 board (IP address 192.168.1.218) and data is displayed by the FASTER system monitor and represented in the virtual tunnel application.

Some minor issues were encountered in the power subsystem when using an external power source. As reported in Table 9, some devices have a current drain peak during startup phase that can cause the system to restart if the power supply is unable to deliver an adequate power level. To avoid restarts an appropriate startup sequence was defined which consists in startup the system with the LCD screen and the camera powered off in order to manage the EPIA EN15000 startup power absorption peak. Once the system is ready and in all the peripherals are in idle mode, the Canon camera is powered firstly, because it also has an absorption peak during startup phase because all the internal subsystem are checked (camera screen, shutter and secure digital read/write operations are performed); then the LCD screen is powered up.

The entire system was subjected to long run tests, in order to verify the perfect matching between the number of acquired images and their ancillary information, contained in the log file provided by the PC/104+ board. This was needed because sometimes, during high system loads, the insufficient data rate may cause the camera memory buffer (32 Mbytes, corresponding to approximately 3 RAW images) to be filled up, preventing the acquisition of additional images. In this case there is no longer matching between the image number and the log number since there is no real-time feedback on the camera shoot signal.

A cross check can still be made if the camera clock has been synchronized with the PC-board internal clock time, reading the *exif*³ data contained in each image where date and time are saved. Long runs of more than 4 hours of operations showed that each image was correctly acquired and saved.

After the first testing phase, a Computer-In-the-Loop (*CIL*) and an Hardware-In-the-Loop (*HIL*) test campaigns were performed to evaluate system response and better understand the interaction with the pilot. The *CIL* layout is shown in Figure 84, where a joystick is used as input device to control aircraft's command surfaces. The aircraft's dynamics is simulated using a Simulink model and according to its position and attitude, both GPS and IMU data are provided to the *FASTER* model.

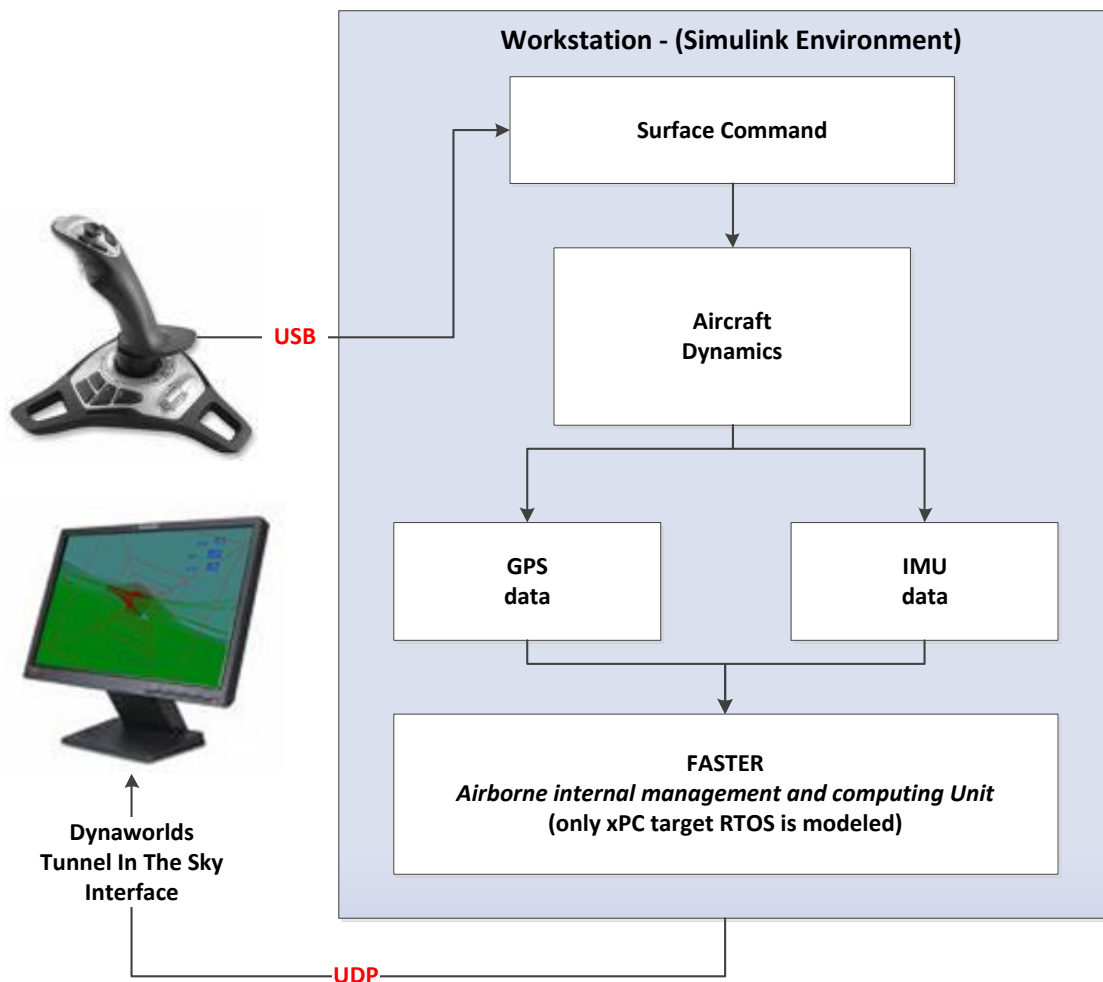


Figure 84: FASTER CIL layout

³ Exif stands for *Exchangeable image file format* and is a specification for the image file format used by digital cameras. The specification uses the existing JPEG or RAW file formats with the addition of specific metadata tags that could contain: date and time information, camera settings like aperture, shutter speed, focal length and ISO value, and a thumbnail for previewing the picture.

The FASTER block contains the same Simulink model used to build the xPC Target real time operating system which works directly in the host machine as detailed in Section 6.5. Finally, the same EPIA EN15000 is used to run the Dynaworlds tunnel in the sky guidance interface using the UDP Ethernet connection provided by the CIL workstation. This setup has been very useful during the FASTER software development and to train the pilot before each flight test campaign, because reproduces the same information that will be given during the flight. Furthermore, it is the fastest way to test visual interface modifications or to evaluate new trajectories.

The HIL setup has been used instead, to evaluate in the real world the performance of the FASTER EM hardware-software combination using only synthetic data coming from the Garmin 18x 5Hz and Crossbow NAV420 emulators.

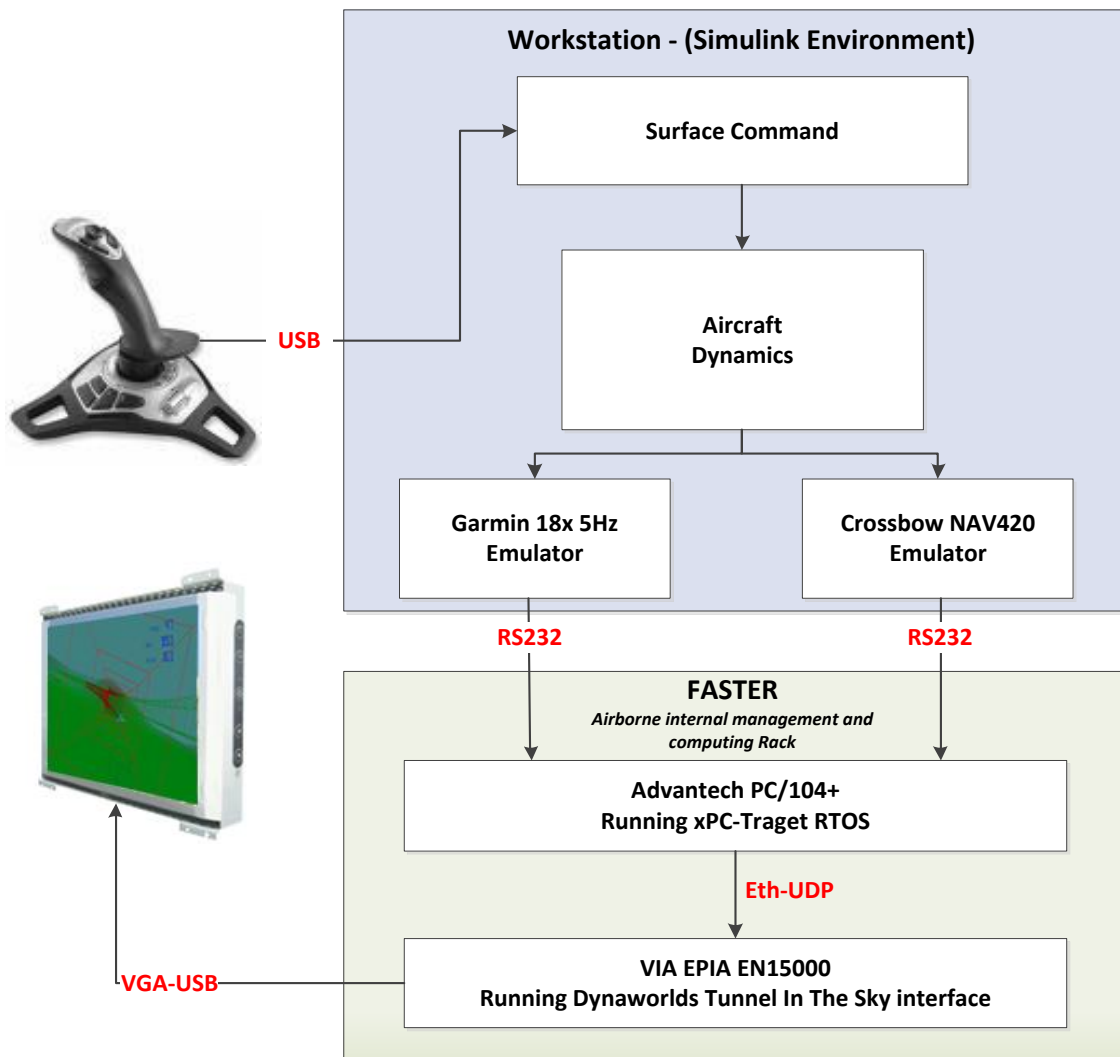


Figure 85: FASTER HIL layout

The two emulators generates the same *nmea* strings for the GPS and the angle mode packet binary data output for the I.M.U. With the HIL setup more accurate simulations of the flight campaigns were made testing the functionalities of the updated version of the tunnel in the sky interface.

The results of the third flight campaign simulation over the Brisighella area are reported in the following images. Figure 86 shows the planned trajectory with the FASTER planning tool (more detail in Chapter 5). Then the waypoint list file has been created and copied inside the memory card by the Advantech PC/104+ board inside the FASTER rack box.

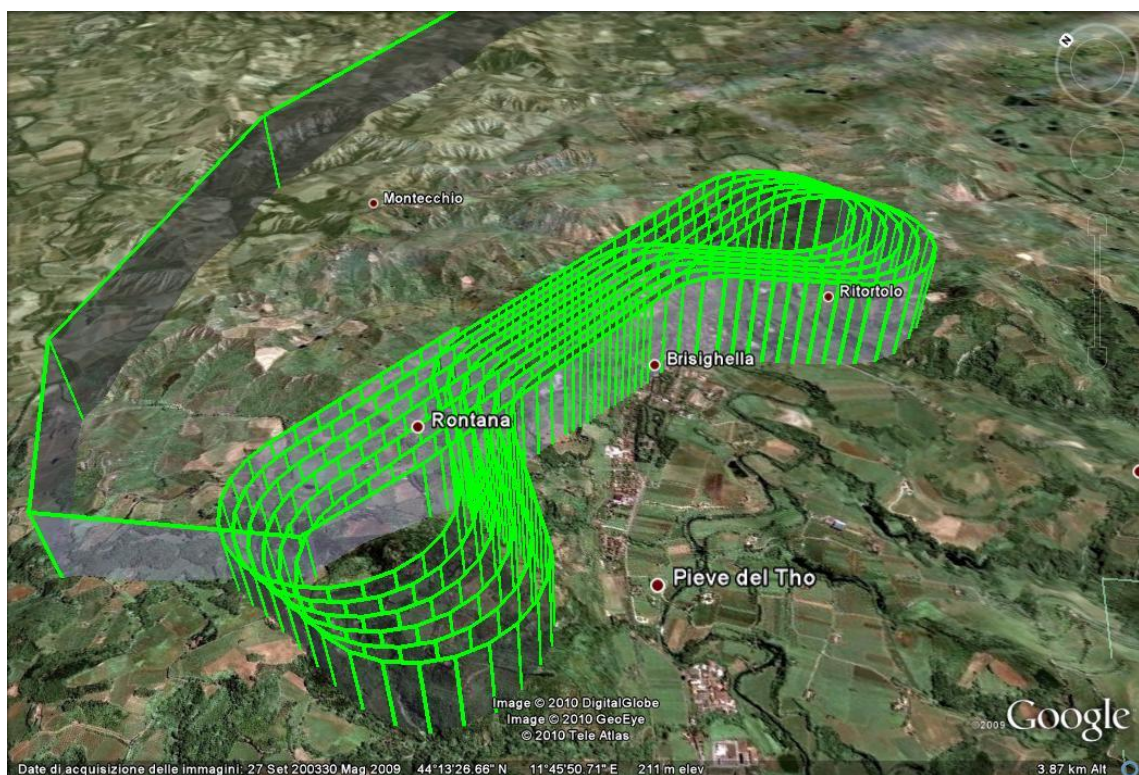


Figure 86: Simulation of the third flight campaign (Brisighella area) using the HIL setup

The entire flight (about 50 min) was simulated using the HIL setup and then the results were analyzed with an appropriate tool developed in Matlab. This tool takes into account both the planned and flown trajectories; for each planned waypoints the script searches for the two nearest waypoints into the flight log. This search is time driven, based on total elapsed flight time; only waypoints at the same mission time percentage ($\pm 10\%$) are searched in order to avoid errors during stripes crossing.

Once the coordinates of the two nearest waypoints are extracted, the straight line passing through that two points is found using the known equations:

$$m_i = \frac{y_{flown\ i+1} - y_{flown\ i}}{x_{flown\ i+1} - x_{flown\ i}}, \quad \text{Eq.5}$$

$$q_i = y_{flown\ i} - m_i x_{flown\ i} \quad \text{Eq.6}$$

then, the distance between the straight line and the planned waypoint is calculated using Eq.7, and defining a index which gives an idea of “how close” are the two trajectories on the plane.

$$d_i = \frac{|y_{planned\ j} - m_i x_{planned\ j} - q_i|}{\sqrt{(1+m^2)}}, \quad \text{Eq.7}$$

The results of the HIL simulation, using a squared 30x30m guidance tunnel are shown in the following figures.

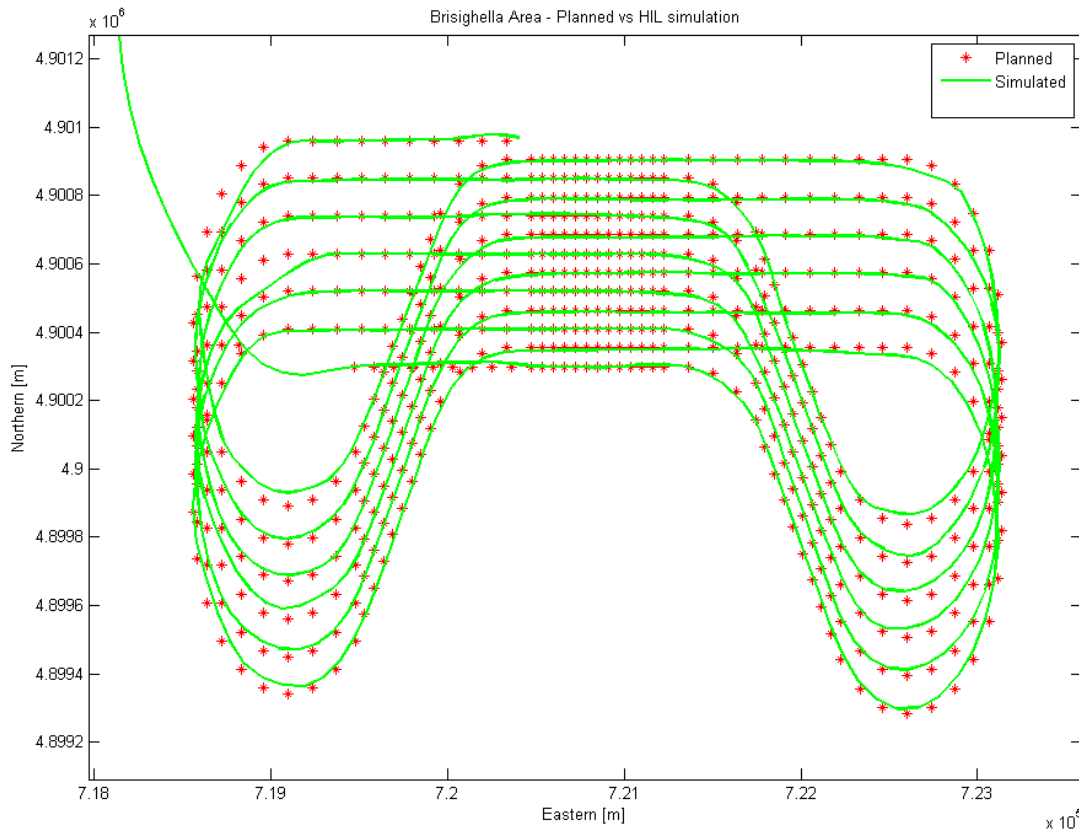


Figure 87: Brisighella area, planned vs HIL simulated trajectory

Results of the test campaigns

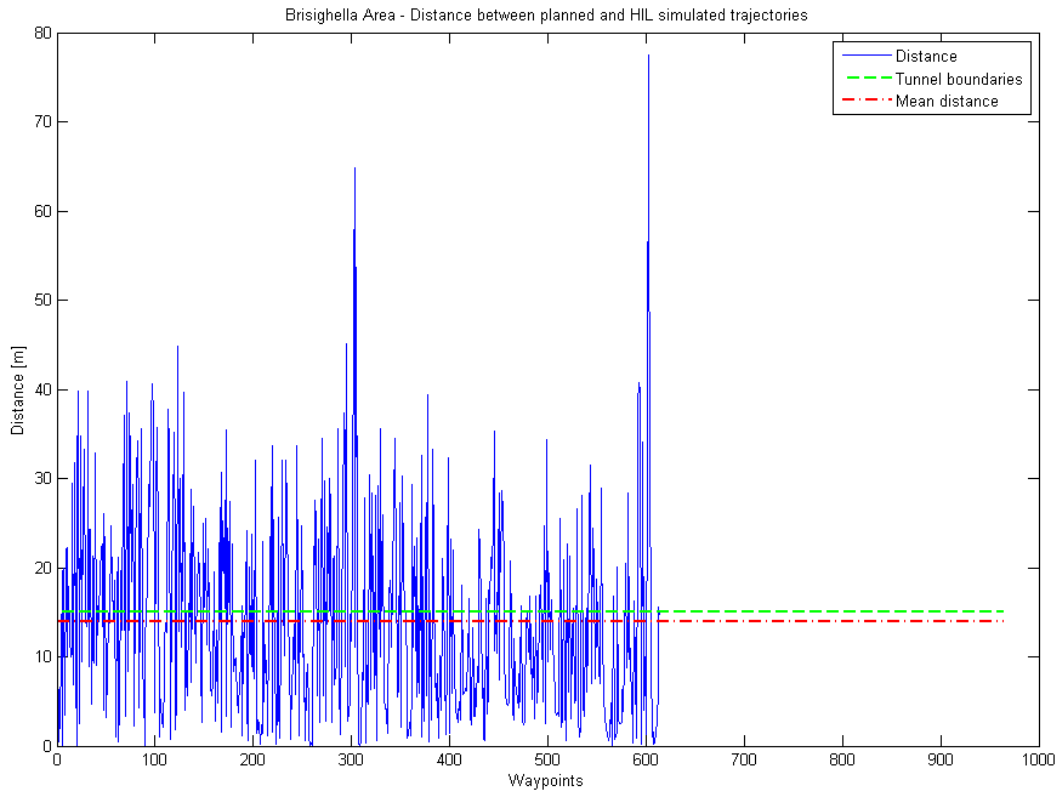


Figure 88: Brisighella area, distance between planned and HIL simulated trajectories, whole flight

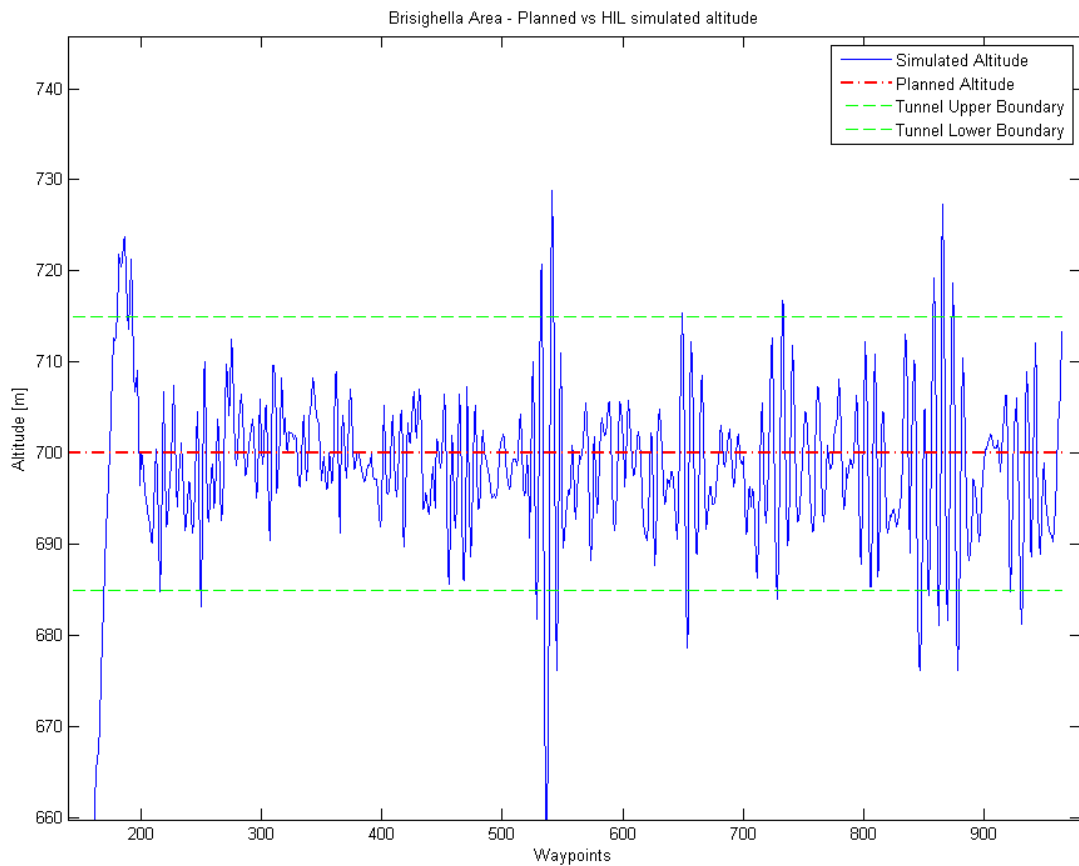


Figure 89: Brisighella area, HIL simulated altitude profile vs planned, whole flight

Figure 87 shows the HIL simulated trajectory in green, while the red dots represent the planned waypoints. The HIL simulation was done without simulating atmospheric conditions, thus in ideal conditions. Notwithstanding a small time lag between the given command and the aircraft response resulted in a non-optimal flight. The absolute mean distance between the planned and simulated trajectory for the whole flight, shown in Figure 88, is 13.93 m just below the tunnel boundary set at 15 m.

7.2 Flight tests

Three flight campaigns were conducted since the assembly of the FASTER Engineering Model. An Ultra Light Aircraft, Tecnam P92-Echo, was used as aerial platform; it is an high wing airplane equipped with a Rotax U912UL engine with a maximum power of 60 kW [Ref.(46)]. It weights 600 kg and reaches a cruise speed of about 180 km/h (51 m/s); the service ceiling is 4500 m (14700 ft).

The airborne internal management and computing unit is placed behind the two seats and the external POD is attached to the fuselage structure in the passenger side (right side looking at the propeller). For safety reasons, in addition to the c-shaped bracket (Figure 90) which fixes the pod to the structure, a flat string which passes under the fuselage and is attached to structure in pilot side, is used to retain the POD adherent to fuselage.

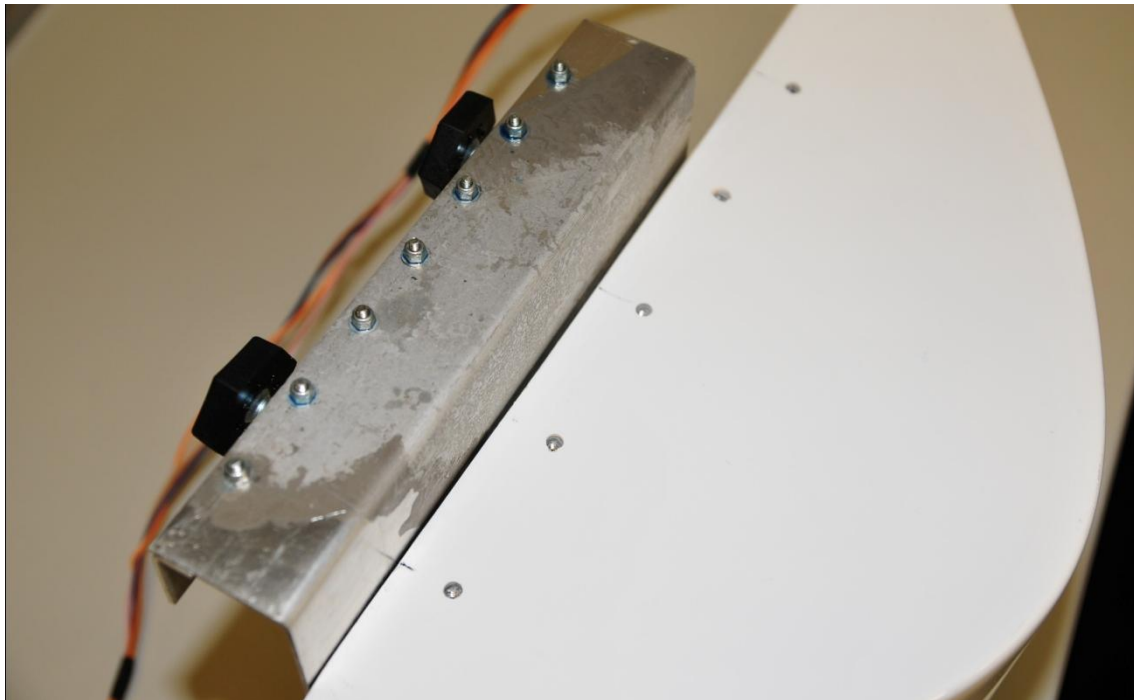


Figure 90: C-shaped bracket used to install the external POD on the passenger side of the P92 fuselage

Wires pass under the door and connect the two unit. The LCD screen has been installed on a metal support that fits above the compass over the dash board, so the screen is placed in a central position and can be easily seen by the pilot without head movements and maintaining into its field of view the outside environment (Figure 91).

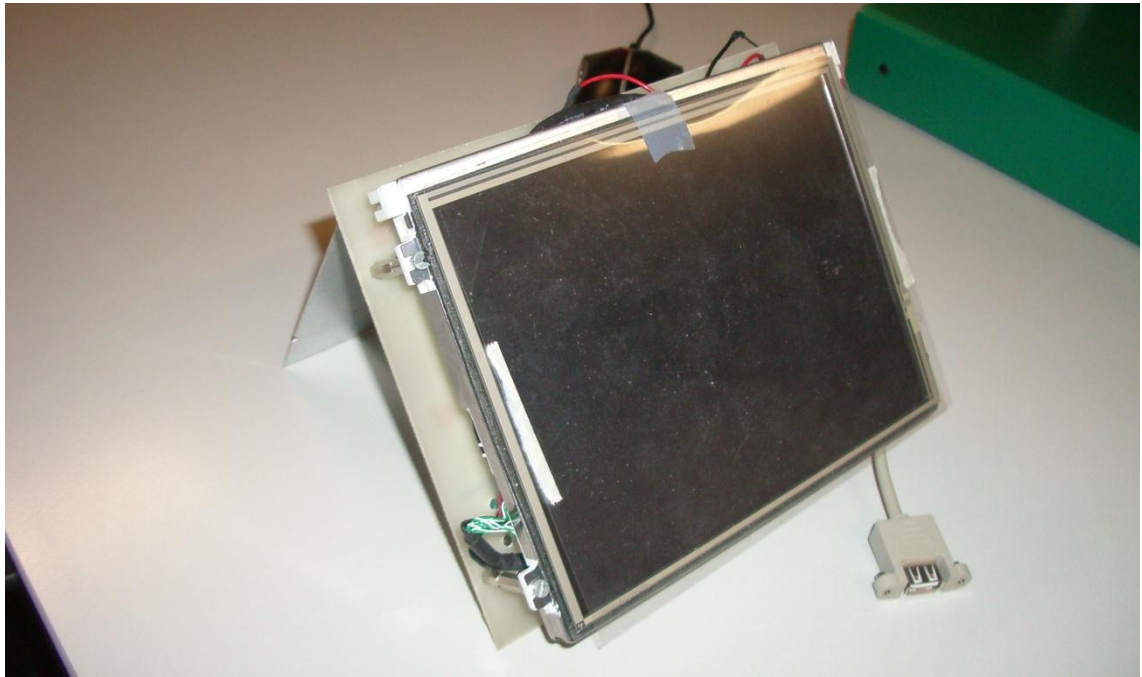


Figure 91: FASTER EM LCD monitor mounted on the metal support



Figure 92:FASTER external POD installed on the Tecnam P92

The camera arm switch, for the three campaigns, has been controlled by an operator which had the role of controlling the system functioning and intervene in case of need. The aircraft fully equipped is shown in Figure 92.

7.2.1 First Test Campaign

During the very first test campaign most of the flight-time was devoted to understand how to mount the two units, inside the airplane, in a fully secure way; this allowed to reduce the installation time for the following two campaigns to only 30 minutes. At that time the tunnel in the sky interface was still in its first release and no fixing ring was used to block the focus ring on the camera lens.

Because the objectives of the first test campaign were relative to the installation of the system on the aircraft, the flight was not planned using the FASTER planner tool but the trajectory was generated selecting several waypoints on Google Earth, giving the guidance tunnel the role to built the whole trajectory interpolating the waypoints. The poor resolution of the first release of the guidance tunnel did not allow the pilot to see the numerical values indicating the ground speed and the flight altitude, so the pilot had to continuously move his look between the FASTER monitor and conventional instruments.



Figure 93: First flight campaign trajectory

No further magnetometer calibration was applied with respect to that made inside the laboratory. The planned trajectory is shown Figure 93. The departure airport was the Verginese airfield near Ferrara.

During the flight, the pilot, which was not trained before takeoff, had serious difficulties trying to follow the tunnel indications, probably because of an uncorrected bias in the tunnel geometry. The position predictor was switched off and no standard maneuvers was used during planning. In addition the colour palette was not producing sufficiently sharp images so the tunnel itself was not clearly distinguishable from the background. The resulting flown trajectory with respect to the planned one is shown in Figure 94.



Figure 94: First flight campaign, planned vs flown trajectory

The pilot tried to follow the planned trajectory for the first part (tunnel side was set at 50 m) and then, after exiting the tunnel to reach the following known waypoint, re-entered the planned trajectory for another small portion of the planned flight. So only the initial part of the flight has been analyzed, and the results are shown in Figure 95, Figure 96 and Figure 97, where the mean distance between the planned and flown trajectories was 6125 m. Also altitude plot shows how the pilot was not able to stay inside the guidance tunnel.

Results of the test campaigns

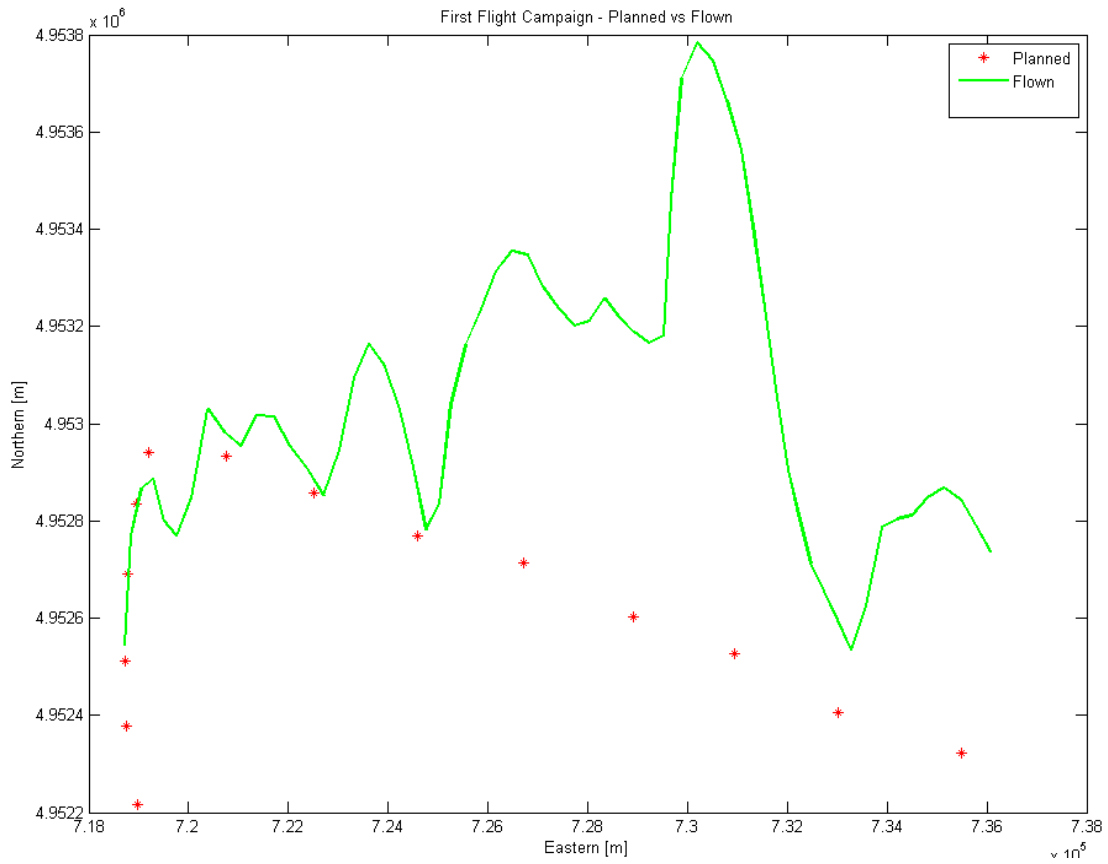


Figure 95: First flight campaign, initial part of planned vs flown trajectory

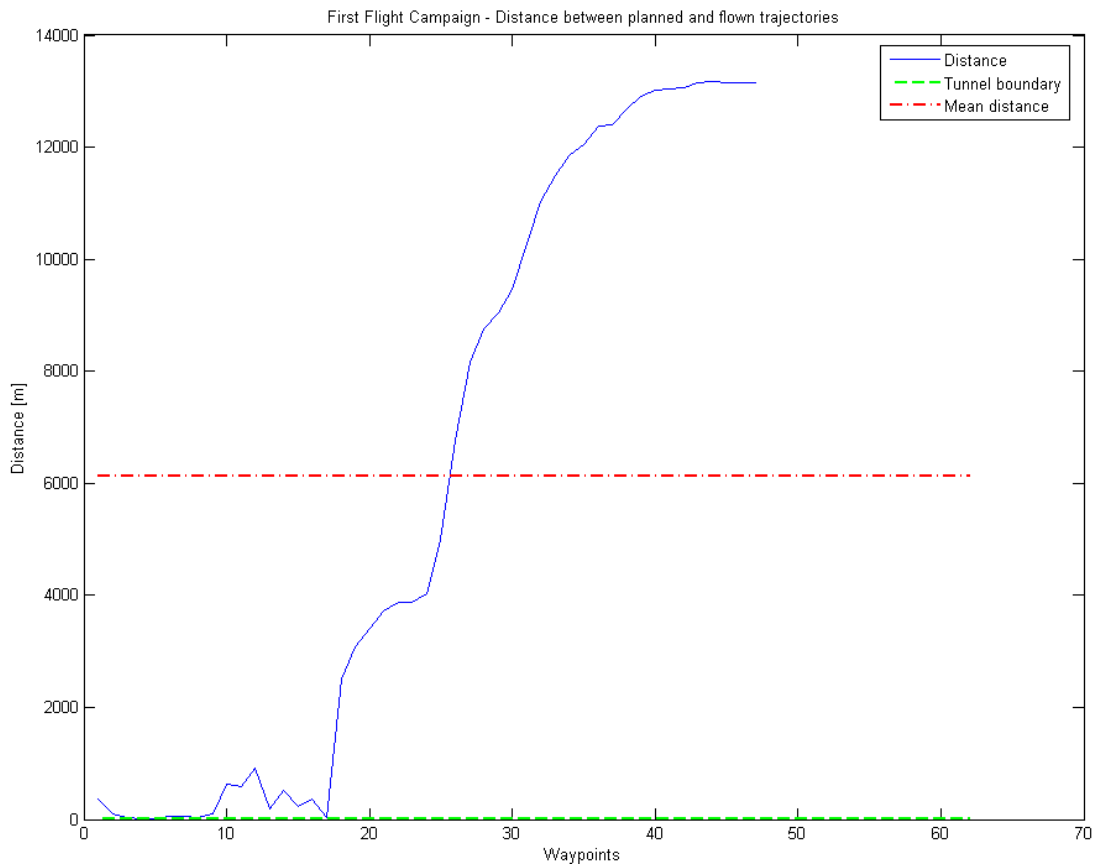


Figure 96: First flight campaign, distance between planned and flown trajectories

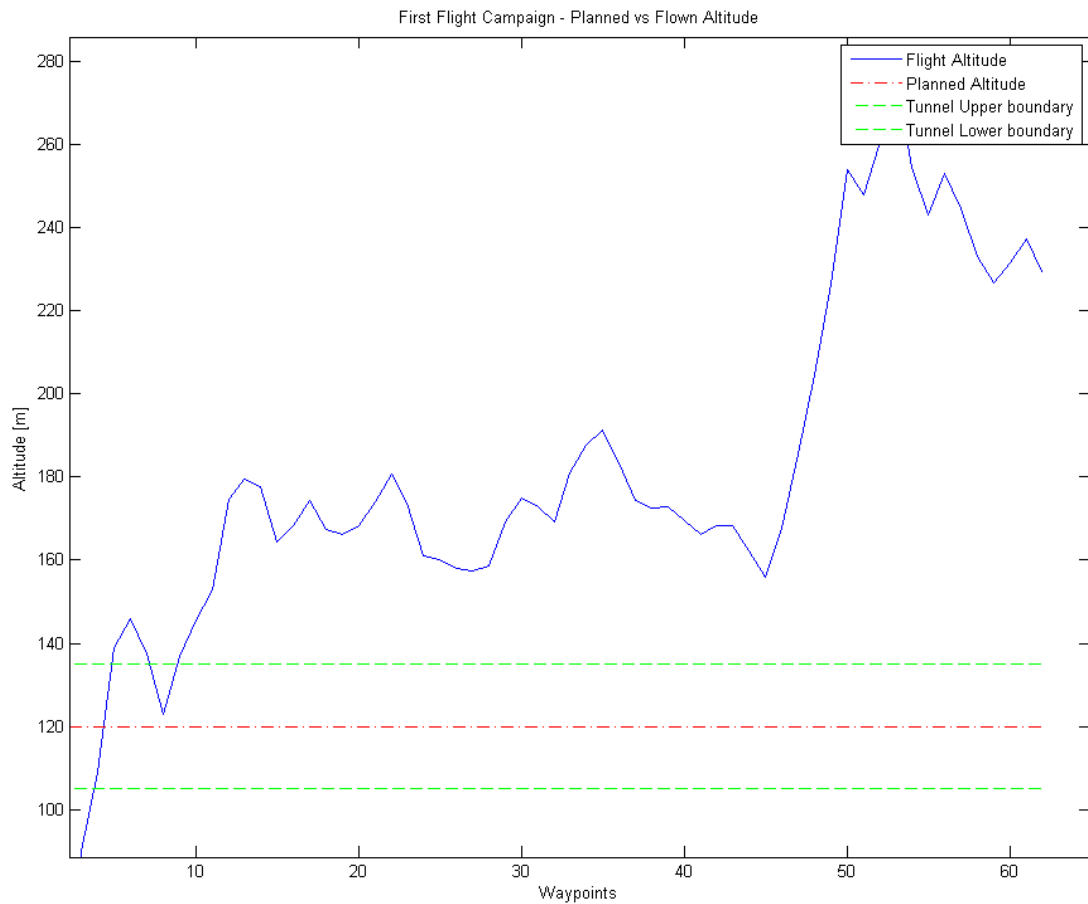


Figure 97: First flight campaign, planned vs flown altitude

Furthermore, because of the prolonged ground operations, during which the system was turned on, the battery went down before completing the entire flight. Although the guidance tunnel did not work correctly the FASTER airborne internal management and computing unit acquired all the information from the GPS receiver and the I.M.U, working, in flight, for more than 50 minutes. Also the camera timing was correct and all images were stored into the hard drive, but unfortunately, due to the rotation of the focus ring, caused by the engine vibrations, only few images were at the correct focus distance.

The experience gained during the first flight campaign was crucial to apply major changes to the guidance tunnel interface and most of problem encountered were fixed. The camera focus ring was blocked at infinity using a plastic band. During the next campaigns an appropriate magnetometer calibration was applied making the calibration (360° turnaround) procedure directly on board the aircraft.

The camera sensitivity was set to ISO 100, in order to avoid electronic noise, the aperture was F/4 while the exposure time was $4 \cdot 10^{-3}$ s because the flight was made in the late afternoon. One of the images correctly acquired was georeferenced and an high

resolution Google Earth layer was created. The computed GSD in 2.9 cm/pixel, and the difference between the 1 m Google Earth database and the high resolution layer is clearly visible in Figure 98.



Figure 98: First flight campaign, high resolution Google Earth layer created from an acquired image

7.2.2 Second Test Campaign

The second test campaign was a closed circuit over the Verginese airfield. Also in this case the trajectory was planned using Google Earth but taking into account standard maneuver rates. Aim of this second test was the verification that the changes applied to the tunnel interface were appropriate to overcome the problems encountered during the first test. The installation procedure was repeated following the check list validated during the first flight.

The new tunnel interface with an augmented screen resolution, better sharpened images, a new colour palette and readable air data values allowed the pilot to maintain the aircraft inside the tunnel for almost the entire flight. The circuit is shown in Figure 99, while the flown trajectory is plotted against the planned one in Figure 100. It is immediately noticeable that during this flight the pilot remained always inside the

guidance tunnel. The position predictor, which provides a 5 s prediction, was activated utilizing a red dot.



Figure 99: Second flight campaign, circuit over Verginese airfield



Figure 100: Second flight campaign, planned vs flown trajectory

The pilot was trained for 30 minutes before takeoff to get used to the new interface; training was performed using the CIL workstation connected to a laptop pc. As shown in Figure 101, the new interface provides a position predictor shown as red dot, if the red dot remains inside the guidance tunnel, the tunnel structure is highlighted. This information is very useful to the pilot because the aircraft can be flown trying to maintain the prediction inside the tunnel, thus anticipating the maneuvers. The air data values displayed over the graphical representation, like in a Head Up Display, allows piloting without watching to the standard analogue instruments down in the dashboard.

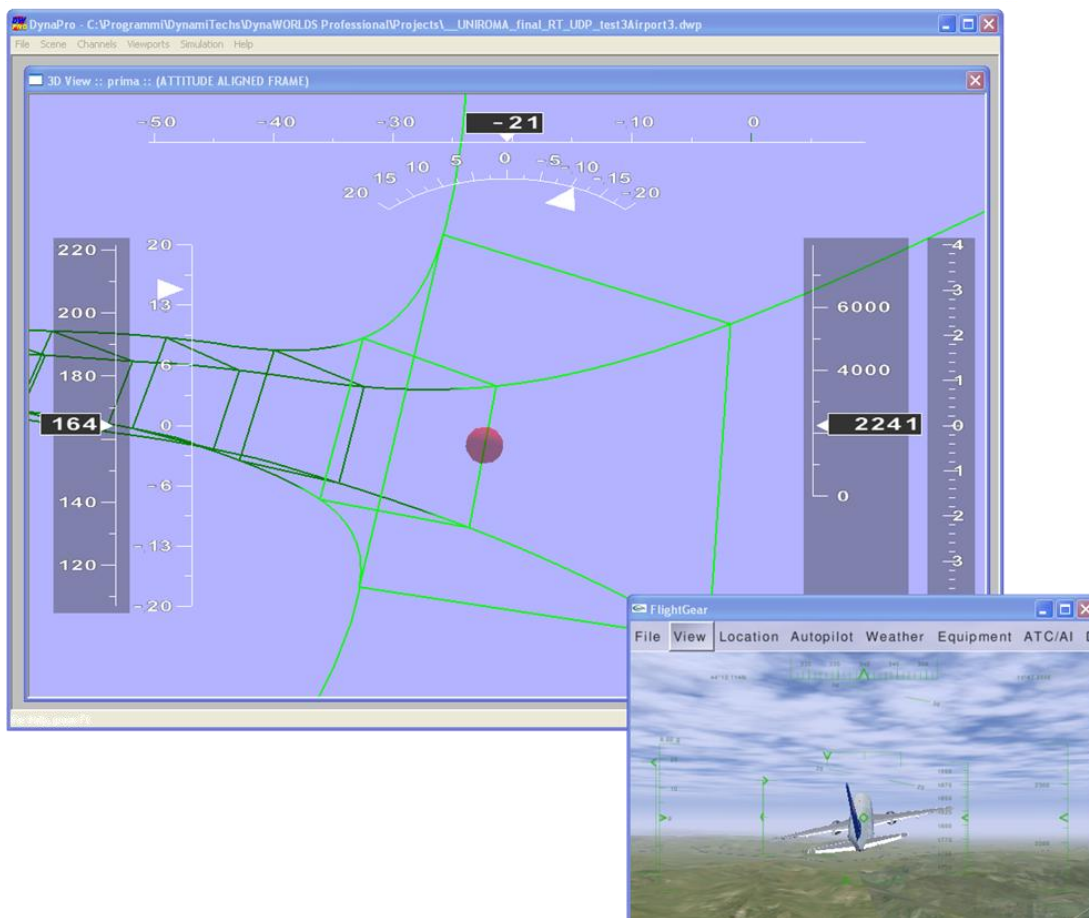


Figure 101: Second flight campaign, Pilot training system

Flight data analysis is shown in Figure 102, Figure 103 and Figure 104. This time, the tunnel was set to 50x50 m and the pilot succeeded in remaining inside the tunnel for almost the whole rectilinear part of the circuit (for what concerns the horizontal trajectory differences) while had no problems in keeping the aircraft inside the tunnel at the planned altitude. During this 6 minutes flight, 164 images were acquired.

Results of the test campaigns

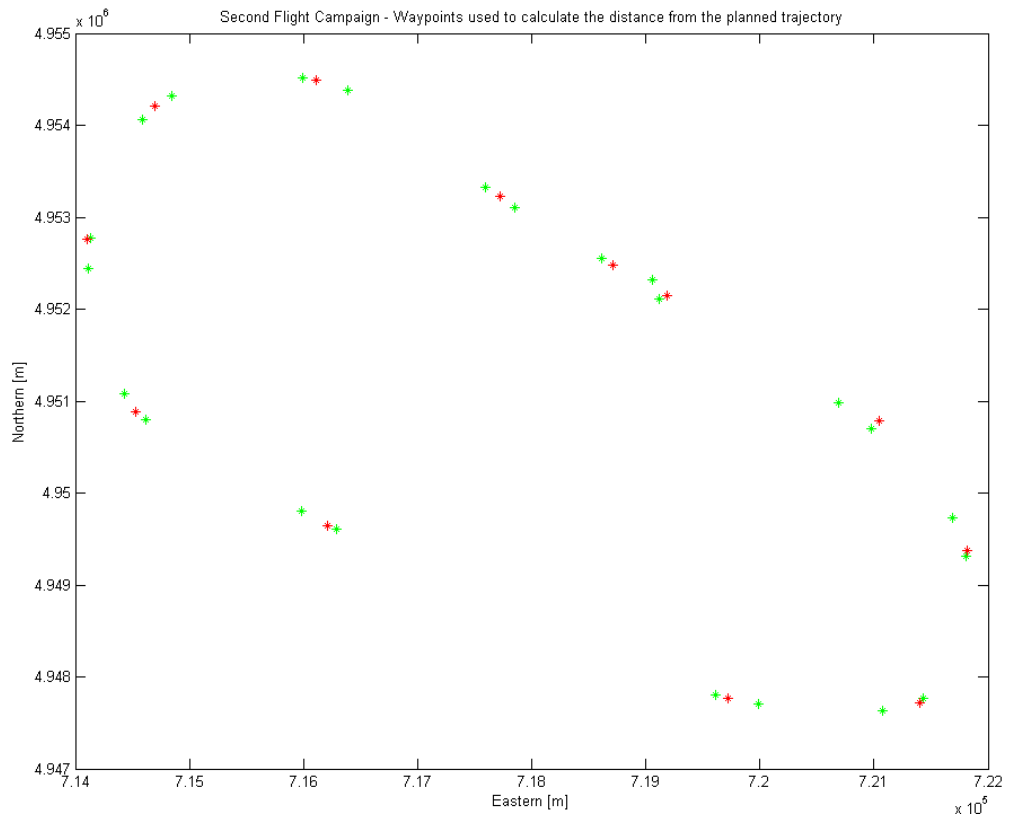


Figure 102: Second flight campaign, selected waypoints of the flown trajectory used to compute the distance from the planned trajectory

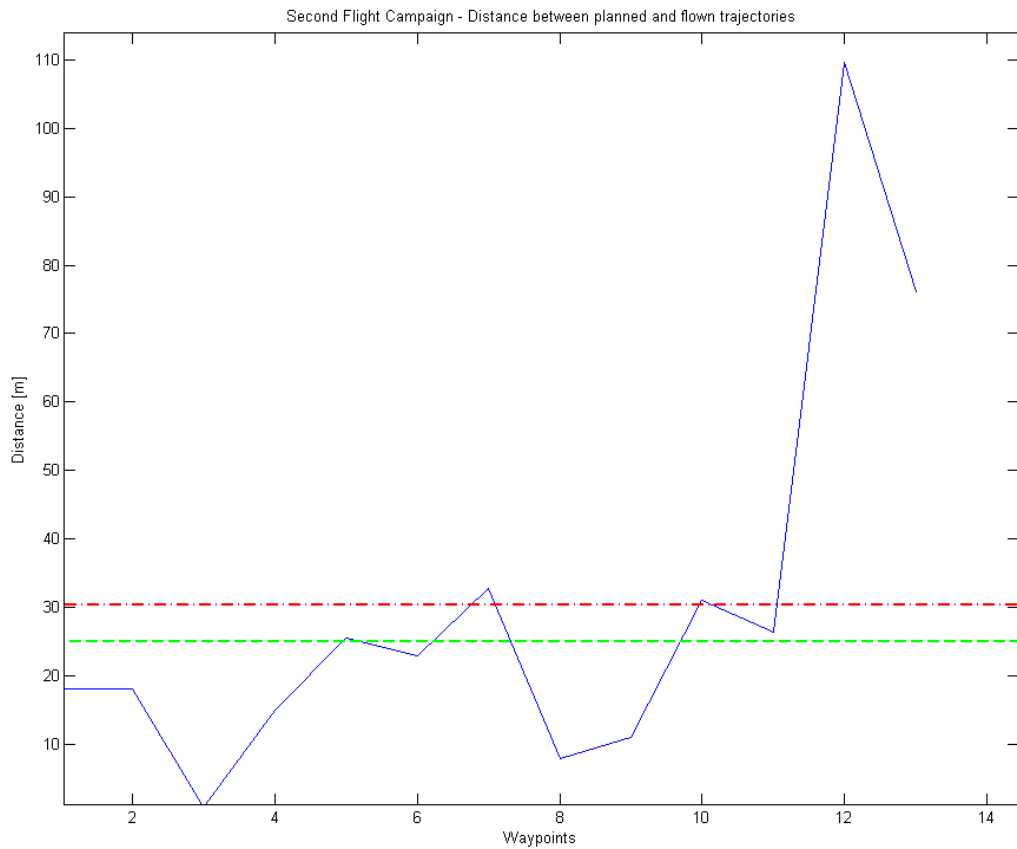


Figure 103: Second flight campaign, distance between planned and flown trajectory

Results of the test campaigns

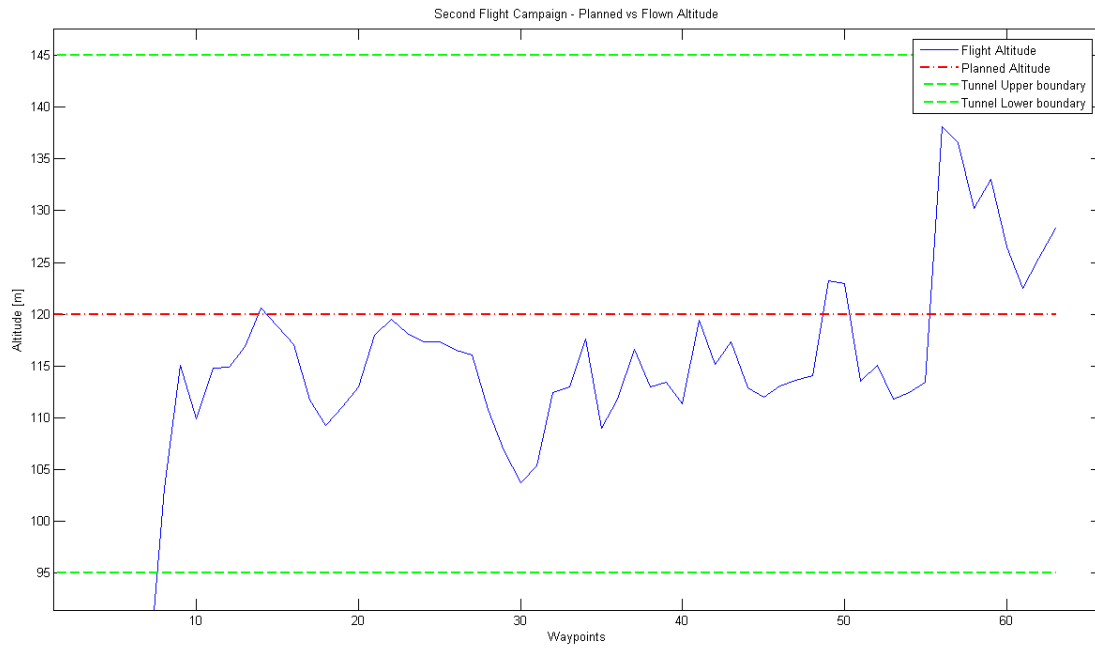


Figure 104: Second flight campaign, planned vs flown altitude

The camera settings for the second test were: focal length 28 mm (equivalent to 46 mm for the APS-C format), ISO 100, aperture F/5 and exposure time of $4 \cdot 10^{-3}$ s. A sample georeferenced image, was used to create an high resolution Google Earth layer



Figure 105: Second flight campaign, Google Earth layer created from an acquired image

7.2.3 Third test campaign

In the third test campaign, for the first time, the FASTER planning tool was used because of the presence of several adjacent flight stripes. In addition, the latest modifications to the waypoints management made to the FASTER EM management software were used. So the tunnel was not completely displayed since the beginning but it was updated every 5 s, taking into account the actual position (Section 6.5.6).

The target area (shown in Figure 106) was defined using the Google Earth interface and then the trajectory was computed using the Matlab script *Faster_planner.m*. The planned trajectory was already presented in Chapter 5 (Figure 42-Figure 49).



Figure 106: Brisighella target area

The aircraft took off from the Villafranca airfield near Forlì and after a transfer of 15 min reached the target area. The transfer flight was planned with only 4 waypoints leaving the graphical interface to generate a newer guidance tunnel according to the pilot maneuvers. A climb was planned between the starting point (15 m AMSL⁴) and the target area entrance waypoint (700 m AMSL). A mountain area had to be over flown in the proximity of the target area, and strong ascending air streams were present making

⁴ AMSL stands for Above Mean Sea Level

difficult to keep the pre-computed heading. The flight analysis is presented in the following figures.

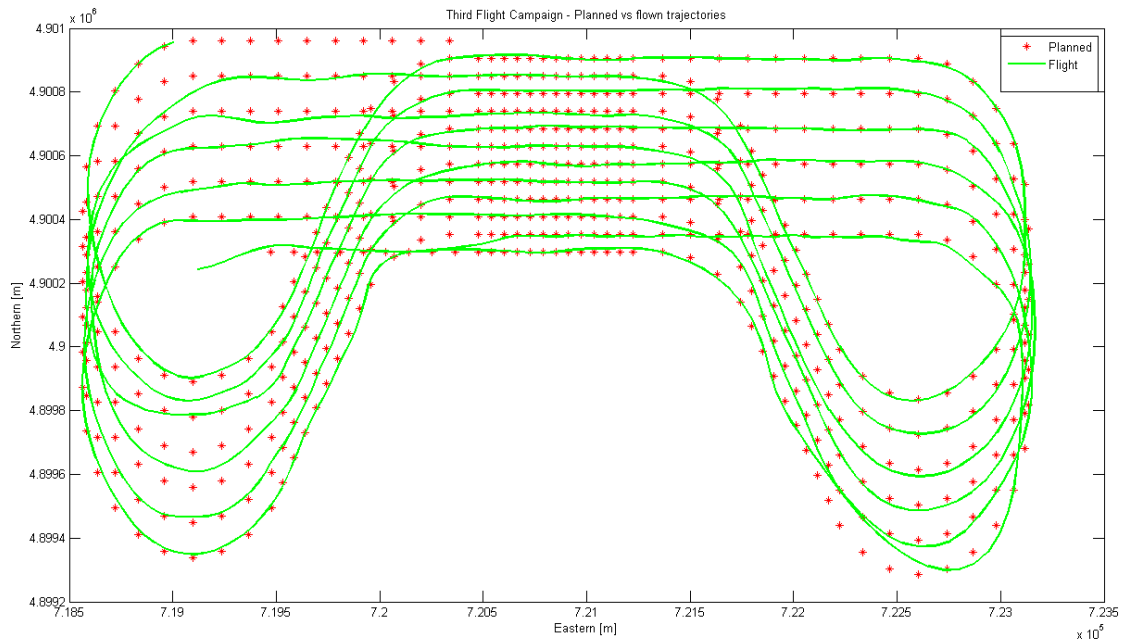


Figure 107: Third flight campaign, planned vs flown trajectories

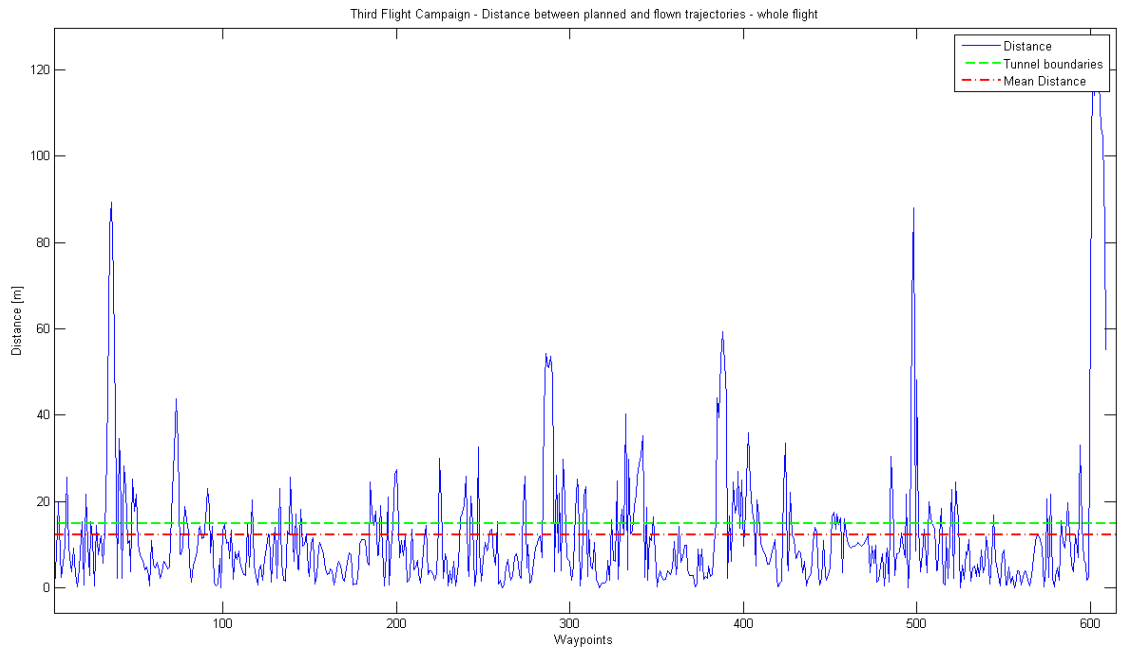


Figure 108: Third flight campaign, distance between planned and flown trajectories

Results of the test campaigns

Figure 107 and Figure 108 show the planned trajectory against the flown trajectory and the computed distance between them. The mean distance is below the tunnel boundaries (12.35 m), which for this flight were set to 15 m (30x30 m tunnel section). Distance peaks are relative to the course turnabouts and mainly due to the adverse meteorological conditions. Flight altitude is plotted in Figure 109, showing that notwithstanding ascending airstreams, the pilot succeeded in remaining almost all the time inside the guidance tunnel. Better results could be obtained looking only at the aircraft behavior during stripe passages.

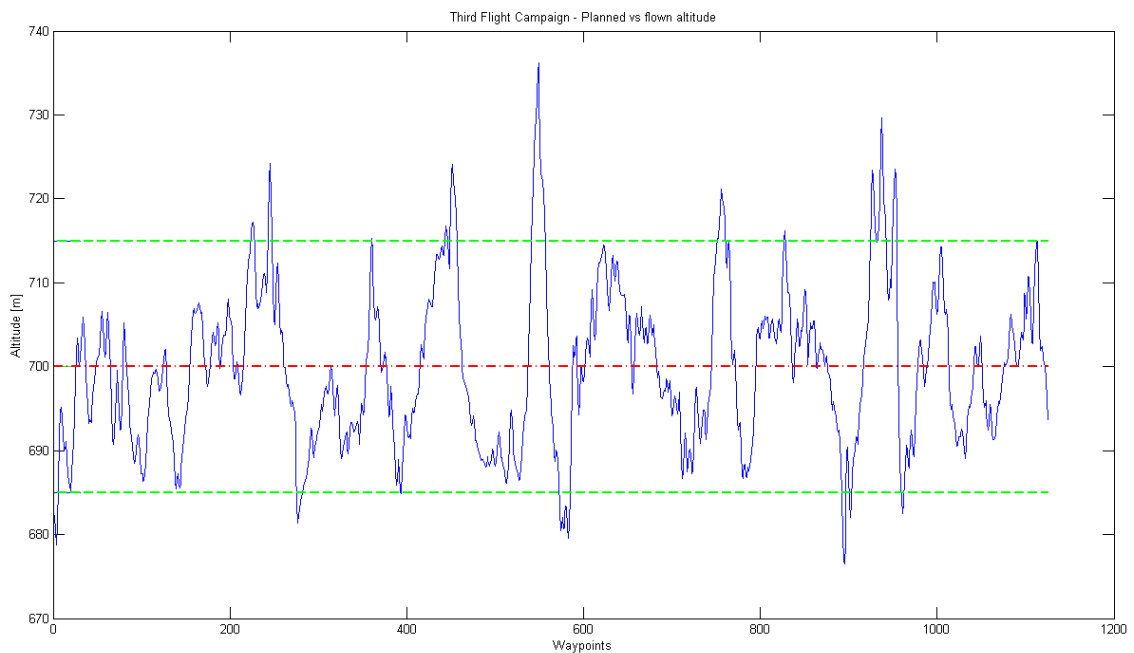


Figure 109: Third flight campaign, planned vs flight altitude

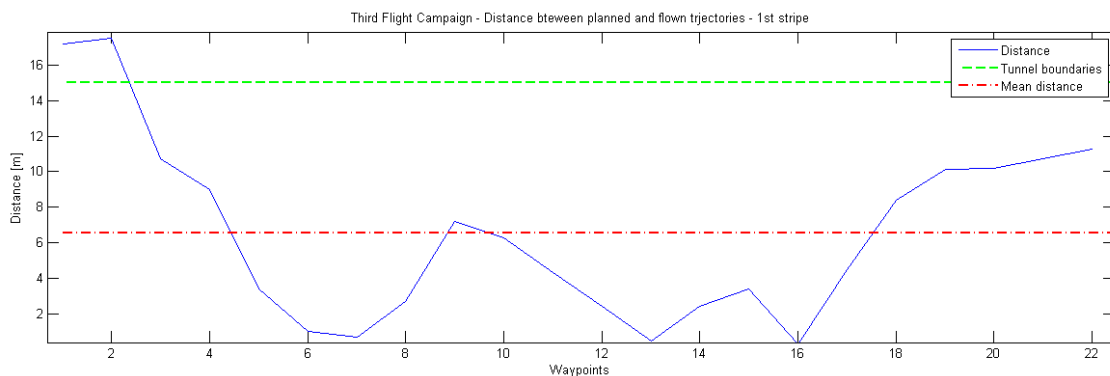


Figure 110: Third flight campaign, distance between planned and flown trajectories, 1st stripe

In Figure 110, the distance between planned and flown trajectories is plotted for the first stripe, showing a mean distance of about 6.3 m. The same happens for the others stripes; the worst case is represented by the 2nd stripe which has a mean distance from the planned of about 9.6 m. The aircraft entered the target zone at 13:27 and exited at 14:04 for a total elapsed time of about 37 min against the 39 min computed by the planning software. During the flight, 1235 images were acquired because the camera was left armed also during maneuvers.

This third campaign, has demonstrated that the visual interface adopted for the FASTER EM, allows the pilot to perform a very narrow (90 m) multi-stripes flight path. Differences between the planned and the flown trajectories, contained within 10%, can be taken into account during flight planning suitably adjusting the overlap percentage. The last test campaign has also revealed that the additional pilot workload is not negligible, especially during long missions. A possible solution to reduce pilot loads is to increase the tunnel size during transferring and turnabout maneuvers, where image acquisition is not working. Then tunnel size will be progressively reduced during the 60 s, re-aligning phase of the 45° procedure turn.

Acquired images were used to built some image mosaic in order to verify the expected along track and across track overlap. To generate mosaics a specific software, PtGUI, was used and an example of the output is shown in Figure 111 and Figure 112.



Figure 111: Brisighella mosaic, cropped image



Figure 112: Third flight campaign, Brisighella mosaic

Chapter 8. Conclusions

In this work a novel concept of photogrammetric and remote sensing instrument has been discussed. The system is a fully-digital, direct georeferencing system used to acquire images in different bands of the electromagnetic spectrum. To define the external orientation parameters, avoiding traditional image scanning and aerial resection, a combination of an inertial measurements platform and a GPS receiver has been used. The system has been completely developed and an engineering model with reduced functionalities has been assembled and tested.

To realize the EM a complete set of hardware parts have been defined according to a requirements list, derived by the analysis of the state of the art technologies actually available in the Geomatics field.

To complete a series of test flight campaign a flight planner tool, able to satisfy all constraints of a photogrammetric campaign, has been developed in order to generate pre-built trajectories to be followed by the pilot. During the flight test campaigns the functioning of the pilot visual interface, expressly adapted for the purpose of this project, was validated. In the last test campaign indeed, the pilot was able to keep the aircraft inside the guidance tunnel almost for the entire mission (39 minutes) with a mean distance from the planned trajectory of less than 13 m.

Over a thousand of images were acquired during the three test campaigns, although only those of the last two were usable for georeferencing and mosaicing purposes. Unfortunately, the work on these last two tasks is not completed yet. This is mainly due to the lack of an high resolution digital elevation model of the over flown areas. Tests were also done on image georeferencing using Google Earth software capabilities, showing the difference between the 1 m satellite imagery database and the very high resolution images acquired from the Ultra Light Aircraft at an altitude of 150m.

Conclusions

The FASTER EM still needs to be fine tuned before the realization of the final system; other tests campaign, with the IMU installed inside the external POD, will be helpful in order to better evaluate the direct georeferencing accuracy of the system. In particular a flight over an airfield with calibration patterns installed could be the most appropriate solution.

Future work shall be focused on the development of an additional stereo imager able to acquire the surrounding elevation model in order to produce orthophotos which are used in topography and for mapping purposes.

Appendix-A Converting Geographical Coordinates to UTM

In the following appendix the method used to convert Geographical coordinates to UTM coordinates is described. Relationship are used in the *GEOtoUTM.m* and *UTMtoGEO.m* scripts. The geometrical problem is shown in Figure 113.

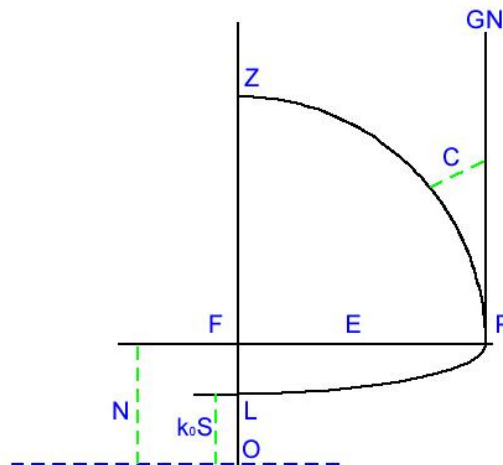


Figure 113: Geographical to UTM coordinates conversion, geometrical problem

In the previous figure P is the point under consideration, F is the foot of perpendicular from P to central meridian (F latitude is the footprint latitude), O is the origin on the Equator, \overline{OZ} is central meridian, \overline{LP} is the parallel of latitude P , \overline{ZP} is the meridian of P , $\overline{OL} = k_0S$ is the meridional arc from equator, \overline{LF} is the ordinate curvature, $\overline{OF} = N$ is the grid northing, $\overline{FP} = E$ grid distance from central meridian, \overline{GN} is the grid north and C is the convergence or meridians (angle between true and grid north) [Ref XX]. k_0 is the scale along the zone central meridian and is equal to 0.9996.

According to the USGS (*United States Geological Survey*), first the meridional arc through the point in question is calculated as follow [Ref. (53)]:

$$M = a \left[\left(1 - \frac{e^2}{4} - \frac{3e^4}{64} - \frac{5e^6}{256} \dots \right) lat - 3 \left(\frac{3e^2}{8} + \frac{3e^4}{32} + \frac{45e^6}{1024} \dots \right) \sin(2lat) \right. \\ \left. + \left(\frac{15e^4}{256} + \frac{45e^4}{256} + \dots \right) \sin(4lat) - \left(\frac{35e^6}{3072} + \dots \right) \sin(6lat) + \dots \right]$$

Converting latitude and longitude to UTM, northing is defined as ($p = long - long_0$):

$$y = K_1 + K_2 p^2 + K_3 p^4$$

and considering that e is the eccentricity of the Earth's elliptical cross-section, $e' = \frac{e^2}{(1-e^2)}$ and $\nu = \frac{a}{\sqrt{(1-e^2 \sin^2(lat))}}$, we have that

$$K_1 = M k_0$$

$$K_2 = k_0 \nu \sin(lat) \frac{\cos^2(lat)}{2}$$

$$K_3 = \left[k_0 \nu \sin(lat) \frac{\cos^3(lat)}{24} \right] [(5 - \tan^2(lat) + 9e'^2 \cos^2(lat) + 4e'^4 \cos^4(lat))]$$

while easting is:

$$x = K_4 p + K_5 p^3$$

and

$$K_4 = k_0 \nu \cos(lat)$$

$$K_5 = (k_0 \nu \frac{\cos^3(lat)}{6}) [1 - \tan^2(lat) + e'^2 \cos^2(lat)]$$

Bibliography

1. *Standalone Three-Axis Attitude Determination from Earth Images*. **Bevilacqua, Alessandro, et al.** San Diego : XX AIAA Conference, 2010.
2. **Wikipedia**. Geomatics. [Online] <http://en.wikipedia.org/wiki/Geomatics>.
3. *Characteristics of New Generation of Digital Aerial*. **Trinder, J.** s.l. : GISdevelopment.net, 2005.
4. *Airborne Digital Imagers: An Overview & Analysis*. **Petrie, Gordon e Walker, Stewart**. Marne-La-Vallée, France : s.n., 2006. ISPRS Commission I Symposium.
5. **Carl Zeiss AG**. VS 40. [Online] <http://www.zeiss.de/c1257088004a21ca/Contents-Frame/609445591b9e91a3c1257391003149c8>.
6. **Canon**. EOS Digital. [Online] <http://www.canon.com/eos-d/>.
7. **Airborne Data System**. Agriview. [Online] http://www.airbornedatasystems.com/index.php?option=com_content&view=article&id=18&Itemid=20.
8. *Airborne Digital Data Capture Systems*. **Petrie, Gordon**. Nessebar, Bulgaria : s.n., 2007. VII International & Technical Conference " From Imagery to MAP: Digital Photogrammetric Technologies".
9. **Trimble - Applanix**. DSS RapidOrtho. [Online] <http://www.applanix.com/solutions/airborne/dss.html>.
10. **Dimac** . Digital Modular Aerial Camera - Wide+. [Online] <http://www.dimacsystems.com/html/products-dimac-wide-plus.html>.
11. **Microsoft**. UltraCamXp Large Format Camera. [Online] <http://www.microsoft.com/ultracam/en-us/UltraCamXp.aspx>.
12. **Intergraph**. Intergraph Z/I Cam - photo -. [Online] <http://www.intergraph.com/photo/default.aspx>.
13. *Design Principles of the LH Systems ADS40 Airborne Digital Sensor*. **Sandau, Rainer, et al.** Amsterdam : IAPRS, 2000, Vol. XXXIII.
14. *Camere Digitali per Riprese Aeree e Terrestri*. **Galetto, Riccardo**. Roma : s.n., 2004.

15. *An Optimally Integrated Direct Georeferencing and Flight Management System for Increased Productivity of Airborne Mapping and Remote Sensing*. s.l. : USGS, 2004, Vol. WG I/4.
16. **Prosilica**. *Prosilica GE4000/4000 C, User Manual*. 2009.
17. **Carl Zeiss AG**. *Distagon T* 2,8/28 ZF, Technical Specification*. 2009.
18. —. *Distagon T* 2,8/21 ZF, Technical Specification*. 2009.
19. **Prosilica**. *Prosilica - GigE cameras*. [Online]
<http://www.prosilica.com/products/ge4000.html>.
20. **Carl Zeiss Ag**. *Carl Zeiss Imaging Lens*. [Online] <http://www.zeiss.com/photo>.
21. **Linder, Wilfried**. *Digital Photogrammetry, a practical course*. s.l. : Springer, 2006.
22. **Konecny, Gottfried**. *Geoinformation, Remote Sensing, Photogrammetry and Geographic Information Systems*. s.l. : Taylor & Francis Inc, 2003.
23. **Wikipedia**. *GIS - Geographical Information Services*. [Online]
http://en.wikipedia.org/wiki/Geographic_information_system.
24. *The Shuttle Radar topography mission*. **Farr, Tom G., et al.** 2007.
25. **Open Geospatial Consortium Inc**. *KML 2.2 – An OGC Best Practice*. s.l. : OGC, 2007.
26. **Snyder, John P.** *Map Projections - A Working Manual*. s.l. : USGS Professional Paper 1395, 1987.
27. **Wikipedia**. *Universal Transverse Mercator*. [Online]
http://en.wikipedia.org/wiki/Universal_Transverse_Mercator_coordinate_system.
28. **METI**. *ASTER GDEM Version 1 Readme file*. 2009.
29. **Salsi, Umberto**. *Le virate Standard*. [Online]
<http://www.icosaedro.it/acm/virate.html>.
30. **Advantech**. *PCM-3353 User Manual*. 2006.
31. —. *Product-Line PCM-3353*. [Online]
http://www.advantech.com/applied/Stack_SBC_Pages/PC_104/PCM-3353.htm.
32. **Garmin International, Inc**. *GPS18 Technical specifications*. 2005.
33. **Garmin**. *GPS18x 5Hz*. [Online]
<https://buy.garmin.com/shop/shop.do?cID=158&pID=13195>.
34. **Crossbow**. *NAV420CA Series User's Manual*. 2007.

35. —. NAV420 Navigation Aided IMU. [Online]
<http://www.xbow.com/Products/productdetails.aspx?sid=181>.
36. **VIA Technologies Incorporated.** *EPIA-EN User's Manual, Version 1.21.* 2008.
37. **VIA Technologies Inc.** VIA Embedded - EPIA page. [Online]
<http://www.via.com.tw/en/products/embedded/ProductDetail.jsp?productLine=1&id=399&tabs=1>.
38. **LiteMAX.** *LiteMAX AD5621GA AD Board - User Guide.* 2007.
39. —. *LiteMAX LI0610 Inverter - User Guide.* 2007.
40. —. *LiteMAX LID08A02 LED Driving Board - User Guide.* 2008.
41. —. *LiteMAX SP0835E Sunlight Readable 8.4" LED B/L LCD - Preliminary Specifications.* 2008.
42. —. High Brightness LCD Monitors. [Online]
http://www.litemax.com/PD_Products_Detail_36_39_142_US_utf-8.html.
43. **Canon Corporation.** *EOS 450D/Rebel XTi Operating Guide.* 2008.
44. **Mini-Box.** *M2-ATX-HV Intelligent Automotive ATX Power Supply, Version 1.1a.* 2007.
45. **Mini-itx.** [Online] <http://www.mini-itx.it/alimentatori/alimentatori-automotive/alimentatore-automotive-6-32v-m2-atx-hv-140w.html>.
46. **Tecnam.** *P92 Echo Classic, Advanced Ultra Light Aircraft datasheet.* 2003.
47. **Mathworks.** *xPC Target 4, User's Guide.* 2009.
48. —. *xPC Target 4, Getting Started Guide.* 2009.
49. **Garmin International, Inc.** *Garmin Proprietary NMEA 0183 Sentence - Technical Specifications.* 2006.
50. **Applied Physics Systems.** *Model 539 High Speed Digital 3 Axis Fluxgate Magnetometer, operating manual and technical reference.* 2010.
51. **Mathworks.** *Simulink Reference.* 2009.
52. *A Fully Automated System for Remote Sensing Application on Ultra Light Aircraft.* **Melega, Nicola, et al.** Milano : AIDAA, 2009.
53. **Dutch, Steven.** Converting UTM to Latitude and Longitude (Or Vice Versa). [Online] <http://www.uwgb.edu/dutchs/usefuldata/UTMFormulas.HTM>.
54. *Digital Earth visualization and web-interface capabilities utilizing 3-D geobrowser technology.* **Foresman, T. W.** 2005.

55. **MIL Standards.** *MIL-PRF89020B, Performance specification Digital Elevation Data (DTED).* 2000.
56. **PC/104 Embedded Consortium.** *PC/104-Plus Specification Version 2.3.* 2008.
57. **VIA Technologies Incorporated.** *EPIA EN-Series Mini-ITX Mainboard Operating Guide.* 2006.
58. *A program for direct georeferencing of airborne and spaceborne line scanner images.*
Muller, Rupert, et al.